

**Design, assembly, and operation  
of a self-regulating DNA  
rotaxane linear actuator**

**Dissertation**

zur Erlangung des Doktorgrades (Dr. rer. nat.)  
der Mathematisch-Naturwissenschaftlichen Fakultät  
der Rheinischen Friedrich-Wilhelms-Universität Bonn

vorgelegt von

**Ze Yu**

aus  
Tianjin, China

Bonn 2021



Angefertigt mit Genehmigung der Mathematisch-Naturwissenschaftlichen Fakultät  
der Rheinischen Friedrich-Wilhelms-Universität Bonn.

1. Gutachter: Prof. Dr. Michael Famulok

2. Gutachter: Prof. Dr. Günter Mayer

Tag der Promotion: 24.03.2022

Erscheinungsjahr: 2022



Part of this thesis is published in:

**Yu, Z.**; Centola, M.; Valero, J.; Matthies, M.; Šulc, P.; Famulok, M. **A Self-Regulating DNA Rotaxane Linear Actuator Driven by Chemical Energy.** *J. Am. Chem. Soc.* **2021**, 143 (33), 13292–13298. doi:10.1021/jacs.1c06226

Further scientific contributions:

Valero, J.; Centola, M.; Ma, Y.; Škugor, M.; **Yu, Z.**; Haydell, M. W.; Keppner, D.; Famulok, M. **Design, Assembly, Characterization, and Operation of Double-Stranded Interlocked DNA Nanostructures.** *Nat. Protoc.* **2019**, 14 (10), 2818–2855. doi:10.1038/s41596-019-0198-7



# Contents

---

<b>Abstract</b> .....	<b>1</b>
<b>1. Introduction</b> .....	<b>3</b>
1.1. DNA and DNA nanotechnology .....	3
1.1.1. Structural basis of DNA.....	3
1.1.2. Kinetic processes in DNA structure assembly .....	9
1.1.3. DNA nanotechnology .....	11
1.1.4. Bio-hybrid DNA nanodevices. ....	14
1.1.5. In silico design and modeling of DNA nanotechnology .....	16
1.2. Interlocked DNA nanostructures.....	19
1.2.1. Interlocked molecules and mechanical bonds .....	20
1.2.2. Interlocked assemblies based on DNA.....	21
1.2.3. Applications of DNA rotaxane and catenane .....	26
1.3. DNA nanotechnology and synthetic biology .....	28
1.3.1. Synthetic biology.....	28
1.3.2. Artificial regulatory circuits .....	30
1.3.3. DNA as a component of synthetic transcriptional regulation .....	32
1.4. DNA and transcription .....	34
1.4.1. T7 RNA polymerase-DNA interactions.....	34
<b>2. Aim of this project</b> .....	<b>40</b>
<b>3. Results</b> .....	<b>42</b>
3.1. DNA rotaxane linear actuator .....	42
3.1.1. Design of the rotaxane actuator.....	42
3.1.2. Assembly and characterization of the rotaxane actuator.....	44
3.1.3. Overview of the mechanism of the rotaxane actuator .....	48
3.1.4. Transcription behaviors.....	49

3.1.5.	Rehybridization of the macrocycle.....	54
3.1.6.	Macrocycle releasing by T7RNAP .....	56
3.1.7.	Movement direction of macrocycle forced by T7RNAP .....	57
3.1.8.	Termination of transcription and dethreading investigation.....	59
3.1.9.	Investigation of the dynamic stability of the macrocycle in the rotaxane by molecular dynamics simulations .....	62
3.2.	Spherical stopper (SST) optimization for the rotaxane actuator.....	66
3.2.1.	Design and assembly of the SST-optimized rotaxane .....	66
3.2.2.	Transcription behavior and comparison .....	67
3.2.3.	Investigation of the dynamic stability of the macrocycle in the SST-optimized rotaxane by molecular dynamics simulations .....	68
3.3.	Investigation of macrocycle-mediated promoter properties.....	70
3.3.1.	Design and assembly .....	70
3.3.2.	Transcriptional behaviors.....	73
<b>4.</b>	<b>Discussion and Outlook.....</b>	<b>78</b>
4.1.	Design and mechanism.....	78
4.2.	The factors that affect the transcription rate in the rotaxane actuator .....	81
4.3.	Interlocked macrocycle-mediated transcriptional control .....	83
<b>5.</b>	<b>Materials and methods .....</b>	<b>85</b>
5.1.	Reagents .....	85
5.2.	Buffer systems.....	86
5.3.	Equipment .....	86
5.4.	Methods.....	88
5.4.1.	UV Absorption Spectroscopy – concentration of ODNs and DNA assemblies ..	88
5.4.2.	DNA annealing program .....	88
5.5.	Gel electrophoresis .....	88
5.5.1.	Agarose Gel Electrophoresis .....	88
5.5.2.	Polyacrylamide Gel Electrophoresis (PAGE).....	89



5.5.3.	Macherey-Nagel Gel and PCR Clean-up kit .....	89
5.5.4.	Freeze 'n squeeze .....	89
5.6.	High Performance Liquid Chromatography (HPLC) .....	89
5.7.	Fluorescence experiments .....	90
5.7.1.	MB fluorescence experiments. ....	90
5.7.2.	Fluorescence-quenching measurements.....	90
5.8.	Atomic Force Microscopy (AFM) .....	91
5.9.	Assembly of DNA nanostructures.....	91
5.9.1.	Assembly of 168 bp ring stoppers. ....	91
5.9.2.	Synthesis of 40 nt single-stranded macrocycle. ....	92
5.9.3.	Assembly of axle.....	92
5.9.4.	Assembly of rotaxane. ....	92
5.9.5.	Assembly of spherical stopper (SST).....	93
5.9.6.	Assembly of rotaxane with one spherical stopper (ROT-sst).....	93
5.10.	Molecular dynamics simulations of DNA nanostructures.....	93
5.10.1.	Modeling construction .....	93
5.10.2.	oxDNA molecular dynamics simulation.....	94
5.10.3.	Simulation with external constant forces .....	94
<b>6.</b>	<b>Appendix.....</b>	<b>96</b>
6.1.	List of Abbreviations .....	96
6.2.	Supplementary Date.....	98
6.3.	Tables .....	100
<b>7.</b>	<b>References.....</b>	<b>106</b>
<b>8.</b>	<b>Acknowledgements .....</b>	<b>114</b>



# Abstract

DNA is not only the carrier of genetic information but also an excellent bottom-up material for constructing nanostructures due to its high degree of programmability. Interlocked DNA nanostructures have a potential use as nanomachines to perform certain tasks at the molecular scale, in which subcomponents can move a large amplitude with respect to each other. Additionally, DNA is also able to interact with motor-like enzymes, such as RNA polymerase. Such interactions can be utilized to generate directional forces to create biohybrid artificial nanodevices capable of autonomous active motion and produce RNA.

In this thesis, T7 RNA polymerase (T7RNAP) and a DNA nanostructure – DNA rotaxane are combined to develop an automatic linear nanoactuator for the following purposes: 1) transferring the linear motion of T7RNAP along the DNA track to the periodic translational displacement of macrocycle threading in rotaxane; 2) self-controlled transcription.

An interlocked macrocycle-reconstructed promoter is proposed to control the transcription of T7RNAP. In this arrangement, the split promoter sequences of the template strand are distributed over the axle and the threading macrocycle in rotaxane, which together constitute the complete promoter sequence. Transcription by T7RNAP is then utilized to control the release of the macrocycle from a single-stranded (ss) gap region in the promoter and deplete the movement range of the interlocked macrocycle on the axle. Upon reaching the terminator sequences of transcription, T7RNAP detaches from the axle, and the whole system can be reset as the macrocycle shifts back and rehybridizes with the promoter gap to reconstitute the double-stranded (ds) promoter structure, which is a prerequisite for the next transcription cycle.

The transcriptional performance of the rotaxane actuator with an interlocked macrocycle-mediate promoter is studied through molecular beacon (MB) fluorescence experiments. Meanwhile, the detailed kinetics in the operation of the rotaxane actuator are also investigated. The dynamic stability of the system after transcription is then demonstrated through gel analysis, AFM, and coarse-grained modelling simulations. An updated rotaxane actuator with a spherical stopper is proposed and compared with the original design. The properties of the macrocycle-mediated promoter are also carefully investigated.

This T7RNAP-DNA rotaxane hybrid nanodevice was shown to produce self-repeating

---

linear motion without any intervention and achieve self-controlled transcription without any intermediate. Moreover, it has the potential to develop delivery systems and self-regulating RNA production automatons at the molecular scale.

# 1. Introduction

## 1.1. DNA and DNA nanotechnology

DNA nanotechnology involves applying the properties of deoxyribonucleic acid (DNA) or other nucleic acids (such as their self-assembly properties) to constitute new manipulable devices or machinery in the nanoscale. While nucleic acids are the carriers of genetic information in organisms, they are instead used as non-biological materials in the field of DNA nanotechnology.<sup>1</sup> The programmability of nucleic acids derives from their strict base-pairing features, which make it possible to design nanoarchitectures precisely and programmatically. Although the basic concept of DNA nanotechnology was first introduced by Nadrian Seeman in the early 1980s, it did not begin to attract widespread attention until after 2000.<sup>2,3</sup> So far, researchers in this field have successfully constructed immobile structures such as 2D and 3D crystal lattices, wireframes, polyhedrons, and other arbitrary shapes as well as functional structures such as nanomachines. Several strategies are employed to assemble structures, such as folding structures (DNA origami) and dynamic reconfigurable structures (toehold strand displacement methods).<sup>4</sup> The contemporary characterization equipment used in DNA nanotechnology applications includes but is not limited to atomic force microscopy (AFM), transmission electron microscopy (TEM), fluorescence microscopes and crystallography. Increasing numbers of techniques are being developed and research on the way to exploit the potential of DNA nanotechnology and produce more practical applications probably in nanoelectronics and nanomedicines is ongoing.<sup>1</sup>

### 1.1.1. Structural basis of DNA

DNA consists of nucleotides (specifically, deoxyribonucleotide) as subunits. A deoxyribonucleotide is composed of a deoxyribose sugar, a phosphate group (5' position of the sugar), and a nucleobase (Figure 1-1a). Four nitrogenous bases are available: adenine (A), thymine (T), cytosine (C), and guanine (G). A and G bases have two-ringed structures and are called purines, whereas C and T bases have just one ring and are called pyrimidines. The nucleotides of DNA are linked in chains via phosphodiester bonds between the deoxyribose sugar with a hydroxyl group (3') and the phosphate group (5') of the next. The sugar-phosphate backbone of DNA is therefore formed within an alternating chain of phosphate groups and sugars as shown in Figure 1-1b.

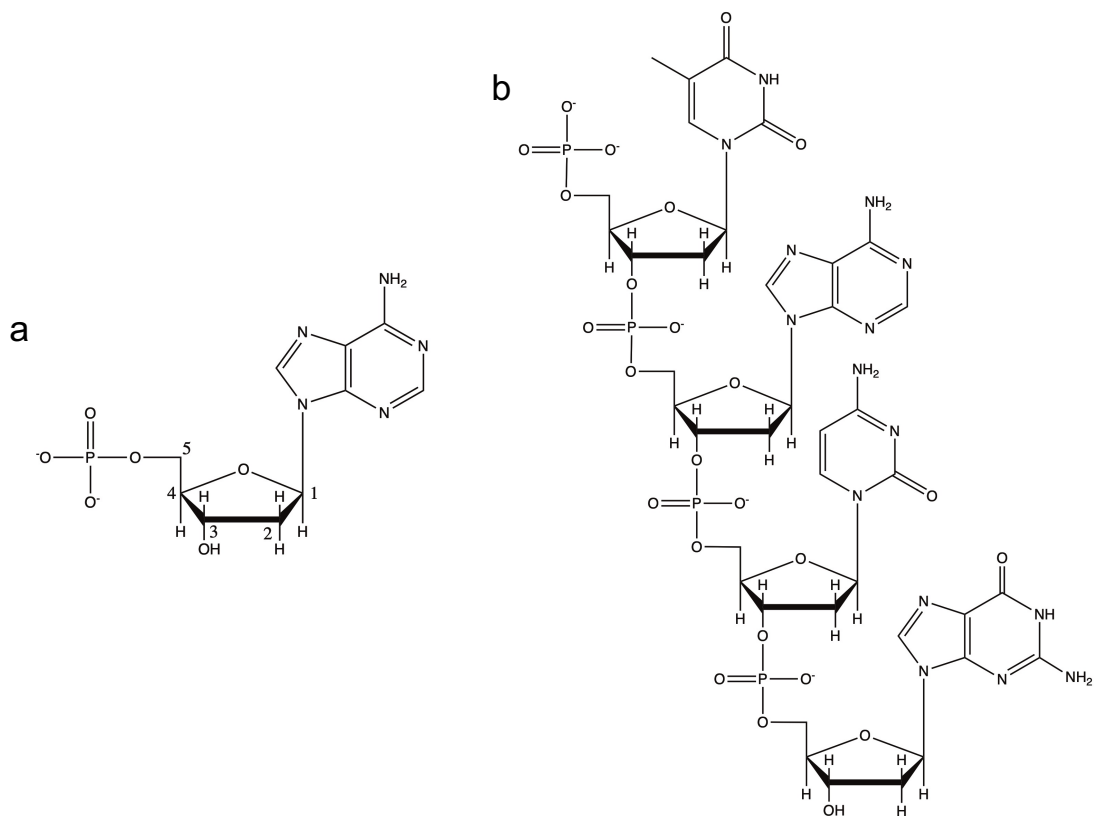


Figure 1-1. Chemical structure of DNA. (a) Structure of a deoxyribonucleotide with an adenine. (b) Structure of a 4 nt oligonucleotide (ODN) containing 4 different types of nucleotides: T, A, C, and G.

People's understanding of DNA's double-stranded (ds) structure most likely refers back to Watson and Crick's study. However, it was Erwin Chargaff who first revealed that, regarding the composition of DNA, the amount of A is always equal to the amount of T and the amount of C is always equal to the amount of G.<sup>5</sup> The results, referred to as Chargaff's rules, identified the door to understand DNA's structure and Watson and Crick opened the door with the key. X-ray diffraction experiments generate an X-shaped diffraction pattern, clearly indicating DNA has a double-stranded helix for DNA, where the sugar-phosphate backbone lies outside of the helical structure and the bases pair together inside and hold the two strands of DNA together.<sup>6</sup>

One of the most important features of DNA is that base pairing is achieved through hydrogen bonding. It should be noted that the two candidates in a typical DNA base pair are not chosen arbitrarily: A is always paired with T, and C is always paired with G. More specifically, as shown in Figure 1-2, an A-T base pair is formed with two hydrogen bonds whereas a C-G base pair is stabilized by three hydrogen bonds that make it more stable. There are no other covalent bonds between the two components in a base pair. These patterns are what we called Watson-Crick base pairs, and the

relationships between AT and CG are complementary. Meanwhile, further experiments showed if the bases of two DNA strands are correspondingly complementary, they will interact with each other to form a double helix structure (A-T, C-G), which is so-called hybridization. Due to the pairing rule of large purines (A or G) always pairing with small pyrimidines (T or C), the diameter of the helix is relatively uniform, about 2 nm.

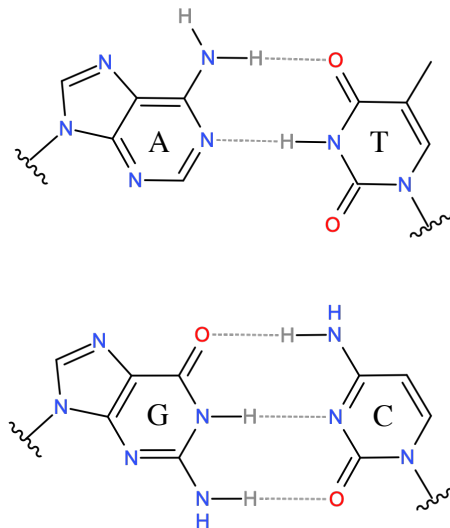


Figure 1-2. Watson-Crick base pairing. The two types of Watson-Crick base pairs: A-T and G-C.

As shown in Figure 1-3, two twisted DNA strands run alongside each other in an antiparallel pattern, which means in a dsDNA, the 5 prime of one strand is always accompanied by the 3 prime of another strand, and vice versa. As can be seen from the figure, the base pairs are arranged in a double helix, much like steps on a ladder.  $\pi$ - $\pi$  stacking between the aromatic planar of adjacent base pairs can also further stabilize DNA's double helix structure. Meanwhile, the hydrophobic effect causes the sugar-phosphate backbone (which is the polar portion of the molecules) to point outward, exposing it to water, while the hydrophobic bases are protected internally, making it easier for them to mutually pair. DNA ends with a double-stranded base pair are called a blunt end, while the ends with unpaired nucleotides (overhang) in either one of the double strands is called sticky end. Stick ends in DNA are well-suited to connecting different sections of DNA structures into one integrated combination, which is extensively applied in DNA nanotechnology.

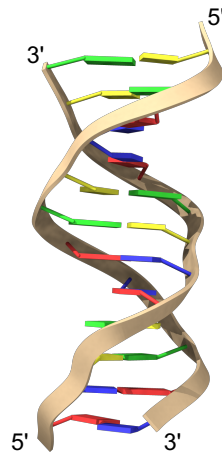


Figure 1-3. Model of an antiparallel double-stranded (ds) DNA. The figure was prepared using the ChimeraX molecular visualization program.<sup>7</sup>

The helical backbone strands and the base pairs form the twisting structure of DNA and create two gaps running along the molecule, which are termed grooves (Figure 1-4). Since the base pairs are asymmetrically attached to the sugar-phosphate backbone, the sizes of the two grooves indicate the differences. A wider major groove and a narrower minor groove are 22 angstroms and 12 angstroms wide, respectively. The outer edges of the bases are also exposed to the grooves and potential donor or acceptor of hydrogen bonding. Thus, these grooves provide an additional site to interact with small ligands and proteins and play important roles in the replication and expression of DNA.

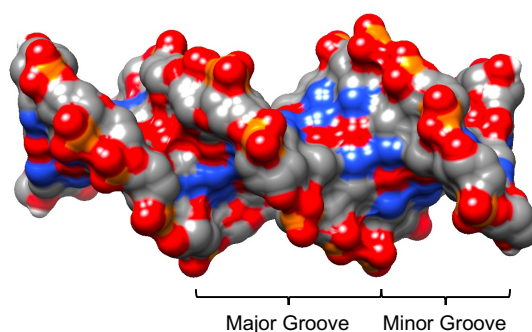


Figure 1-4. Model of the major and minor grooves of DNA. The figure was prepared using the ChimeraX molecular visualization program.

Most of the DNA structures found in cells is what we call B-form DNA, which has a right-handed helix conformation. The structure parameters of B-form DNA are as follows: 10.5 bp per turn, 0.34 nm interval per bp, 3.4 nm per pitch (the height per



complete turn of the helix),  $34.6^\circ$  twist per bp, and 2 nm diameter. Other conformations such as A-form and Z-form are less favorable in nature. The structure of a B-form DNA molecule can also be determined by the sequence of nucleotides containing different bases. It is reported that the sequence containing poly A-tracts showed an inherent curvature in dsDNA (Figure 1-5).<sup>8</sup> Meanwhile, for a 21 bp dsDNA (two complete turns) with a A6N5A5N5 sequence pattern (6 and 5 bp A-runs separated by two 5-bp random sequences), the motif presents a  $19^\circ$  bending toward the minor groove of the A-tracts. Hence, the periodically repeated design with A-tracts leads to cyclization of DNA through short oligonucleotides (ODNs) assembly. In addition, introducing a delicate design mismatch loop can also bend a dsDNA to structure to a certain angle.<sup>9</sup>



Figure 1-5. Model of dsDNA curvature as induced by A-tracts. The figure was prepared using the ChimeraX molecular visualization program.

Besides intermolecular double-stranded formation, DNA can also fold in an intramolecular fashion, as shown in Figure 1-6.<sup>10</sup> The most typical structure formed within one DNA strand is a stem-loop conformation called a hairpin structure. Its base-paired ends are connected with an unpaired loop, which is extensively utilized in the construction of DNA nanostructures and functional parts of DNA nanodevices. Notably, it also occurs very frequently in RNA structures.<sup>11</sup> The secondary structures of DNA can be formed within one DNA strand and involve G-quadruplex and i-motif structures, which are formed by noncanonical (Hoogsteen) base pairs. Even so, these two structures still play important roles in biological functions and the design of DNA nanostructures.<sup>12</sup>

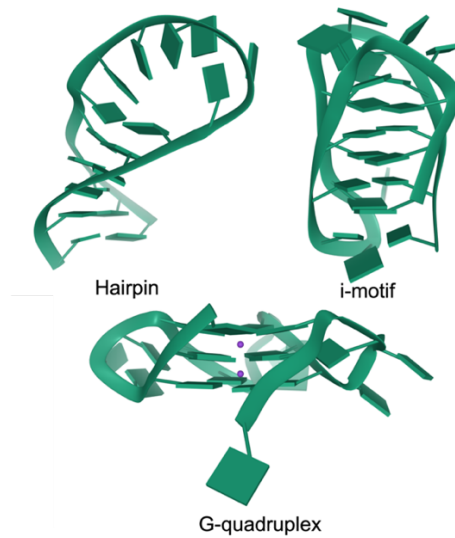


Figure 1-6. Models of DNA secondary structures: hairpin, i-motif, and G-quadruplex, (PDB database: 1ELN, 2GVO, 3CDM), respectively. The figure was prepared using the ChimeraX molecular visualization program.

Another famous DNA structure named Holliday junction (Figure 1-7) was first put forward by the Holliday group in the 1960s. As this contains the symmetric sequence design, a branch migration can be observed in this junction.<sup>13</sup> Seeman developed the design in an asymmetric manner and the structure can be stably presented with multiple intersections (3 to 6 or more)<sup>14</sup> and be used to build more complicated 2D or 3D DNA structures. To summarize, the arrangement of bases (sequence) in DNA strands determines the way DNA molecules connect with the overall structures of different systems. Crucially, the arrangement of bases is programmable and controllable.

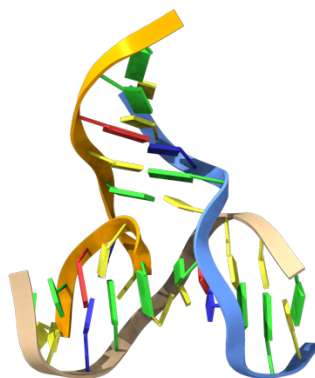


Figure 1-7. Model of a DNA three-way junction (PDB database: 1EKW). The figure was prepared using the ChimeraX molecular visualization program.

### 1.1.2. Kinetic processes in DNA structure assembly

In addition to the structural DNA basis, non-equilibrium DNA systems have also been extensively studied. These systems have been designed to incorporate kinetic DNA processes such as hybridization, dissociation, strand displacement, and reconfiguration.

Hybridization is one of DNA's essential properties, which is determined by several sequence parameters and solution conditions. It is also important for present purposes as it allows for the construction of more complicated DNA nanoarchitectures. As noted above, DNA strands will hybridize together when they have complementary sequences (A-T and C-G) (Figure 1-8). Since GC base pairs are more stable than AT base pairs due to their extra hydrogen bond, GC content (i.e., the percentage of GC base pairs in a DNA sequence) provides a basic image for assessing the stability of hybridization. Regarding solution conditions, pH, concentrations of salt ions, nonaqueous solvents and temperature are the important factors for DNA hybridization. Under certain environmental conditions, the hybridization kinetics can be predicted from the sequence to provide a preliminary assessment for the further rational design and assembly of DNA structures.

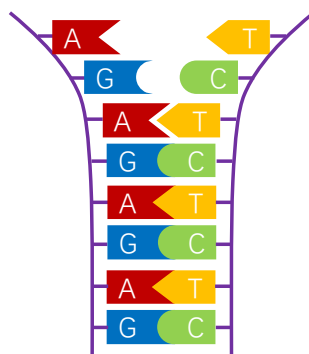


Figure 1-8. Schematic representation of DNA hybridization.

DNA dissociation, also known as DNA melting or DNA denaturation, is a process in which the hydrogen bonds in the DNA double strands are broken, thus leading the double strands to unwind into a single strand. DNA dissociation can be induced by heating. As temperature increases, changes in DNA structure can be easily recorded by measuring the Ultraviolet absorbance and stabilization of a dsDNA with certain sequences by  $T_m$  (temperature of melting) of DNA,<sup>15</sup> which is defined as the temperature at which 50% of DNA dissociation when heated, as illustrated in Figure 1-9.  $T_m$  can be calculated empirically. The stability of the DNA structure presented by

the  $T_m$  parameter should be considered in the initial stage of the design process. In addition, a number of biological processes, such as transcription and replication, can also cause DNA unwinding. During transcription, DNA melting occurs at the promoter sequence associated with the polymerase and initiates the transcription process.<sup>16</sup> Hence, dissociation information allows the stability of the DNA structure to be assessed and also provides the possibility of understanding interactions between DNA and certain enzymes.

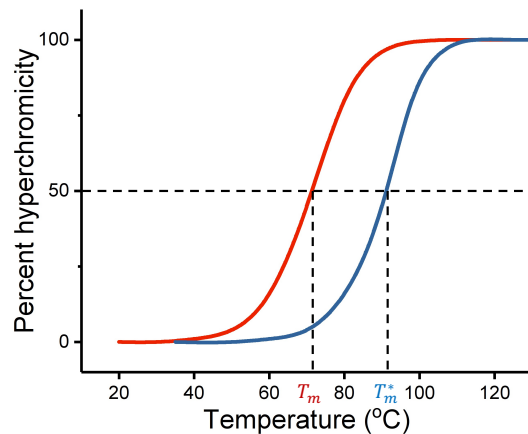


Figure 1-9. Schematic diagram of melting curves of dsDNA.  $T_m$  and  $T_m^*$  represent the melting temperatures at which 50% of DNA dissociates when heated.

Strand displacement occurs when additional strands partially or fully hybridize and further replace one or more of the strands that have been hybridized (Figure 1-10). Strand displacement is initial at a toehold domain (complementary single-stranded (ss) overhang), and progresses with the branch migration procedure.<sup>17</sup> The rate of strand displacement depends on the length and sequence composition of the toehold parts. This rate can be quantified and estimated through simulations and provide a reference for further modification.<sup>18</sup>

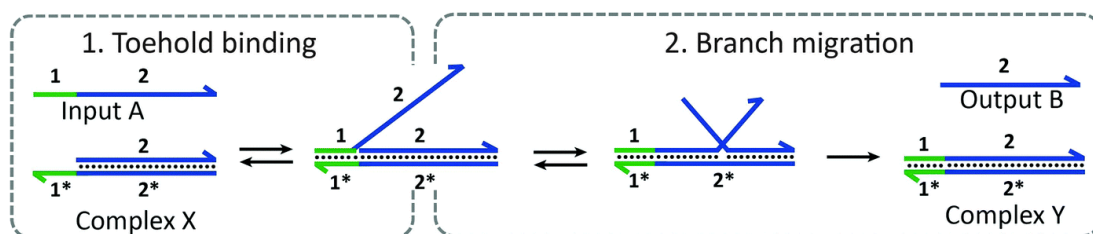


Figure 1-10. Schematic representation of the toehold-mediated strand displacement. The toehold region of strand A hybridizes with the double-stranded complex X, thus starting branch migration. When branch migration is complete, strand B will be released and a new double-stranded complex Y will be formed, completing the strand

displacement. The figure is taken from reference<sup>19</sup>.

Although DNA reconfigurations and DNA allostery are the most complex processes within the study of the kinetics of DNA interactions, they occur in almost every DNA related process. They take place when DNA structures are formed by adding extra strands, undergo conformational changes when meeting with specific metal ions or H<sup>+</sup>, or interaction with different small molecules, proteins, etc.<sup>20</sup> The high flexibility and polymorphism of DNA make complex reconfigurations possible. Reconfiguration of DNA can be pre-designed and utilized to realize special functions and perform predefined tasks.

### 1.1.3. DNA nanotechnology

**Structural DNA nanotechnology.** The comprehensive application of DNA's structural properties is the foundation of structural DNA nanotechnology. The concept of structural DNA nanotechnology dates back to the 1980s, when Nadrian Seeman first postulated and demonstrated immobile synthetic nucleic acid junctions.<sup>2,14</sup> In the intervening years, a wealth of research has been carried out and more and more increasingly complexity of DNA nanoarchitectures are being fabricated using robust designs and rational combination of DNA structures. The complex design of DNA nanoarchitectures are derived from two basic strategies: the multiple-stranded method and the template folding method (DNA origami) (see Figure 1-11).

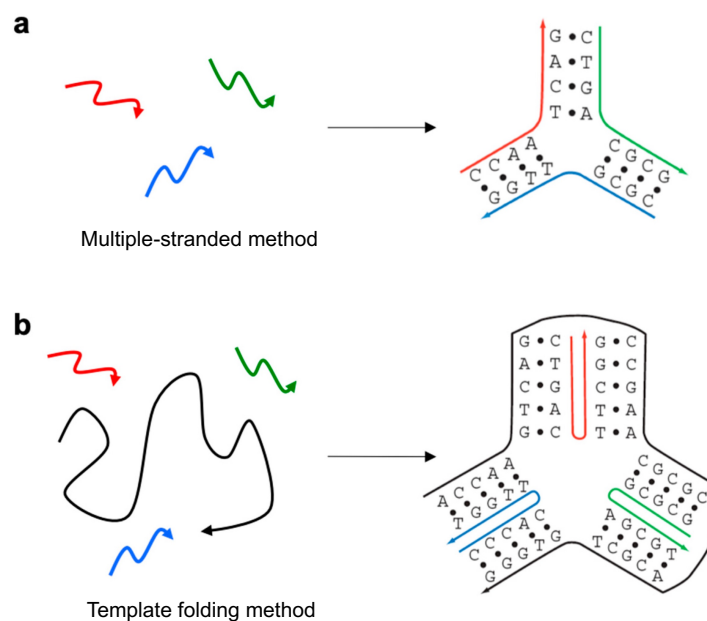


Figure 1-11. Schematic representation of two DNA nanostructure design strategies: (a)

---

Multiple-stranded method. (b) Template folding method. The images are taken and slightly modified from reference<sup>21</sup>.

For the multiple-stranded method, the DNA strands are assembled into several subunits, which then join to form a larger structure through sticky-end hybridization. This method was first exemplified through the assembly of a DNA tube<sup>22</sup> (Figure 1-12). The assembly consists of 10 ODNs and can be divided into two parts. Each part contains a square assembled from four three-way junctions and is extended with four sticky ends. The two subcomponents are first assembled and ligated into a 3D cube structure. A further developed method called DNA tiles is based on synthetic short ODNs containing several domains that bind to neighboring ODNs<sup>23</sup>. Multiple strands can be hybridized periodically or in a program to assemble larger 2D or 3D structures such as a DNA canvas. Meanwhile, ligation is a powerful tool to help to assemble complex DNA structures. To connect two DNA fragments, DNA ligase recognizes the 5'-phosphate group at one end of a strand of DNA and the 3'-OH of the other and then joins them together.<sup>24</sup> Ligation can be performed within the blunt- and sticky-ends of DNA, although the sticky-ends combine two fragments of DNA in advance to prepare for more efficient ligation. Ligation forms DNA connections amongst different DNA fragments that are more stable and irreversible, meaning that the resulting DNA structures can withstand more complicated conditions.

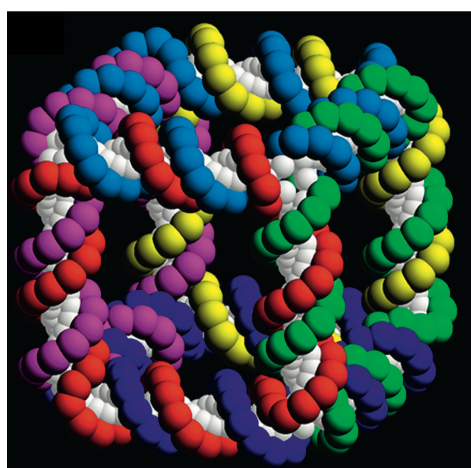


Figure 1-12. Model of a DNA tube. The image is taken and slightly modified from reference<sup>25</sup>.

The most famous structure developed through structural DNA nanotechnology is DNA origami. The method was proposed by Paul Rothemund in 2006, who demonstrated that DNA nanostructures with any designed shapes can be formed by folding a long circular ssDNA from bacteriophage M13 (7249 nt), called a scaffold, via hybridization

with various short DNA strands called staples (20 to 60 nt), as shown in Figure 1-13.<sup>26</sup> The staples hybridize to different positions on the scaffold, thus folding the scaffold into the desired shape. The staple strand sequences are generated using a computer-aided design program based on the known sequence of the scaffold. Next, the assemblies are performed in a lab by mixing the strands and procedural annealing with certain temperature programs. To date, various DNA origami objects have been created, varying from two-dimensional structures to three-dimensional structures and plate or brick-shaped structures to arbitrary shape structures such as gridiron and wireframe.<sup>27</sup>

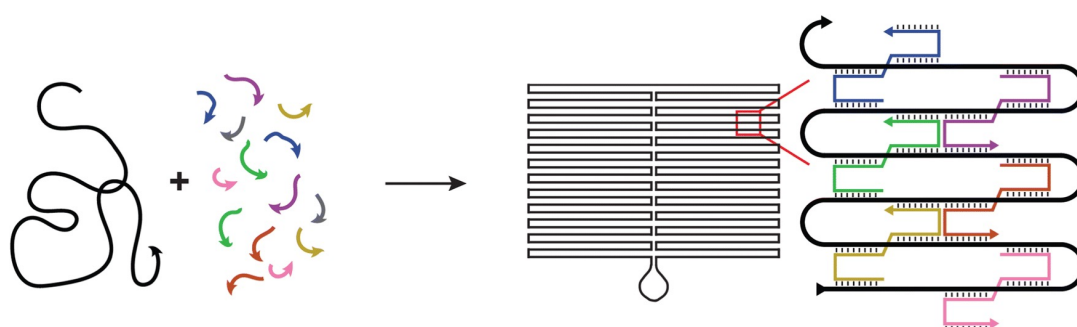


Figure 1-13. Schematic representation of the assembly of DNA origami. A long single-stranded (ss) DNA scaffold (black) is folded up into a dsDNA shape, which is cross-linked by 'staple' strands (colored). The image is taken and slightly modified from reference<sup>28</sup>.

**Dynamic DNA nanotechnology.** Dynamic DNA nanotechnology pertains to the construction of nucleic acid systems with dynamic functions that are related to the overall structure. Dynamic DNA nanotechnology often combines the kinetic DNA interactions detailed above to design strand displacement cascades that can be used in DNA computation and the construction of nanomechanical devices including but not limited to DNA switches, DNA walkers, and other DNA motors.<sup>29</sup>

As shown in the example in Figure 1-14, a DNA walker is a type of DNA nanomachine that extensively applies strand displacement to implement linear motion along a defined track.<sup>30</sup> One popular method is to manually add control strands containing toehold domains, while another strategy is to incorporate with DNase or restriction enzymes to cleave the strands, create unequilibrated hybridization and thus force the walker to move, which can be designed for stochastic walking.<sup>31</sup> The idea for the DNA walker was inspired by natural nanomotors such as dynein and kinesin.

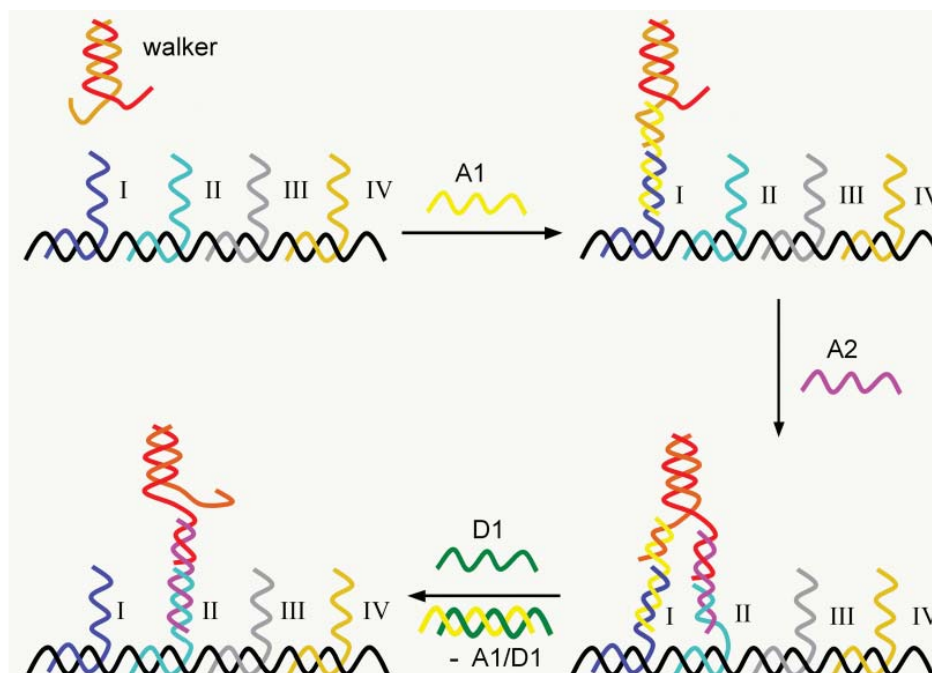


Figure 1-14. Schematic representation of the operation of a DNA walker on a DNA “track” with 4 stations. The image is taken and slightly modified from reference<sup>32</sup>.

Another application of the dynamic DNA nanotechnology is in DNA computing.<sup>33</sup> The cascades of strand displacement reactions can be utilized to perform Boolean logic operations. A molecular computer is a concept based on using inter- or intramolecular interactions as signals to simulate traditional computers with electric signals. This means basic Boolean logic operations like AND, OR, and NOT gates can be achieved through the creation of DNA strand displacement circuits in which hybridization or dehybridization of the certain strands generates different signals like fluorescence, which are related to the formed DNA structures. Recently, a system of logic gates containing 130 DNA strands was implemented as a four-digit circuit that can calculate the square root of integers 0-15.<sup>34</sup> Apart from DNA walkers and DNA computing, various dynamic DNA nanotechnology schemes have been demonstrated and are still evolving.

#### 1.1.4. Bio-hybrid DNA nanodevices.

Artificial nanomaterials might encounter problems when applied to living organisms.<sup>35</sup> As such, it is necessary to consider the biocompatibility, biodegradability, and functional effectiveness of the material in vivo. Interestingly, DNA is not only a biomolecule that can be used as an intermediate to improve the functionality of synthetic materials, but also as a biomaterial to construct artificial nanodevices from



the bottom up with the help of DNA nanotechnology. The advantage of DNA over synthetic materials also lies in its biocompatibility and potential to interact with other biomolecules, for instance, protein-DNA interactions, in which specific DNA-binding domains of the proteins recognize corresponding DNA sequences and bind with the grooves of the DNA helix. Thus, researchers can refine DNA nanotechnology by incorporating DNA-reactive proteins to realize self-assembling bio-hybrid systems with potential biocompatible applications.

Qu et al. described another DNA walker where the motion of the walker is propelled by exonuclease III (Figure 1-15).<sup>36</sup> In their research, exonuclease III digested the hybridized DNA tracks, realizing part of the DNA walker. Subsequently, the released DNA sequence immediately hybridized with the adjacent strand on the track. In this process, the walker is driven forward by the digestion reaction and moves stochastically.

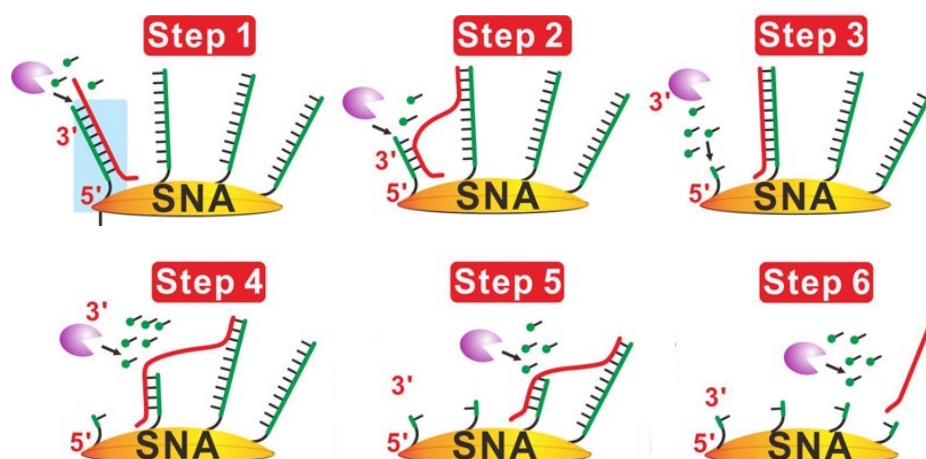


Figure 1-15. Schematic representation of the exonuclease III-driven DNA walker that moves on the SNA surface. The image is taken and slightly modified from reference<sup>36</sup>.

Yehl et al. designed a DNA-based motor that can move along RNA tracks and driven by RNase H (Figure 1-16).<sup>37</sup> RNase H hydrolyses RNA tracks hybridized with DNA that is modified on the surface of the motor. This causes the motor to leave the original position and roll to a nearby location where the RNA tracks are uncleaved. Meanwhile, the spherical motor will travel in a self-avoiding manner.

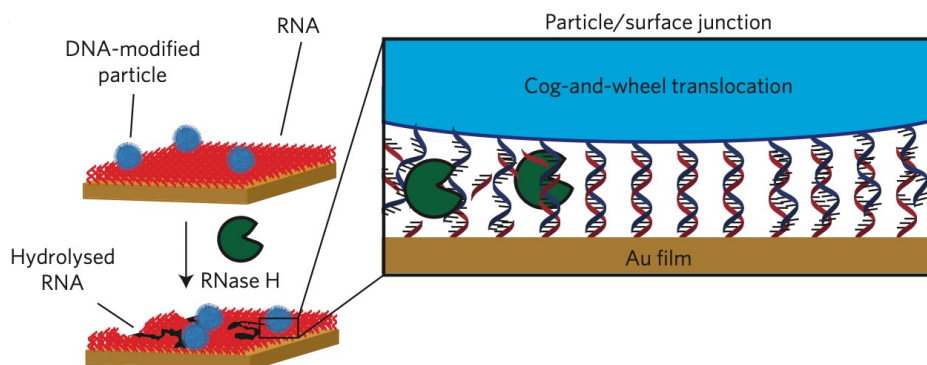


Figure 1-16. Schematic representation of a DNA coated nanoparticle motor driven by RNase H hydrolyzing RNA tracks hybridized with DNA. The image is taken and slightly modified from reference<sup>37</sup>.

### 1.1.5. In silico design and modeling of DNA nanotechnology

As DNA nanotechnology continues to rapidly develop, computer-aided design and molecular dynamics simulation are playing an increasingly important role in DNA nanoengineering prediction and manufacturing. These methods provide simple and quick feedback on the structures of the target DNA assemblies, while also allowing for the simulation of relaxed and equilibrated situations of large DNA nanoarchitectures in silico. This consumes less time and laboratory materials, while also maximizing the efficiency of employing DNA nanotechnology in applications of interest.

Structural DNA nanotechnology has proliferated due to the help of computer-aided design tools like caDNA<sup>38</sup> and Tiamat<sup>39</sup> and simulation methods such as CanDo<sup>40</sup>. Additionally, further developed top-down design methods like DAEDALUS<sup>41</sup> and PERDIX<sup>42</sup> allow users to depict the target systematic design by creating a graphic containing vertices and edges, automatically rendering the corresponding DNA wireframe and generating the sequences of staples based on the specific scaffold. Inexperienced researchers can also get started quickly. Due to these continual developments, it can be expected that more interesting DNA nanoarchitectures will be fabricated in the near future.

Computer-aided design software makes designing DNA nanostructures as simple as stacking building blocks, while the molecular dynamics simulation can predict the most likely shape of the built structure under different conditions and exploit the possible

interaction details by adopting a broad view of the dynamic "evolution" of the system.

Atomistic simulations offer the most detailed representations of DNA and provide the possibility of simulating the full features of DNA to investigate DNA's various detailed interactions, such as those with ligands.<sup>43</sup> However, as the number of atoms increases, the difficulty and time needed to conduct atomistic simulation also increase sharply. This then limits the application of atomistic simulation in large systems, such as DNA origami containing thousands of base pairs.

Coarse-grained (CG) models, using the coarse-grained or simplified representations with a reduced set of degrees of freedom, are able to simulate the complex systems with hundreds of thousands of atoms (such as DNA) in a cost-effective way. A CG model called oxDNA has recently attracted a lot of attention. In this model, each nucleotide is represented as a rigid body that has three interaction sites (Figure 1-17).<sup>44</sup> Each site can interact mutually and with a high degree of anisotropy. The model is in good agreement with experiments within structural and mechanical properties as well as the thermodynamic properties of ss and ds DNA.

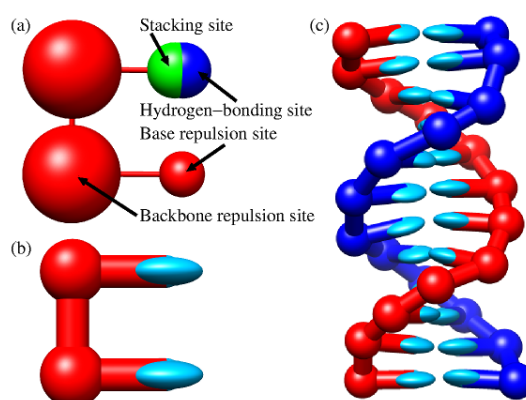


Figure 1-17. Schematic representation of oxDNA model. (a) Model interaction sites. (b) Visualization of the nucleotides in oxDNA. And (c) Representation of a 12-bp dsDNA in oxDNA. The image is taken and slightly modified from reference<sup>45</sup>.

Subsequently, upgraded model oxDNA2 supplements the possibilities of simulating DNA systems in different concentrations of  $\text{Na}^+$  other than the original 0.5 M. It also introduces partial effective charges to simulate the influence of ion condensation on the electrostatic properties of DNA in some specific cases.<sup>46</sup>

To date, the model has been used to generate important information for various research on DNA nanotechnology, such as the above-mentioned toehold-mediated strand displacement, DNA walkers, and large DNA systems represented by DNA

---

origami, all of which have achieved great consistency with experimental data.<sup>47</sup> This model allows researchers to simulate the characteristics of the DNA system of interest prior to starting the laboratory work, thus saving time and costs. Moreover, it creates the possibility of entering deeper mechanical mechanisms of experimental phenomena, which are difficult to explain or explore under current laboratory conditions.

## 1.2. Interlocked DNA nanostructures

Molecules are aggregates containing groups of atoms, where the forces present in them are recognized as chemical bonds (possibly electrostatic, covalent or metallic bonds). Chemistry beyond the scale of molecules is referred to as supramolecular chemistry. This is based on the complex organization of different molecules, ions, or even radicals, which congregate to form higher ordered adducts. Notably, the intermolecular forces within the complexes are significantly weaker than the covalent bonds that connect the atoms intramolecularly. In supramolecular chemistry, those molecules that are mutually recognized and assembled through non-covalent interactions such as electrostatic,  $\pi$ -stacking or hydrophobic effects, usually refer to self-assembly. In addition to the above-mentioned covalent and non-covalent interactions, another type of bonding that is increasingly attracting attention is mechanical bonding.<sup>48</sup> Mechanical bonding does not involve literally connecting different entities "chemically", but rather confining them "mechanically", much like how pieces of rope are tied together. Molecules that contain mechanical bonds are called mechanically interlocked molecules (MIM). Two typical representations of MIM are catenanes consisting of two or more rings interlocking together like keychains, and rotaxane, where one or more rings are threaded within a dumbbell-like subunit, as illustrated in Figure 1-18.<sup>49,50</sup> To construct mechanically interlocked molecules such as these, specific methods that can mutually limit each component and not separate them must be followed. The strategy begins with traditional covalent synthesis or self-assembly. However, the movable components are ultimately detached and aggregated with mechanical bonds rather than chemical bonds. The building strategy for MIM varies from organic synthetic chemistry to the application of DNA nanotechnology.<sup>51</sup> Although MIMs consisting of small molecules benefit from their compact structures, they are hard to synthesize. By employing DNA nanotechnology, the construction of MIMs becomes highly programmable, synthesis-friendly, and easy to assembly, due to DNA's programmability.<sup>52</sup> Its virtue also resides in its biocompatibility, water-solubility, potential to interact with other biomolecules, and easy modification and functionalization with other molecules or nanoparticles.<sup>53</sup> On the other hand, DNA structures are often large and quite flexible. Thus, the main challenge with interlocked DNA molecules is how to maintain the mechanically interlocked subunits without them becoming dissociated or dethreading.

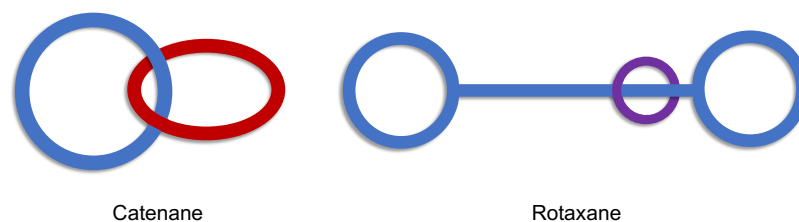


Figure 1-18. Schematic representation of catenane (left) and rotaxane (right).

The widespread creation of interlocking molecules opened up the field of molecular machines, which was largely initiated by Stoddart.<sup>49</sup> The inherent interlocked characteristic of catenanes and rotaxanes provide the opportunities to build up molecular switches and machines, in which the components can move a large amplitude relative to each other and can be controllable or autonomous. The research on this area has continued to grow and was finally recognized with the 2016 Nobel Prize in Chemistry.<sup>49,50</sup> So far, how to design novel molecular machines with practical features has been a continual issue researchers have sought to address.

### 1.2.1. Interlocked molecules and mechanical bonds

The first examples of mechanically interlocked molecules were reported in the 1960s, by Schill for the catenane and Harrison for the rotaxane.<sup>54</sup> Subsequently, the incorporation of theory in supramolecular chemistry has prompted the development of interlocked structure construction, including but not limited to design aspects, synthesis strategies, and production yields. To date, quantitatively synthesis of various interlocked molecules has been possible, which has also contributed to the fabrication of molecular devices that possess interlocked features.<sup>49</sup>

MIMs that present unique mechanical bonds allow the sub-components possessing a certain degree of freedom to move a large amplitude relatively to each other. As the most described examples in research, catenanes and rotaxanes show similar but exclusive properties due to the different ways that they trap their interlocked components.<sup>49,50</sup> Catenanes display unusual topologies which are akin to links in key chains and are difficult to disengage. Contrastingly, rotaxanes are likely to separate because the only obstacle preventing their interlocked components from threading is the relatively bulky stoppers which will deform under certain conditions. Therefore, rotaxanes demand more sophisticated designs in order to be valid entities.

To supplement, IUPAC nomenclature recommended that, the precursors of interlocked catenanes and rotaxanes (in which the subunits are still connected by covalent or

noncovalent interaction) are called pseudocatenanes and pseudorotaxanes, respectively.<sup>55</sup> The ring-like components in the structures are called macrocycle, while the catenanes and rotaxanes containing two or three macrocycles are called [2] or [3]catenane and [2] or [3]rotaxane, respectively. In particular, a rotaxane without any threaded macrocycle is called dumbbell (just stoppers connecting by axle).

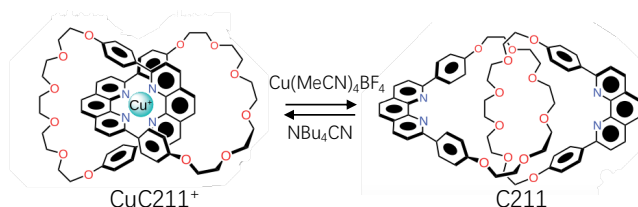


Figure 1-19. Cu(I)-templated synthesis of [2]catenane C211 by removing Cu(I) from the center of a complex  $\text{CuC211}^+$  with  $\text{CN}^-$  ions. The image is taken and slightly modified from reference<sup>56</sup>.

The mechanical bonds in catenanes and rotaxanes significantly alter the properties of interactions that take place between sub-components. Sauvage reported a Cu(I)-templated synthesis of [2]catenane C211 by removing Cu(I) from the center of a complex  $\text{CuC211}^+$  with  $\text{CN}^-$  ions (Figure 1-19).<sup>56</sup> They found a phenomenon of enhanced stability in metals coordinated with topologically linked ligands. They termed this effect as the "catenand effect". The enhanced strength of this kind of non-covalent interaction comes from the loss of degrees of freedom due to the formation of a mechanical bond. Moreover, a mechanical bond can also reduce the kinetic reactivity of the sub-component due to the increased steric hindrance, as exemplified by the slower hydrogenation of an alkene on the thread of a rotaxane compared to an equivalent non-interlocked analogue.<sup>57</sup> Besides, a concentrated effect in the interlocked reactants making a co-localized condition will be present within the interlocked molecules.

## 1.2.2. Interlocked assemblies based on DNA

By incorporating the unique properties of mechanical bonds with DNA nanotechnology, a series of DNA catenane and rotaxane structures have been developed, which demonstrate great potential for the construction of interlocked systems based on DNA.

**DNA rotaxanes.** The first example of dsDNA rotaxanes emerged from the Famulok group in 2010 (Figure 1-20).<sup>58</sup> The design of the dsDNA rotaxane significantly based on the assembly of dsDNA rings (Figure 1-20a). The A-tract segments that can provide

---

the inherent curvature are heavily utilized in the dsDNA rings, as they offer less tension and a relatively higher production yield.<sup>8,59</sup> A macrocycle — a smaller dsDNA ring relative to the stoppers — is firstly incubated to be threaded through the dsDNA axle with a single-stranded gap region that is complementary to a single-stranded part in the macrocycle.<sup>53</sup> Afterwards, two stoppers (also dsDNA rings but relatively larger and extended by three-way junctions) complete "capping" on the ends of the axle through the hybridization of the sticky ends on each part, forming a pseudo-rotaxane structure. The subsequent addition of releasing oligonucleotides (ROs) displaces the macrocycle from the gap of the axle and transforms the pseudo-rotaxane into an interlocked rotaxane. The formation of the structures can be confirmed by gel electrophoresis and atomic force microscopy (AFM). Meanwhile, the macrocycle and the gap on the axle were modified with a fluorophore and a quencher pair. The interlocking status can be validated by a fluorescence spectroscopy in real-time. Interestingly, the threading stability is highly dependent on the sizes of the macrocycle and the stoppers. For dsDNA ring stoppers, dethreading of the macrocycle occurs even if the stoppers are bigger in size than the macrocycle.<sup>58</sup> However, if the ring stoppers are replaced by spherical stoppers that combine two rings with four-way junctions and are much more rigid and bulky, the macrocycle has little possibility to escape (Figure 1-20b). The following research focused on the use of a much stiffer axle that contains two duplexes through paranemic crossover (PX) structures (Figure 1-21a).<sup>60</sup> By combining the PX axle with spherical stoppers, the rotaxane structures with enhanced rigidity are beneficial for application in the nanodevices that efficiently transmit mechanical force.

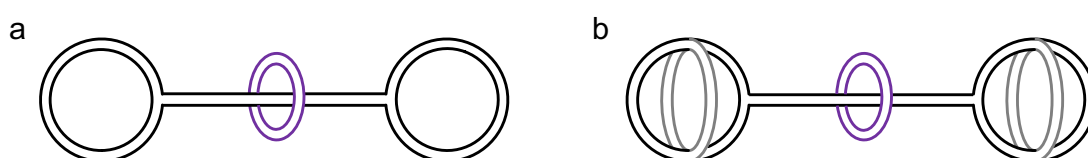


Figure 1-20. Schematic representation of dsDNA rotaxanes. (a) a dsDNA rotaxane with ring stoppers. (b) a dsDNA rotaxane with spherical stoppers.

ROs can liberate the hybridized macrocycle from the axle of rotaxane (pseudo-rotaxane) and make the rotaxane interlocked mainly through toehold-mediated strand displacement. Switching between the pseudo-rotaxane and the interlocked rotaxane can also be achieved by light-induced reconfiguration through the modified sequence with azobenzene derivatives (Figure 1-21b).<sup>61</sup> Light-controlled switching provides additional benefits relating to the elimination of waste generation within the strand displacement approach. Another tool for strand replacement, pcPNA (pseudo-complementary peptide nucleic acid) was developed to improve the hybridization with the target sequence, due to the invasive binding characteristics of pcPNA even without



a toe domain.<sup>62</sup>

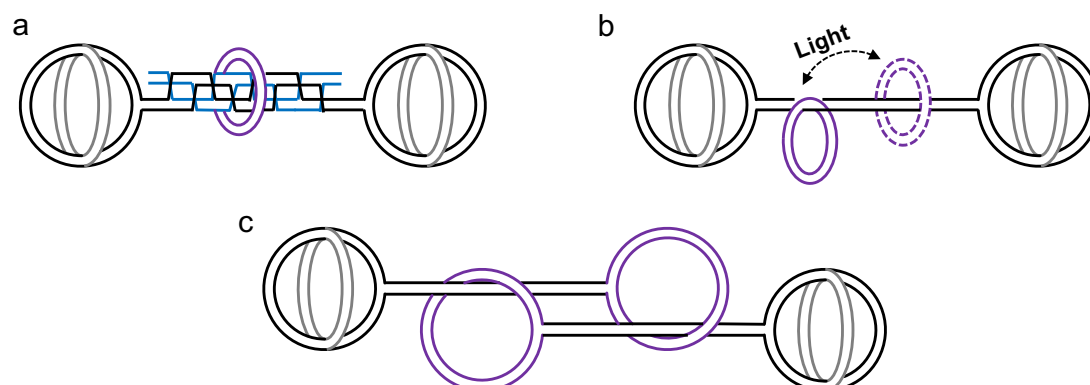


Figure 1-21. Schematic representation of dsDNA rotaxanes. (a) A PX100 rotaxane. (b) A light-controlled rotaxane. (c) A daisy chain rotaxane.

A more complex design is termed a daisy chain rotaxane (DCR), containing two macrocycles connecting with different axles, threaded on the axle of the rival and confining mutually as stoppers (Figure 1-21c).<sup>63</sup> The structure is analogous to macroscopic bearings or muscles, which can be applied in those DNA nanodevices that need to control or guide the linear movement with defined boundaries. However, as the design complexity increases, the formation yield of the interlocking assemblies drops significantly. Therefore, it is recommended to consider it in more complex proposals.

**DNA catenanes.** The ssDNA catenanes have been described previously. Notably, they can be assembled and switching-controlled by adding extra stimuli. This includes changing the pH for forming i-motif and metal ions ( $\text{Hg}^{2+}$  for the T- $\text{Hg}^{2+}$ -T structures,  $\text{K}^+$  for the G-quadruplex formations) or applying the strand displacement strategy.<sup>64,65</sup>

Willner group specializes in synthesizing DNA catenanes that consist of multiple ssDNA rings and possess reconfiguration functions. The most typical example reported a seven-ring interlocked DNA catenane features two bigger ones with five smaller ones (Figure 1-22a).<sup>66</sup> The rings in the structure were formed by ligation with the help of complementary splint ODNs. Simultaneous reconfigurations of different combinations among the rings can be achieved, producing up to 16 different isomers of the catenane. The dynamic switching between the isomers realized by the addition of the corresponding RO/antiRO (an oligonucleotide complementary to the RO, or called fuel/antifuel) through the strand displacement mechanism and can be observed via fluorescence spectroscopy by introducing fluorophore modifications. Other secondary structures such as G-quadruplexes and specific DNA interactions can also

---

be applied on the assemblies of DNA catenanes.<sup>67</sup> Nevertheless, the single-stranded feature of this class of DNA catenanes would be a hindrance for measurement in AFM.

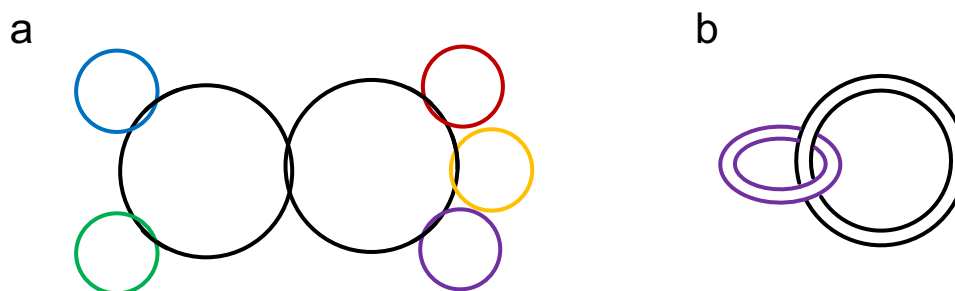


Figure 1-22. Schematic representation of DNA catenanes. (a) A 7-rings ssDNA catenane. (b) A dsDNA catenane.

In contrast, dsDNA catenane structures present robust, homogeneous and well-defined shape characteristics, which can easily be evaluated by using ultrahigh-resolution AFM without the need for external markers (like nanoparticles) to discriminate the different rings in an indistinct pattern. The dsDNA catenanes allow for incorporation with functional DNA groups that require more rigid spatial separations, thus turning them into the scaffolds with controllable switching. In this instance, the on/off switching is performed in a reversible, quantitative way by adding ROs to change the mobility of the rings (Figure 1-22b).<sup>68</sup>

**Single-stranded tile and DNA origami-based interlocked nanostructure.** More solid and rigid interlocked DNA structures have been reported through incorporation with DNA tiles and DNA origami.

Julian Valero reported a DNA rotaxane with single-stranded tile stoppers that consist of 97 oligodeoxynucleotide strands and assembled into a square-shaped structure (Figure 1-23).<sup>69</sup> The single-stranded tile stoppers extend with a sticky end which is used to form a connection with a dsDNA axle. The dimension of the single-stranded tile stoppers should be bulky enough to maintain the threading of the macrocycle with a 14 nm diameter. Additionally, AFM can more easily capture the structures and accurately determine the position of the macrocycle. However, a sufficient salt concentration is necessary to prevent the single-stranded tile structure from disassembling.

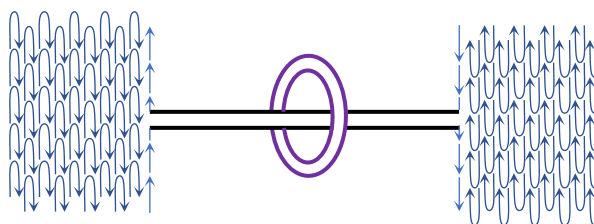


Figure 1-23. Schematic representation of a single-stranded tile-based rotaxane. The arrow indicates the 3'-end of the individual strand.

Jonathan List designed and produced a type of large DNA origami rotaxane nanoarchitectures that can perform long-range movements (Figure 1-24a).<sup>70</sup> In this arrangement, the rotaxanes are based on dumbbell-shaped DNA origami structures, which are attached with a flexible DNA origami hinge structure that is closed by adding closing strands and then detached by the addition of releasing fuel strands, which is called a "clipping" strategy. Two alternative designs present the dimensions of around 140 x 40 nm or 90 x 71 nm, where the axle of each contributes at least 60 nm of length and can reach up to 355 nm. Meanwhile, switching between the mobile and hybridized states in the rotaxanes is achieved by employing a strand displacement strategy and can be observed through TEM and AFM.

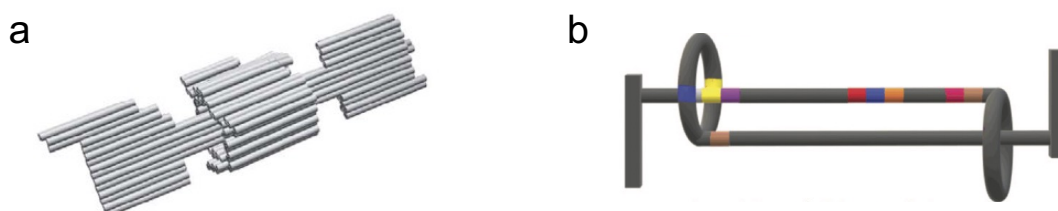


Figure 1-24. Schematic representation of DNA origami-based rotaxanes. (a) A DNA origami rotaxane, and (b) A DNA origami-based daisy chain rotaxane. The images are taken and slightly modified from references<sup>70,71</sup>.

Yu-Chen Chao illustrated a DNA origami-based daisy chain rotaxane structure, which can extend up to 310 nm and contract to 160 nm with the application of a fuel/antifuel strategy (Figure 1-24b).<sup>71</sup> The DNA origami-based daisy chain structure is sufficient bulky that the switching in this system can be measured by TEM. Switching between expanded and contracted configurations provides an opportunity to develop so-called "nanomuscles", which perform repeated mechanical movements on the nanoscale.

---

### 1.2.3. Applications of DNA rotaxane and catenane

Various research applications of interlocked DNA molecules have demonstrated the possible routes towards practicality for these artifacts. Mechanically interlocked molecules allow the interlocked components to move freely within the confinement defined by the stoppers or another ring. This kind of movement enables researchers to construct dynamic nanodevices such as logic gates.

Finn Lohmann reported a [3]rotaxane-based shutter system, in which two DNA macrocycles of different sizes can alternatively or simultaneously bind to the "stations" (gaps) located on the axle (Figure 1-25a).<sup>72</sup> These different binding patterns can be defined as each state in logic gates. Therefore, it may be possible for the system to finally be used to perform logic operations.

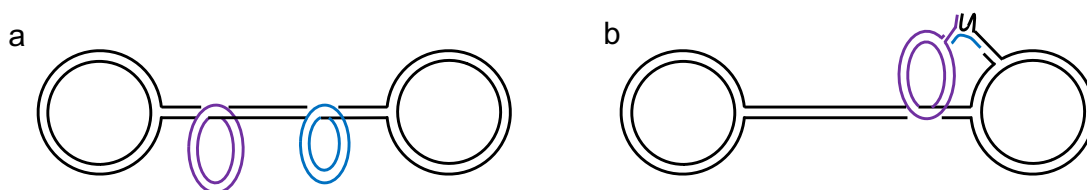


Figure 1-25. Applications of dsDNA rotaxanes. (a) A [3]rotaxane for logic gates, and (b) A rotaxane incorporated with split DNzyme.

The position switching in rotaxane can also allow for the control of interactions such as oxidative catalysis. Mathias Centola exploited a split DNzyme-based nanostructure in which a dsDNA rotaxane was applied as a scaffold to carry the different domains of the DNzyme on the macrocycle and one of the stoppers (Figure 1-25b).<sup>73</sup> The re-integration of the DNzyme can be controlled through the position switching of the macrocycle trapped within the rotaxane. Moreover, the whole system can be switched on and off in multiple cycles making it advantageous relative to other systems that are limited in their reversibility.

Apart from strand displacement, the switching in interlocked molecules also responds to temperature change. Yinzhou Ma demonstrated a thermal-responsive DNA joint based on [2]catenane, which allowed for reversible switching between the hybridized and interlocked states in response to different temperatures (Figure 1-26).<sup>74</sup> The sensitive temperature range can be fine-tuned by modifying the length or the sequence of the hybridized region of the catenane.

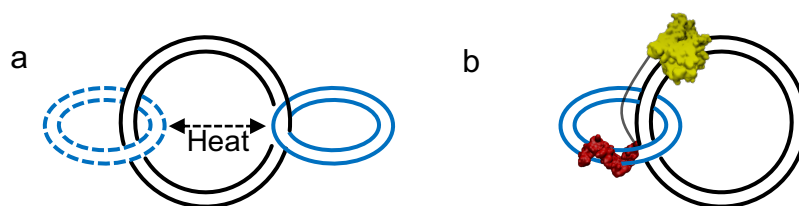


Figure 1-26. Applications of dsDNA catenanes. (a) A thermal-responsive catenane joint, and (b) A dsDNA catenane nanoengine powered by a T7RNAP-zif fusion protein.

An enzyme-driven DNA motor was reported by Julian Valero, which incorporates a T7RNAP as its engine (Figure 1-26b).<sup>75</sup> Two dsDNA rings are interlocked to form a catenane structure. Next, the polymerase binds with one ring of the catenane through a zinc-finger subunit fused to the polymerase and recognizes the other ring as a template for transcription while constantly rotating the ring unidirectionally. The system produced long, repetitive RNA transcripts that can be exploited to guide the motion of the motor along a predefined ssDNA track.

In summary, the research on interlocked DNA nanoarchitectures is of interest in DNA nanotechnology, due to their highly integrated structures and intrinsic dynamics. They have the potential to become vessels for the development of artificial molecular machines to address the Brownian motion dominated in the molecular scale, cooperate with other biomolecules to generate linear (rotaxane) and rotary (catenane) motions, and continuously produce RNA with the help of RNA polymerase.

---

## 1.3. DNA nanotechnology and synthetic biology

Self-assembly in the artificial nanostructure construction is only one aspect of DNA properties. As the carrier of genetic information, DNA can inherently interact with proteins within a network. Such proteins play essential roles in almost all biological processes in an organism, such as DNA replication and transcription. In recent decades, synthetic biology has come to the fore as an emerging field of science and attracted increasing attention, using engineering approaches to design and construct genetic circuits with novel functions.<sup>76,77</sup> In this context, DNA nanotechnology can be retrofitted with synthetic biology to create unique biological systems that do not appear in nature.

### 1.3.1. Synthetic biology

Synthetic biology is an interdisciplinary area, described as "designing and constructing biological modules, biological systems, and biological machines or, re-design of existing biological systems for useful purposes".<sup>78</sup> It draws on and combines knowledge and methods from different disciplines, such as systems biology, bioinformatics, biophysics, and bio-nanotechnology. To date, it has been implemented in a variety of industries, including agriculture, energy, environment, and medicine.<sup>79</sup>

Synthetic biology draws on the idea of engineering approaches to create biological systems with new features by combining the highly programmable and modular biological components. There are two different levels of schemes that are geared towards this aim: top-down strategies and bottom-up strategies. Top-down strategies modify the living cell with new functions through genetic engineering, while bottom-up strategies construct new genetic circuits from scratch by combining modular biomolecular components, ultimately leading to the creation of an "artificial cell".<sup>80</sup>

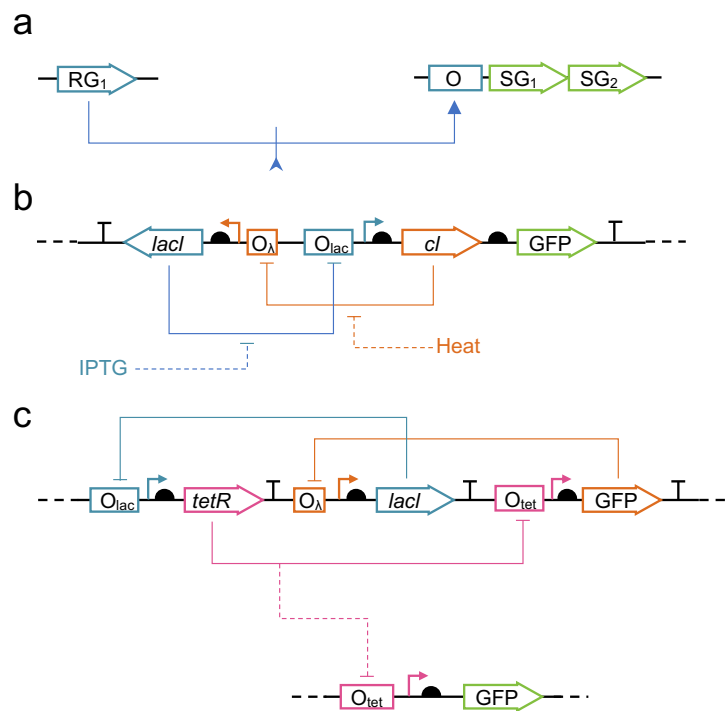


Figure 1-27. Schematic representation of genetic circuits. (a) A bistable circuit containing a transcriptional repressor gene and operators. (b) A genetic toggle switch containing two repressors that can inhibit one another. (c) A genetic oscillator containing three regulator genes positioned in a daisy chain arrangement. Abbreviations: O, operator; GFP, green fluorescent protein; RG, repressor gene; SG, structural gene. The arrows represent the transcriptional directions. The annotations follow the SBOL visual standard (sbolstandard.org). The image is taken and slightly modified from reference<sup>81</sup>.

The emergence of synthetic biology dates back to 1961, when Jacob and Monod first proposed their famous theory of the operon model of gene regulation (Figure 1-27a).<sup>82</sup> In 1978, the discovery of restriction enzymes allowed for the easy reconstruction of DNA and analysis of new gene combinations.<sup>83</sup> By the mid-1990s, further developments in DNA sequencing expanded the catalog of biological components available to scientists. In 2000, the publication of two papers in the journal *Nature* reported the first synthetic genetic circuits, a toggle switch<sup>84</sup> (Figure 1-27b) and a repressilator circuit<sup>85</sup> (Figure 1-27c). Both the switch and the repressilator were composed of a set of similar biological components, such as promoters, and used GFP expression as a reporter to monitor the behavior of the genetic circuit, thus demonstrating the modular characteristic of synthetic circuit construction. The scale and scope of synthetic biology have expanded dramatically over the past two decades. iGEM [www.igem.org] and Biobrick [http://hdl.handle.net/1721.1/21168] have played

---

an important role in attracting the interest of researchers, and at the same time, the complexity and robustness of synthetic genetic circuit construction have followed an upward trend.<sup>86</sup>

### 1.3.2. Artificial regulatory circuits

With the development of synthetic biology, precise and programmable construction of the genetic circuits has become increasingly important.<sup>87</sup> The control of gene expression will help to optimize the production pathway of biopharmaceuticals, while also improving the yield and preventing overload and toxicity to the host cell.<sup>88</sup> Gene expression involves many intermediate steps, all of which can be regulated (in principle). From DNA to protein, the entire process can be regulated at different levels: transcriptional (when DNA is transcribed to RNA), post-transcriptional (when RNA is processed into mRNA), translational (when RNA is translated into a protein), and post-translational (after a protein is made). For an artificial gene expression system that expects to maximize yield and reduce redundancy, it is desirable to control expression at the transcriptional level. This is because only transcriptional control can ensure that the process will not produce superfluous intermediates.<sup>88</sup>

Transcription regulators, such as transcription factors, are a group of proteins that are associated with the level of gene transcription during transcription initiation.<sup>88</sup> They have DNA-binding domains and are able to recognize the special DNA sequences, thus activating (activator) or repressing (repressor) transcription. However, transcription regulators are not unique to each gene transcription being transcribed and they may be involved in a variety of gene expression activities.<sup>88</sup> For most of the time, transcription regulators also function in collaboration, to ensure that they can synergistically control transcription and have it occur at the right time and in the right amount.

In particular, repressor proteins have been extensively used to construct genetic circuits including transcriptional downregulation. A well-known example is the "repressilator".<sup>85</sup> In 2000, Elowitz and Leibler constructed an artificial genetic circuit in *E. coli* containing a negative feedback loop for the expression of three regulatory proteins (repressors). This was executed as a temporal oscillator, also known as a repressilator. The circuit periodically synthesizes green fluorescent protein (GFP) and allows for its expression behavior to be analyzed through its fluorescence signal. These results suggest that it is possible to design and synthesize artificial genetic circuits by reconstituting naturally occurring biological components, such as DNA promoter sequences and repressor proteins.



Compared with protein regulators, nucleic acid-based regulatory elements offer the opportunity to regulate gene expression through base pairing, which enjoys the benefits of being highly programmable, specific, and predictable.<sup>89</sup>

Riboregulators (RNA-based regulators) can be incorporated into genetic circuits and regulate the gene expression at the post-transcriptional level. In 2004, Collins et al. demonstrated an RNA-based regulatory system that uses ncRNA (non-coding RNA) to activate or silence gene expression by hybridizing the RBS (ribosome binding site) region of the mRNA (Figure 1-28).<sup>90</sup> This artificial riboregulator exploits the highly specific interactions between RNAs through base pairing and acts as a modular biological component incorporated into the synthetic genetic network to control the gene expression of interest at the RNA level.

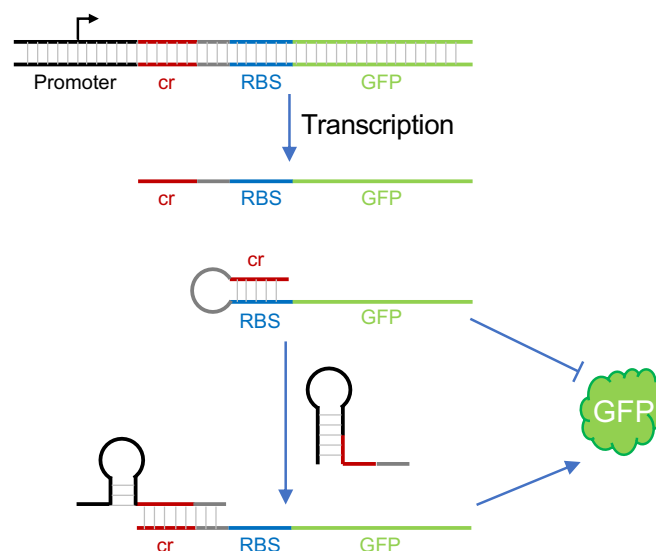


Figure 1-28. A riboregulator enabling post-transcriptional control of GFP expression. Abbreviations: cr, cis-repressed sequence; RBS, ribosome binding site; GFP, green fluorescence protein. The image is taken and slightly modified from reference<sup>90</sup>.

Similarly, RNA-centric regulation systems have been developed. Other examples of these include a de-novo-designed toehold switch<sup>91</sup> and the STARs (small transcriptional activating RNAs)<sup>92</sup>. Additionally, various artificial regulatory strategies have been reported and are still rapidly emerging.<sup>81</sup>

---

### 1.3.3. DNA as a component of synthetic transcriptional regulation

Typically, DNA is usually the target of regulatory components, such as the transcription regulators detailed above. In addition to coding genes, some non-coding sequences of DNA are also necessary and significant, such as cis-regulatory elements (CREs), which are the DNA sequences located close to related gene sequences and regulate the transcription of neighboring genes.<sup>93</sup> These sequences always contain the binding regions for transcription regulators or other molecules associated with the transcriptional regulation. The most well-recognized CREs include promoters, enhancers and silencers. For instance, promoters are DNA sequences that are usually located upstream of the adjacent gene and can be recognized by RNA polymerase and initiate transcription. Promoters typically contain the binding sites for RNA polymerase and TATA box sequences<sup>94</sup> that have lower melting points and are therefore preferable for initiation. Promoters can cooperate with other regulatory regions (such as enhancers, silencers) to control the level of gene transcription.

DNA can also be used as artificial regulatory components, in analog to transcription regulators. DNA-based regulatory components can combine the merits of transcription regulators which control gene expression during transcription initiation and riboregulators that precisely control the gene expression through programmable base pairing.

Pioneering efforts to construct regulatory circuits using DNA-based regulatory components largely focused on manipulating the interactions between RNAP, especially T7RNAP and related promoter sequences to enable more favorable binding of RNAP to DNA templates, by complementing an incomplete promoter region (Figure 1-29).<sup>95-97</sup> Another strategy, albeit a more complicated one, is to make the upstream region of the promoter sequence single-stranded and have it serve as an anchor for its complementary sequence-RNAP fusion, to activate the transcription upon binding.<sup>98</sup>

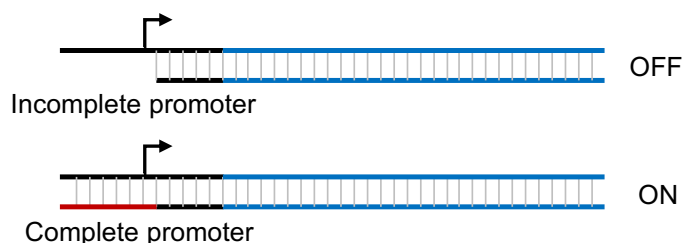


Figure 1-29. Brief schematic representation of DNA-based regulatory mechanism.

In this case, DNA nanotechnology (or nucleic acid nanotechnology more broadly) can be effectively integrated within genetic networks. It has been developed and refined for decades and offers the advantages of predictable self-assembly and programmable toehold mediated strand displacement, while also allowing for the construction of static and dynamic two- or three-dimensional nanostructures with arbitrary geometries. By incorporating these impressive features of nucleic acid nanotechnology, synthetic biology is poised to expand significantly in scope and scale. Even so, there are several challenges that remain to be considered:<sup>99</sup> (1) DNA nanotechnology focuses primarily on hybridizations between DNA strands and ssDNA sequences are always used to initiate reactions. ssDNA is more susceptible to damage than dsDNA because the chemically reactive groups in its nucleobases are more exposed. (2) Delicate annealing programs are necessary to assemble some DNA nanostructures. (3) The intracellular environment is completely different from the conditions in the buffer solution. (4) Artificial DNA nanostructures cannot be easily fabricated by the cells themselves, such that they cannot be replicated on a large scale.

Cell-free approaches to synthetic biology have attracted much attention, both from academia and industry.<sup>100</sup> Such approaches allow for the design of complex synthetic genetic circuits but without having to deal with the constraints of the cellular environment. Thus, by utilizing cell-free approaches, artificial DNA nanostructures can be more easily integrated into the design of synthetic genetic circuits.

---

## 1.4. DNA and transcription

Transcription is a biological process that is carried out in the early stage of gene expression. In this process, DNA's genetic information is transcribed into RNA copies, namely RNA transcripts. RNA polymerase (RNAP) is the main enzyme involved in this process, which reads the DNA template progressively and uses NTPs as substrates to synthesize the RNA transcripts. Transcription can be divided into three phases: initiation, elongation, and termination. Initiation takes place during the beginning of transcription, where RNAP recognizes and binds to a specific DNA sequence, namely the promoter that is located upstream of the gene. Elongation is the process by which RNAP reads the DNA template and produces the RNA product. Subsequently, final termination happens when RNAP encounters another specific DNA sequence, called the terminator. At this point, transcription stops, and the RNA transcripts are released. In living organisms, transcription is not completely spontaneous. Instead, it has a different regulatory scheme for each gene and occurs only when needed. Thus, the study of transcriptional details also facilitates a greater understanding of transcriptional regulation.

### 1.4.1. T7 RNA polymerase-DNA interactions

A well-studied and extensively used polymerase is T7 RNA polymerase or T7RNAP. Its relative molecular mass is 99K.<sup>101</sup> T7RNAP can recognize specific dsDNA sequences as the promoter to initialize the transcription, trigger the elongation process, and perform RNA synthesis. Due to its smaller size and highly controllable manners, T7 RNAP has become a good candidate for collaboration with DNA nanostructures. The properties of T7 RNAP-DNA interactions provide the basis for designing concise transcriptional circuits and constructing T7-RNAP-DNA hybrid nanodevices.

**T7 promoter.** As shown in Figure 1-30, the T7 promoter is made up of two complementary strands: a template strand (non-coding strand) that applies as the template of RNA synthesis, and a non-template strand (coding strand) that displays the same sequence with synthesized RNA (U instead of T). It has a highly conserved sequence within the class II and III T7RNAP promoter sequences, from the position -17 to +2 which is relative to the first base (+1) of template for RNA synthesis.<sup>101</sup> When this area of research was in its infancy, with the help of complementary footprinting experiments, studies on the interactions between T7RNAP and the corresponding promoter showed that the base pairs of both template and non-template strands in the promoter (from position -21 to -2) are protected by the polymerase.<sup>102</sup> The covered

sequence consists of three functional determinants. The sequence of position -17 to -12 in the upstream region determines a recognition site for polymerase, which is mostly located on the template strand and is not a requirement for the presence of a double-stranded feature.<sup>103</sup> Most importantly, in preparation for transcription initiation, a section of the promoter sequence close to the polymerase is required to be melted in the formation of the "open" complex (position -11, +2).<sup>104</sup> Among them, the sequence from position -6 to +2 in minimal is melted in this bubble structure, where the template strand is protected by the T7RNAP and the non-template strand is exposed to the environment and allowed to be digested by endonucleases.<sup>105</sup> It is necessary for the sequence adjacent to the unwinding sequence (most probably the sequence from position -11 to -7) to keep a double-stranded helix to constitute a viable open complex structure, which is also required for recognition by the polymerase.<sup>105</sup>

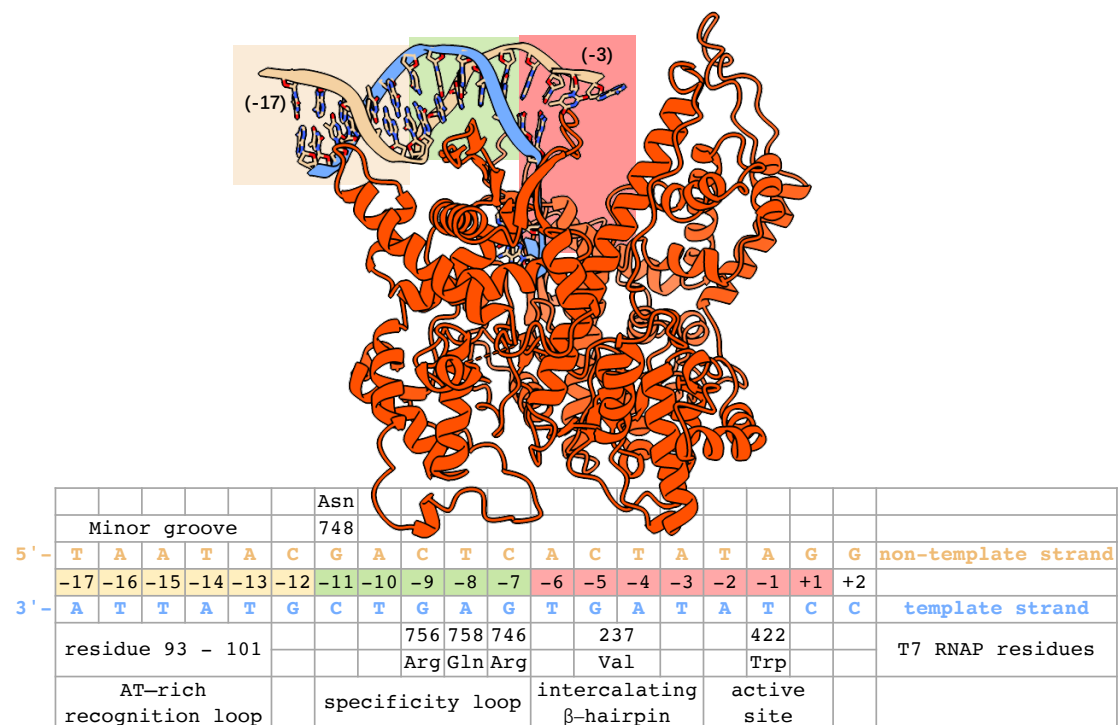


Figure 1-30. Schematic representation and interactions of T7RNAP-promoter complex. The sequences with green and yellow background are two binding sites of T7RNAP-promoter complex, and the sequence with red background is the unwinding region of T7RNAP-promoter complex. The image is based on PDB ID: 1CEZ and prepared with the ChimeraX molecular visualization program. The table below lists the residues or domains of T7RNAP that interact with corresponding nucleobases during transcription initiation.

---

Contemporary crystallography research into T7RNAP with a blunt-ended promoter DNA (-17, -1) further confirmed the detailed interaction among this binary complex.<sup>106</sup> Three major interacting sections of T7RNAP bind with the promoter sequence and stabilize the open complex. (1) T7RNAP inserts a flexible surface loop or AT-rich recognition loop (residues 93 to 101) into the minor groove formed by the base pairs from position -17 to -13 of the promoter sequence. This AT-rich region of its inherent flexibility can form a wider and shallower minor groove than the common B-form DNA helix due to the distortion caused by the flexible surface loop of the polymerase. (2) The residues 746, 756, and 758 of T7RNAP interact with G-7, G-9, and A-8 of the template strand in the major groove of the T7 promoter, while the residue 748 hydrogen bonds G-11 of the non-template strand interact with them directly through water-mediated hydrogen bonding. These interactions between both strands in the helix play the essential roles in recognition by the polymerase. (3) A  $\beta$ -hairpin loop of T7RNAP intercalates into the interval between base pairs -4 and -5, manipulating the melting of the promoter sequence. This loop containing residue 237 parks on the base pair -5 to maintain the upstream bubble structure and provides an additional binding site with the melted template strand that is protected by the polymerase during transcription. (4) The residue 422 of T7RNAP stacks on the -1 base of template strand inducing a sharp bend and directs to the +1 base to initiate RNA synthesis.

**Fast elongation.** When the T7RNAP escapes from the above initiation complex (IC) with the T7 promoter, a large conformational change will occur as the promoter recognition loops break up the interaction with the promoter sequence and move away.<sup>107</sup> In particular, the difficulty of releasing of T7RNAP from IC varies across the different types of templates that are on common linear double helix DNA. Although the IC is less stable ( $t_{1/2} < 1$  min), if it is on a supercoiled template, the IC will show a high stability that is much more difficult to escape ( $t_{1/2} > 14$  min).<sup>108</sup> An elongation complex further forms above the binary system to produce the RNA transcript. The elongation complex is composed of an approximately 10 bp transcription bubble with an 8 bp DNA-RNA hybrid. During elongation, the complex moves powered by a Brownian ratchet mechanism, where the elongation complex reversibly slides around the 3'-end of the RNA until the binding of a next complementary NTP in the active site facilitates the polymerase to transcribe the downstream base.<sup>109</sup> The approximate rate of synthesizing transcripts in elongation is 200–300 nt per second in lengths of thousands of nucleotides.<sup>101</sup> Compared to the fast elongation process, the initiation complex formation and release are much slower and should be the rate-limiting step in transcription. Previous research presented a high energy barrier that is  $26 \pm 3$  kcal/mol for the initiation step of transcription on the fully double-stranded template.<sup>110</sup>

**T7 terminators.** T7RNAP recognizes two types of specific sequences to pause or terminate the elongation process in transcription (Figure 1-31).<sup>101</sup> The class I terminator appears in the late downstream of T7 genome, which is significant to arrest and terminate the transcription process. It is composed of a GC-rich sequence that can transcribe to RNA transcripts with the potential to form a hairpin structure after following a series of U bases.<sup>101</sup> After the hairpin configuration is formed, the interaction between T7RNAP and RNA is evaluated to disrupt 8 to 14 nt away from the 3'-end of the RNA, while a portion of the DNA-RNA hybrid is disrupted as well. The association of the RNA transcript and elongation complex is weakened by the above disruption and further reduced by the U-rich downstream incorporating in a run of less stable A-U base pairs, resulting in the dehybridization of the RNA-DNA template and termination of transcription.

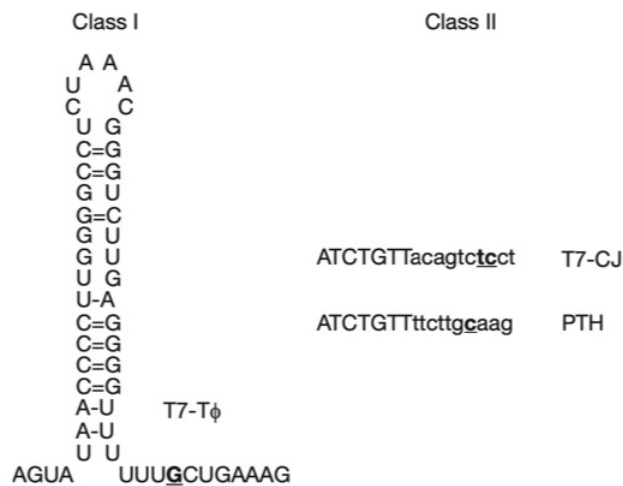


Figure 1-31. Sequences of two types of terminators: Class I terminator (left) and Class II terminator (right). The image is taken from reference<sup>101</sup>.

Another type of T7 terminator was found in the human parathyroid hormone gene, namely, class II,<sup>111</sup> which has a highly conserved sequence ATCTGTT sequence in the non-template strand from 5' to 3'-end. It was found that the class II sequence located at the concatemer junction (without the last T) of the T7 DNA functions as a pause site, while additional T bases downstream in the conserved sequence would provide the considerable termination effect. In contrast with the class I terminator, the class II terminator does not appear in any apparent secondary structure of RNA. The class I and class II terminators display completely different mechanisms when instigating the termination process since the T7RNAP with mutations that consistently stops at the class I terminator ignores the presence of the class II terminator. Correspondingly, there is a gap in the termination efficiency of class II terminator and class I terminator,

---

which is 55% and 80%, respectively.<sup>112</sup> However, several class II terminator sequences set up in tandem will dramatically enhance the termination efficiency.

**Bypassing Gaps in the DNA template.** Based on the studies detailed above, the fully complementary double-stranded helix of promoter sequence is not necessary to initialize the transcription. For the upstream binding site from -17 to -12, only the template strand is needed, such that the presence of a full double-stranded helix is not a requirement.<sup>103</sup> For the binding site in the open complex in initiation from position -11 to -7, both strands are essential for the recognition of T7RNAP. This is because the interaction sites of this binary are distributed across both the template and non-template bases.<sup>105</sup> Meanwhile, for the non-template strand, in the melting region of open complex, deletion of the non-template strand until position -4 upstream cannot affect the binding event.<sup>113</sup> The binding affinity weakens when the non-template strand is removed to position -6, even though the promoter-specific initiation still runs at a high rate. In addition, the absence of the non-template strand from position +1 to +5 has no impact on T7RNAP recognition with the promoter.<sup>110</sup> And further removal of the message region of the non-template strand has little effect on subsequent elongation and RNA synthesis. The template strand is the most important in transcription, as it provides the most, if not all, of the recognition sites for the polymerase, as well as the template for coding and the carrier for RNA transcript in the certain step in elongation. However, a single nucleotide break or multiple nucleotide gap in the template strand cannot completely stop transcription from proceeding.<sup>114</sup> Studies on the effects of single-stranded breaks on the template strand found that T7RNAP can efficiently bypass the one nucleotide vacancy and perform further elongation. This generates accurately transcribed RNA downstream, except the one nucleotide that was shortened.<sup>114</sup> Meanwhile, the template strand containing 1 to 5 nucleotides gap can be still efficiently transcribed, although, with a 10 nt gap, the efficiency of the transcription dramatically dropped down to a low level of around 10% compared to if there were no gap in the template (Figure 1-32).<sup>115</sup> The resulting transcripts still contain the rest of the information of the template strand downstream, most likely due to the assistance of the complete non-template strand.



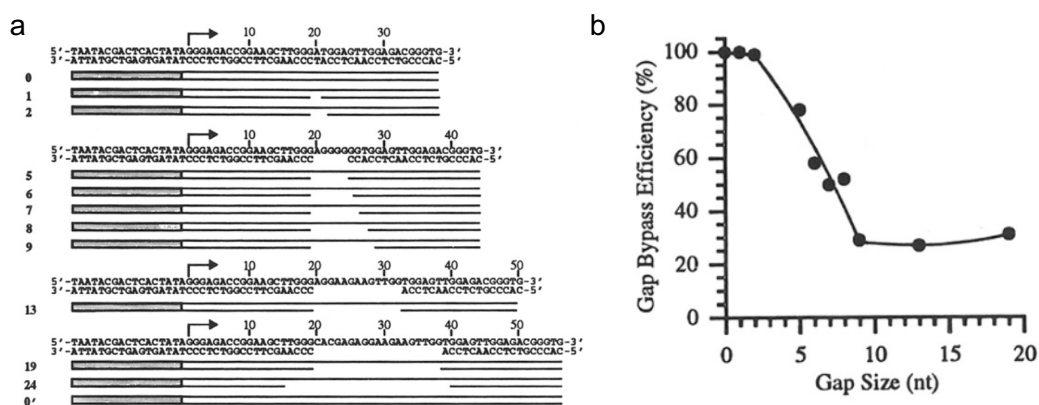


Figure 1-32. (a) Gaps in the template strand. (b) Corresponding bypass efficiency. The image is taken from reference<sup>115</sup>.

**DMSO effects.** Dimethyl sulfoxide (DMSO) is extensively utilized in the research of cell biology and pharmacology as a "universal" solvent. Previous reports have found that DMSO performs an "acceleration" function in the context of transcription.<sup>116</sup> It was also noted that low concentrations of DMSO can enhance the transcription rate of polymerase and increase the efficiency of RNA synthesis. The elevated activity of RNA polymerase is most likely related to the altered polymerase structure in the presence of DMSO (lower than 20%) in the aqueous solution. This discovery not only shed the light on the alternative structure and running mechanism of RNA polymerase in the DMSO-mixed solvent but also provided a powerful tool for the application of RNA polymerase-based strategies.

To sum up, all the elements of the T7RNAP-DNA interaction explored above have the potential to regulate T7RNAP transcription and may be used to develop novel T7RNAP-DNA hybrid nanomachines in DNA nanotechnology and to establish artificial genetic networks in synthetic biology, or to collaborate on application that involve both fields.

---

## 2. Aim of this project

Rotaxanes are dumbbell-shaped structures that allow for the inherent linear motion of mechanically interlocked macrocycles within their confinement.<sup>117</sup> They have great potential for constructing linear nanodevices that generate linear motion by altering the relative spacing between the subunits in response to additional stimuli. By employing DNA nanotechnology, the construction of MIMs become highly programmable and synthesis-friendly, due to DNA's programmable feature.<sup>52</sup> DNA shows another advantage in that it is able to interact with proteins, especially motor-like enzymes, such as RNA polymerase, which can be used to generate directional forces. RNA polymerase-DNA hybrids make it possible to construct biohybrid artificial nanodevices that can perform linear motion automatically and repetitively. Such self-controlling and self-moving DNA nanostructure with biohybrid features are perfect platforms for constructing actuators. Moreover, it has the potential to develop delivery systems and self-regulating RNA production automatons at the molecular scale

In this thesis, T7 RNA polymerase (T7RNAP) and DNA rotaxane are combined to develop an automatic linear nanoactuator for the following purposes: 1) transferring the linear motion of T7RNAP along the DNA track to the periodic translational displacement of macrocycle threading in rotaxane; 2) self-controlled transcription, as presented in Figure 2-1.

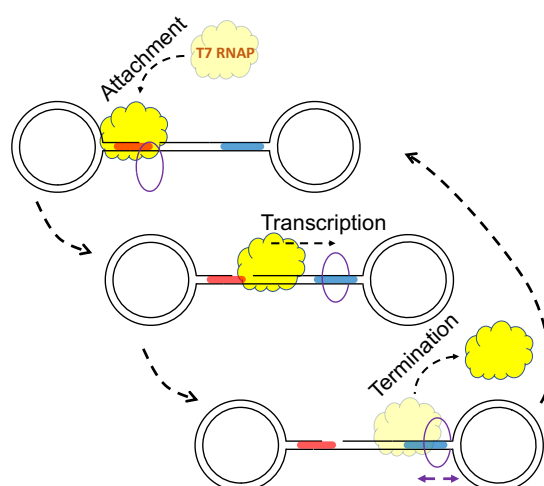


Figure 2-1. Schematic representation of the self-regulating DNA rotaxane actuator.

The brief framework of the "results" is listed below.

In chapter 3.1, the design of this molecular linear actuator is elucidated in the beginning. An interlocked macrocycle-reconstructed promoter is proposed to control the

transcription of T7RNAP. Gel electrophoresis and atomic force microscopy are used to confirm the effective assembly of the actuator. Subsequently, the effect of the macrocycle-mediated promoter on the transcriptional behavior of the actuator is investigated by molecular beacon (MB) fluorescence experiments. Moreover, an on/off switch of transcription controlled by external releasing ODN is also evaluated.

To understand the mechanism of the rotaxane actuator, macrocycle rehybridization after termination, macrocycle releasing by T7RNAP, the direction of macrocycle movement, and the macrocycle dethreading in the rotaxane were sequentially investigated. Fluorescence-quenching methods are utilized to determine the situation of the macrocycle and reveal the detailed operation mechanism of this DNA rotaxane actuator.

Supplement modelling simulations are performed to estimate the macrocycle dethreading in this rotaxane system. The rotaxane with a ss-macrocycle is first simulated to test the dynamic stability of the rotaxane actuator. Further simulations are used to simulate the situation of the macrocycle during transcription through exerting constant forces on it. Experimental explanations related to the macrocycle dethreading are complementary to the simulations.

In chapter 3.2, an optimized rotaxane system with a spherical stopper is designed to improve the dynamic stability compared to the original design. Experimentally, the optimized rotaxane is assembled and characterized. Two rotaxane systems are assessed and compared in terms of their transcriptional behaviors. Modelling simulations confirm that the optimized rotaxane with a spherical stopper can effectively prevent the macrocycle from dethreading.

In chapter 3.3, the properties of the macrocycle-mediated promoter are investigated by comparing the transcription performance of dumbbell/rotaxane systems with activation strands (macrocycle, linear template for macrocycle and promoter gap ODN).

---

## 3. Results

### 3.1. DNA rotaxane linear actuator

In this chapter, a molecular linear actuator is demonstrated, which is composed of T7RNAP and a DNA rotaxane. The rotaxane operates between two states: a static state where a threading macrocycle is hybridized with the axle; and a dynamic state in which the macrocycle is interlocked and can move freely within the dumbbell structure of rotaxane. The driving force of system comes from transcription by T7RNAP. T7RNAP can only initiate the transcription when the rotaxane is in the static state. Once transcription starts, T7RNAP can convert the system from static state to dynamic state. In this process, T7RNAP pushes the macrocycle away from the original binding site in the promoter sequence and confines it in the direction of transcription, as well as deciding the range of motion of macrocycle between the polymerase and the stopper connecting to the downstream part of the axle. During the elongation of transcription, the polymerase moves along the axle, while the range that macrocycle can move become gradually smaller, leading to an overall displacement of the macrocycle from the original anchoring region towards terminator sequences of T7RNAP in the axle downstream. The chemical energy released by NTP hydrolysis during transcription powers the entire process. The transcription cycle terminates at the end of the axle, where located two successive class II terminator sequences of T7RNAP, causing the release of T7RNAP from DNA template. Meanwhile, the macrocycle is free to move along the axle and to rebind to the promoter region, providing the possibility that T7RNAP can bind to the promoter and initiate a new transcription cycle. This results in an autonomous translational movement of the macrocycle along the axle, which actuates sequentially and again without the need for further intervention.

#### 3.1.1. Design of the rotaxane actuator

The rotaxane actuator consists of three main parts: two bulky stoppers, a ssDNA macrocycle and a dsDNA axle containing a 12 nt single-stranded region. The stoppers are 168 bp dsDNA rings, which is already described in the previous works.<sup>53,58</sup> The macrocycle is a 40 nt ssDNA ring, which is spatially smaller compared to bulky stoppers that can prevent it dethreading from the axle. A 20-nt reporter ODN can hybridize to the macrocycle if necessary, providing reporter groups such as a biotin or a fluorophore modification (Supporting Table 1). The macrocycle can also be blocked

by T7RNAP (~ 6 nm in diameter estimating from the crystal structure of T7RNAP, PDB: 1CEZ) due to its smaller dimensions (Figure 3-1a).

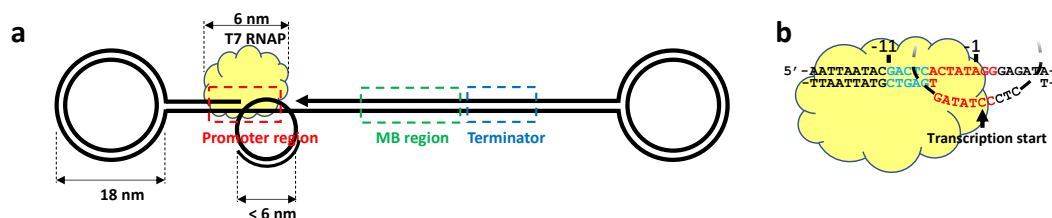


Figure 3-1. Design of the DNA rotaxane-based linear actuator. (a) Schematic representation of the rotaxane actuator with dimensional parameters of the ring stopper, the macrocycle, and the T7RNAP. MB (molecular beacon) region: a coding sequence for producing RNA that can bind with molecular beacon. (b) Schematic representation of the structure of the macrocycle-reconstituted promoter for T7RNAP. Red: a part of promoter sequence that would be unwound during transcription initiation. Blue: a double-stranded binding site for T7RNAP. The non-template strand is on top, and the template strand is on the bottom. Arrow: starting point of the transcription.

The dsDNA axle contains three functional sections: a promoter sequence and two terminator (class II) sequences<sup>112</sup> for T7RNAP as well as a coding region that is complementary to a molecular beacon (MB) allowing fluorescence monitoring of RNA transcripts produced during transcription. When a transcription cycle starts, a T7RNAP will recognize and bind to the promoter region on the axle, causing the formation of an transcription bubble (Figure 3-1b).<sup>105</sup> As shown in Figure 3-1b, there are two functional parts in this transcription bubble: an essential binding region for T7RNAP (the bases from position -7 to -11) and an unwinding region to prepare transcription (the bases from position -6 to +2). The axle is designed to be double-stranded except that the template strand of the promoter region contains a 12 nt single-stranded gap (the bases from position -5 to +7). The threaded macrocycle contains the complementary sequence that binds to this gap (the bases from position -5 to +5) to construct a macrocycle-mediated promoter. In this structure, the gap is partially filled (10 bp, less than on helical turn) by its complementary sequence in the macrocycle, which enables that T7RNAP has the enough capability to initiate transcription and release the macrocycle from this promoter gap. Crucially, the downstream portion of the gap region is involved in the formation of transcriptional bubble to ensure that once released, the macrocycle tends to move toward the downstream axle. (Figure 3-1b).

Therefore, this design ensures that: i) the hybridization of macrocycle to the gap of the

axle can control the transcription directly, because it contains the segment of promoter sequence in template strand that is necessary to initiate transcription; ii) the macrocycle will be released from the gap of the axle as long as the transcription bubble is formed; iii) when the macrocycle hybridizes with the promoter gap, T7RNAP will push the macrocycle toward the transcription direction during the transcription initiation process by binding to the promoter.

### 3.1.2. Assembly and characterization of the rotaxane actuator

Prior to the assembly of rotaxane, the precursors (macrocycle, stoppers and axle) have to be synthesized and if necessary, purified. The 40-nt ssDNA macrocycle was assembled as Figure 3-2. A splint ODN was used to enclose the linear template strand to form a circle shape structure. And the T4 DNA ligase was added to ligate two ends of the linear template to form a ssDNA ring (macrocycle).<sup>118</sup> Subsequently, as shown in Figure 3-2b, urea PAGE was utilized to dehybridize the splint ODN from macrocycle and further extracted the macrocycle from linear template strand and other higher polymerized structures (like dimer or trimer), due to a little lower electrophoretic mobility of macrocycle structure compared to linear template.

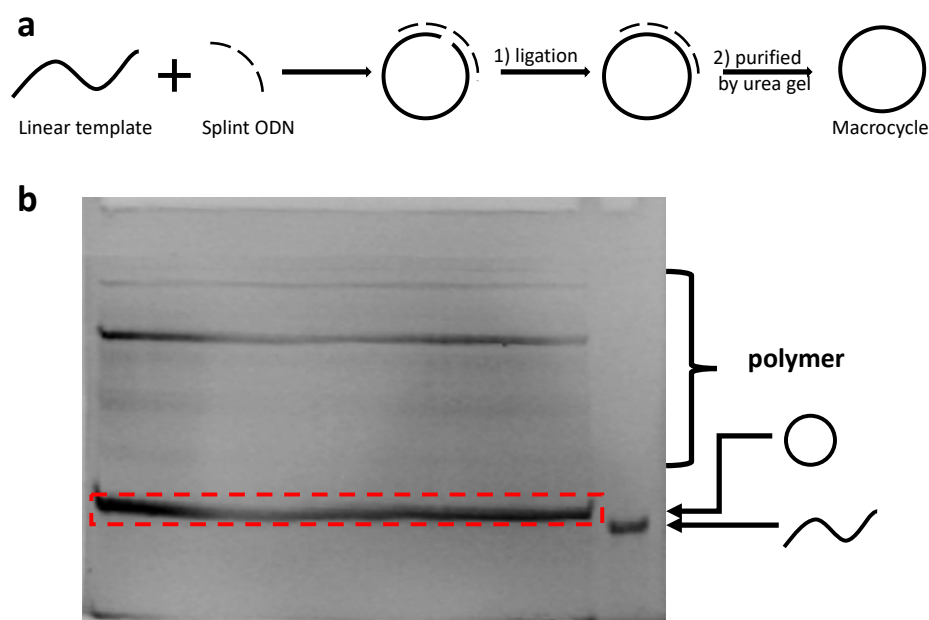


Figure 3-2. Assembly and purification of the macrocycle. (a) Schematic representation of the assembly process of the macrocycle. (b) A 12% PAGE Gel with urea (8.3 M) for purification of the macrocycle (1x TBE buffer, 50 min at 200 V).

The 168bp ring stoppers were assembled by mixing the relevant ODNs with sodium and magnesium ions containing buffer, and then heating the mixture to 95 °C and subsequent cooling to the room temperature by annealing program.<sup>53</sup> The crude products of stoppers were purified by HPLC and checked by agarose gel electrophoresis (Figure 3-3a). The axles were assembled by mixing the relevant ODNs. No further purification was required.

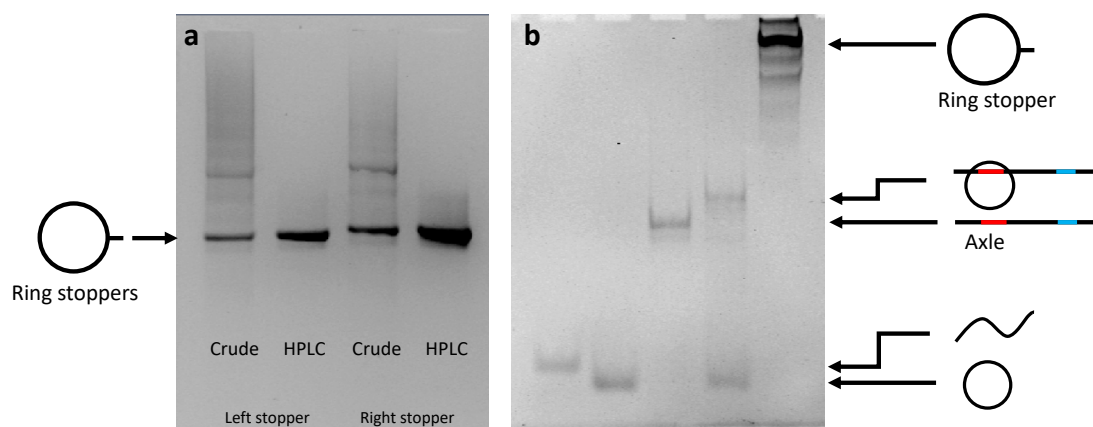


Figure 3-3. Gel analysis of the precursors for the rotaxane assembly. (a) Gel analysis (agarose, 2%, 20 min at 160V) of stoppers before and after HPLC purifications. (b) Gel analysis (PAGE, 9% containing 10 mM MgCl<sub>2</sub>, 50min at 150V) of macrocycle hybridization with the axle.

And the expected rotaxane was assembled by the capping method as described in the previous report.<sup>53</sup> Basically, the macrocycle was firstly threading onto the axle, which is guided by the interaction between the single-stranded gap of axle and its complementary sequence in the macrocycle. The successful threading of the macrocycle was confirmed by PAGE gel (Figure 3-3b). And then, two bulky stoppers with sticky ends were hybridized to the two ends of the axle to form a dumbbell shape structure. T4 DNA ligase was applied to ligate all the nicks in the structure, enhancing the stability of the whole structure. After assembly, the rotaxane was purified by weak anion exchange (WAX) HPLC (Figure 3-4).

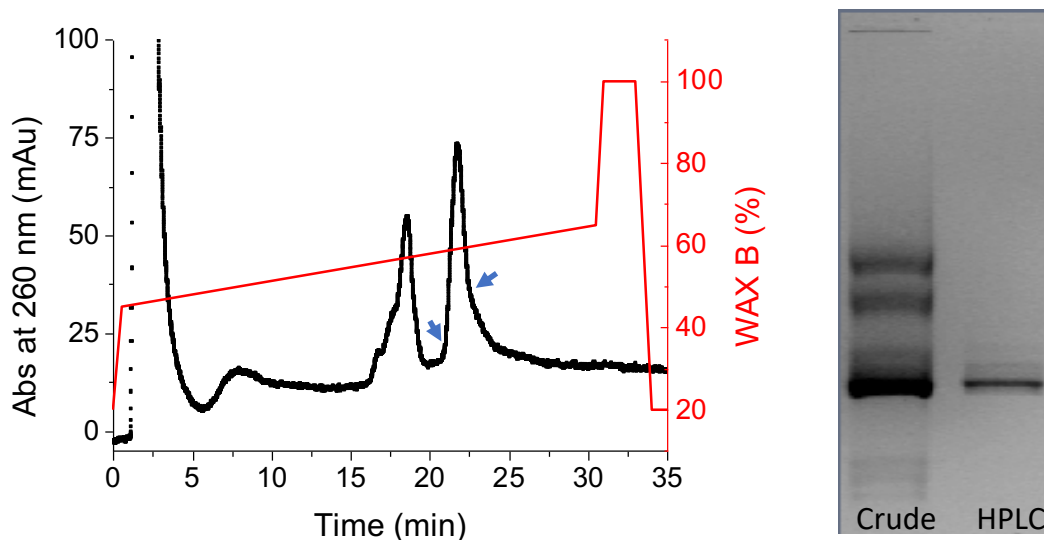


Figure 3-4. HPCL purification of the rotaxane (left panel). Gel analysis (agarose, 2.5%, 100 min at 120 V) of HPLC product of the rotaxane (right panel).

The correct formation of the rotaxane was verified by agarose gel electrophoresis (Figure 3-5, Supporting Figure 1 for a repeat, and Supporting Table 2-3 for the sequence design for the rotaxane). Lanes 1-5, and 8 (Figure 3-5) present the respective mobility of the precursors for the rotaxane assembly (stoppers, stoppers with axle and dumbbell structure). Lane 6 exhibits the rotaxane in the static state (the macrocycle is hybridizing with the promoter gap). Lane 7 shows the hybridized rotaxane in the presence of a release-ODN (RO, 20 nt, Supporting Table 1) which can bind to the macrocycle with the 10 nucleotides where macrocycle hybridizes to the promoter gap, and thus release the macrocycle from the axle to form an interlocked rotaxane. The product migrates between the hybridized rotaxane and the dumbbell structure even though the RO hybridizes to the macrocycle adding extra molecular weight and charge. This apparent slight shift in gel was also observed in other interlocked DNA nanostructures.<sup>58</sup>



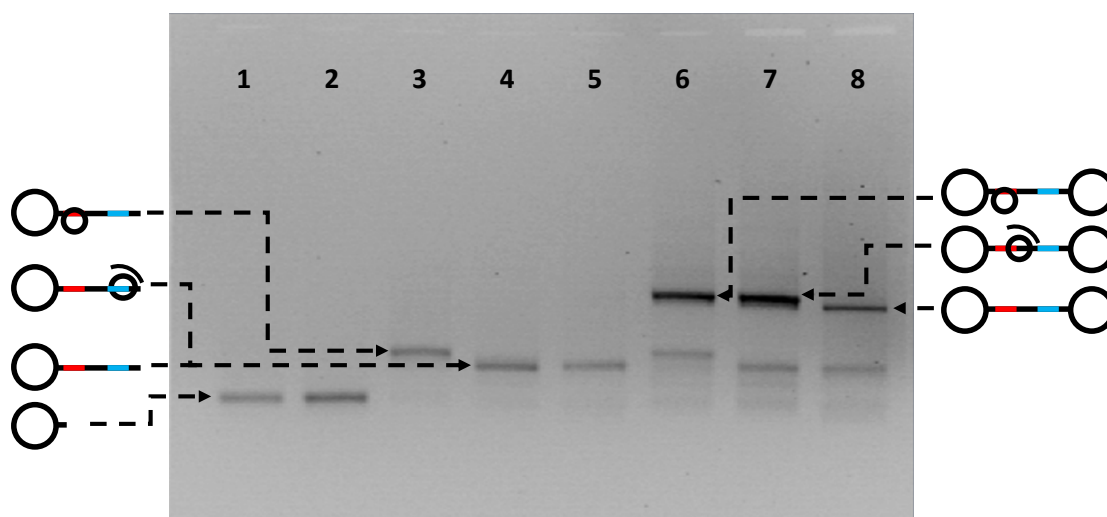


Figure 3-5. Gel analysis of the rotaxane assembly (Agarose, 2.5%, 100 min at 120 V). Lane 1, left stopper; lane 2, right stopper; lane 3, assembly of left stopper and the axle with the threading macrocycle; lane 4, adding RO to lane 3; lane 5, assembly of left stopper and the axle; lane 6, rotaxane; lane 7, adding RO to lane 6; lane 8, dumbbell structure.

Atomic force microscopy (AFM) was performed to further demonstrate the formation of the rotaxane. As shown in the Figure 3-6a, several dumbbell structures were observed on a mica surface that preincubated with poly-L-ornithine. In the presence of a complementary strand with a biotin modification (biotin-ODN) which can hybridize to the macrocycle as an indicator, small knots were found to adhere the axle close to one of the stoppers in the structures. The biotin-ODN can only hybridize to the free part of the macrocycle hybridizing to the promoter gap and allow the macrocycle to remain in the bound state, which is different from the above-mentioned RO (Supporting Table 1). The macrocycle itself is not visible, presumably due to its single-stranded nature. ssDNA structures that localize close to dsDNA regions are often barely visible in AFM scans. To clearly confirm the presence of the macrocycle in the rotaxane, streptavidin, as an indicator, was utilized to bind to biotin-ODN hybridizing with the macrocycle. As shown in Figure 3-6b, the AFM measurement in the presence of streptavidin showed that most of the dumbbell structures are connected to a bright dot with a height of about 4 nm that corresponds to streptavidin, indicating that the macrocycle co-localizes with the dumbbell and strongly suggesting the formation of the designed DNA rotaxane.

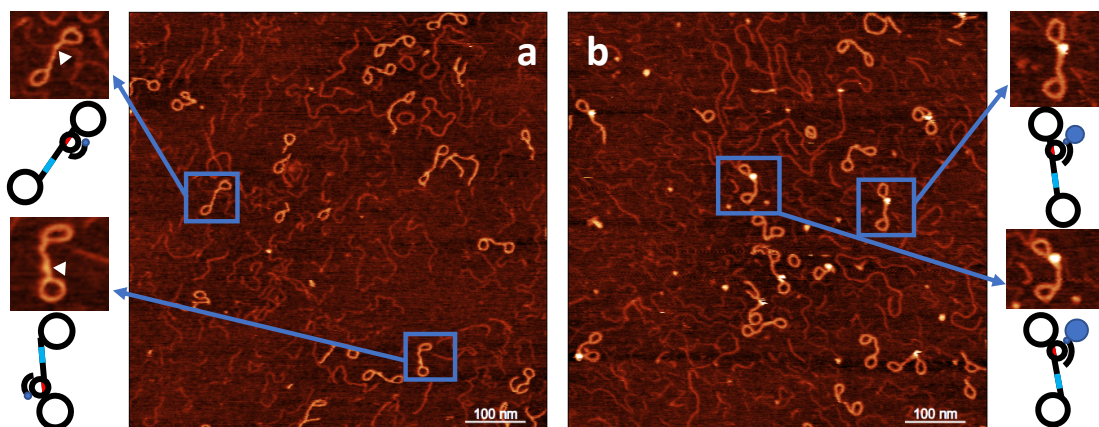


Figure 3-6. AFM measurements of the rotaxane with different indicators. **(a)** AFM measurement of the rotaxane in the presence of biotin-ODN. **(b)** AFM measurement of the rotaxane in the presence of biotin-ODN and streptavidin. White angles are pointing to the knot on the axle.

### 3.1.3. Overview of the mechanism of the rotaxane actuator

As illustrated in Figure 3-7, the designed mechanism of the T7RNAP-driven DNA rotaxane actuator starts from state (a), passes states (b) – (f), and finally returns to the state (a), as a full cycle. The designed T7-promoter region of the axle incorporates the necessary template sequence on the macrocycle, providing the complete recognition site for T7RNAP (Figure 3-1a, Figure 3-7a). When the T7RNAP recognizes and attaches to the promoter sequence, a transcription bubble will be formed to initialize transcription, releasing the macrocycle thereafter due to the unwinding between the macrocycle and promoter gap during the initiation of transcription (Figure 3-7b). The T7RNAP reads and traverses the template strand and produces RNA transcripts (Figure 3-7c, d). The RNA production contains the complementary coding sequence for the MB ODN for fluorescence monitoring. Meanwhile, T7RNAP pushes the macrocycle away from the promoter gap towards a state in which the macrocycle moves in the minimal range along the axle (Figure 3-7e). Once the T7RNAP reaches the downstream end of the axle where two subsequent terminators are located, the transcription will suspend, and the T7RNAP will drop from the axle (Figure 3-7f). At that moment, the lack of the necessary part of the template strand in the promoter hinders the reattachment of T7RNAP and the promoter. Owing to the interlocking nature, the macrocycle wanders and hybridizes to its original binding site driven by the Brownian motion along the rotaxane axle. The rehybridization of macrocycle reconstitutes the system and binds to promoter gap again (state(a)), which serves as a prerequisite to be recognized by T7RNAP and initiates new transcription cycles.

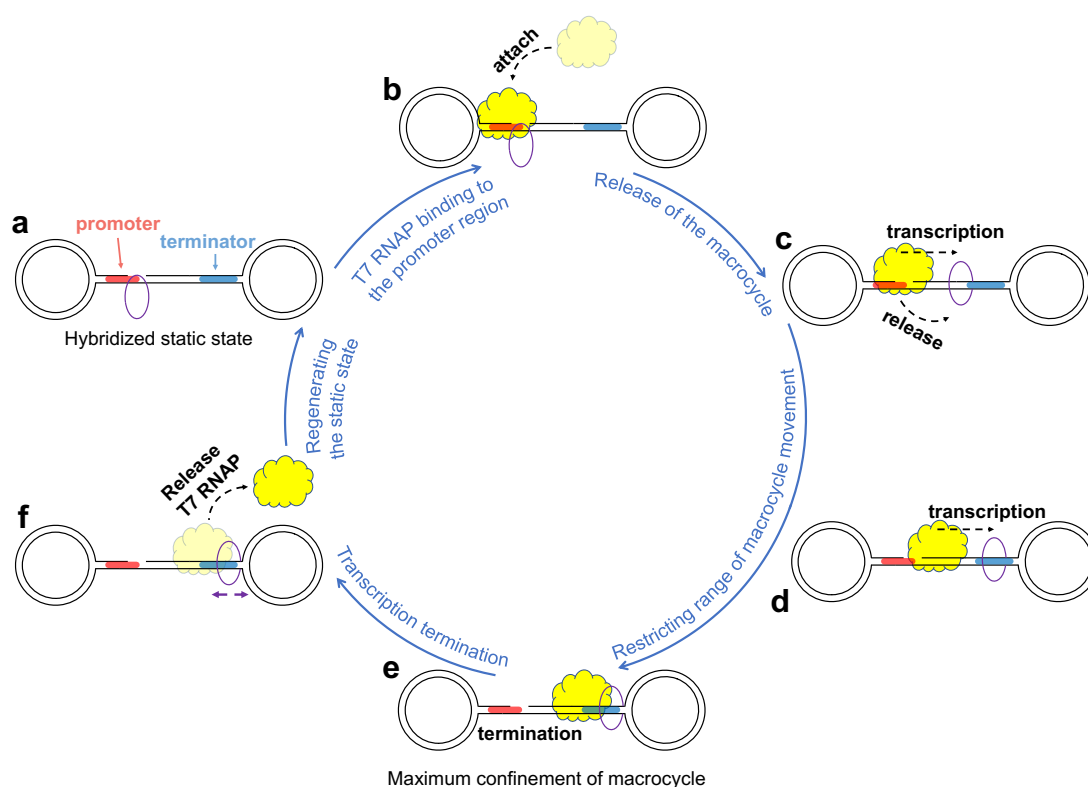


Figure 3-7. Schematic representation of a full operation cycle of the rotaxane actuator with T7RNAP. (a) Rotaxane in the static state with a hybridized macrocycle. (b) T7RNAP (yellow cloud) bind to the macrocycle-reconstituted promoter; (c) Initiation of transcription and macrocycle releasing from promoter region; (d) Transcription depletes the moving range of the macrocycle, making it closer to the downstream stopper; (e) Termination of transcription and maximum confinement state of the macrocycle; (f) T7RNAP detaches, and the macrocycle moves freely along the whole axle. The macrocycle binds to the promoter gap to reconstitute the static state and starts a new cycle.

### 3.1.4. Transcription behaviors

The real-time MB fluorescence experiments of the rotaxane actuator were performed to investigate the transcription process which is the fundamental operation of the system. The transcription rate of the system was analyzed and quantified in this section. The 2'-OMe RNA-MB is labeled with a 3'-FAM and a 5'-DABCYL fluorophore/quencher pair, which is designed to be a hairpin structure in solution and can be opened by RNA transcripts produced during the transcription of the rotaxane actuator and then show the increasing fluorescence signal (Figure 3-8a). As illustrated in Figure 3-8b and c, the MB fluorescence signals of the transcription process and relative transcription rates

are presented respectively. As a negative control, the dumbbell structure without MB coding sequence presents a negligible fluorescence signal (Figure 3-8b, green). And the dumbbell lacking the macrocycle that contains the essential part of the promoter region shows similar results (Figure 3-8b, black). As a positive control, the dumbbell with promoter gap ODN (pGO, Supporting Table 3) that can fill promoter gap and construct the full promoter sequence, shows a noticeably increasing signal during the transcription (Figure 3-8b, blue). The rotaxane hybridizing with the threading macrocycle shows a certain increasing signal of transcription during the whole 120 min, however, the signal level is much lower than the positive control (Figure 3-8b, red). The distorted helix of the promoter region that combines the macrocycle and the rest promoter sequence on the axle would be the most likely cause. In comparison with the interlocked rotaxane, the dumbbell in the presence of a non-threading macrocycle presents more than 2.5-fold less of the signal level of transcription (Figure 3-8b, magenta). The macrocycle is always bound with a biotin-ODN in this experiment. For a better comparison, Figure 3-8c shows the corresponding relative transcription rates of the samples in Figure 3-8b. And Figure 3-9 presents that the experiments are constantly and significantly reproducible by p-values.

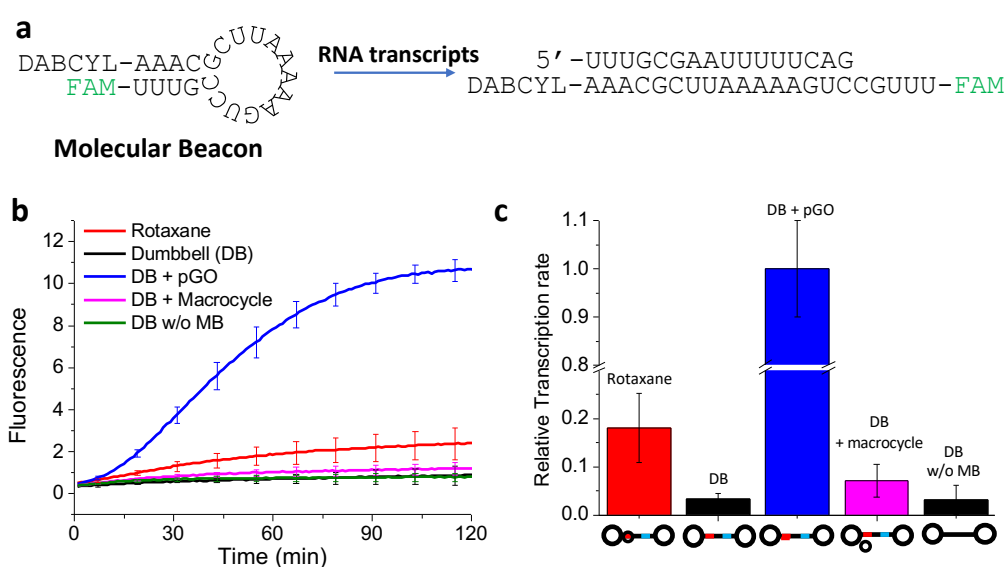


Figure 3-8. Molecular beacon (MB) fluorescence experiment for the transcriptional behaviors of the rotaxane. (a) Schematic representation of the MB and hybridization between RNA transcripts and MB. (b) Transcription performances of rotaxane in the presence of biotin-ODN (red), dumbbell structure (black), dumbbell with promoter gap ODN (pGO, blue), dumbbell with the macrocycle and biotin-ODN (magenta), and dumbbell without MB sequences (green) at 25 nM template concentration. Error bars: S.D.,  $n = 3$ . (c) Relative transcription rates from (b), same colors as in (b).

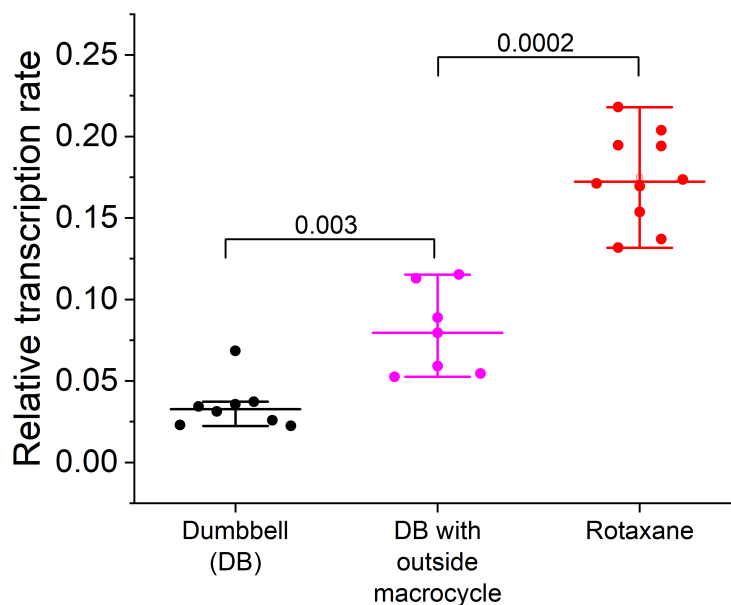


Figure 3-9. Relative transcription rates of dumbbell (black), dumbbell with outside macrocycle (magenta) and rotaxane (red). Error bars: S.D.,  $n = 7$  for dumbbells and  $n = 9$  for rotaxane. Significant differences between samples were verified by p-values: 0.003 for dumbbell sample compared with the dumbbell with outside macrocycle sample and 0.0002 when comparing the dumbbell with outside macrocycle and rotaxane, respectively.

Based on these results, it can be concluded that: i) the transcription can be almost completely turned off in the presence of the ss-gap in the template strand of promoter sequence; ii) the promoter gap can be partially filled using a macrocycle containing the complementary sequence, and the transcription will be restored to a certain extent, but the efficiency is not as good as that of a fully double-stranded promoter that hybridizes with pGO; iii) the non-interlocked macrocycle is less capable of restoring the transcription than the macrocycle that is interlocked with the rotaxane; and iv) the T7RNAP is tightly regulated by the interlocked macrocycle in this rotaxane system.

The transcription rate was quantified by a calibration curve based on the MB fluorescence signals corresponding to the different concentrations of the coding strand of the rotaxane axle (see Supporting Table 3 for the sequence) that has the identical sequence to RNA transcripts produced by the transcription of rotaxane (Figure 3-10a). The different concentrations of this ssDNA strand were combined with the RNA-MB and the fluorescence signals were recorded by plate reader over 120 min (Figure 3-10b). The calibration curve was based on correlation between ssDNA concentration and the fluorescence signal at 30 min time point (Figure 3-10c).

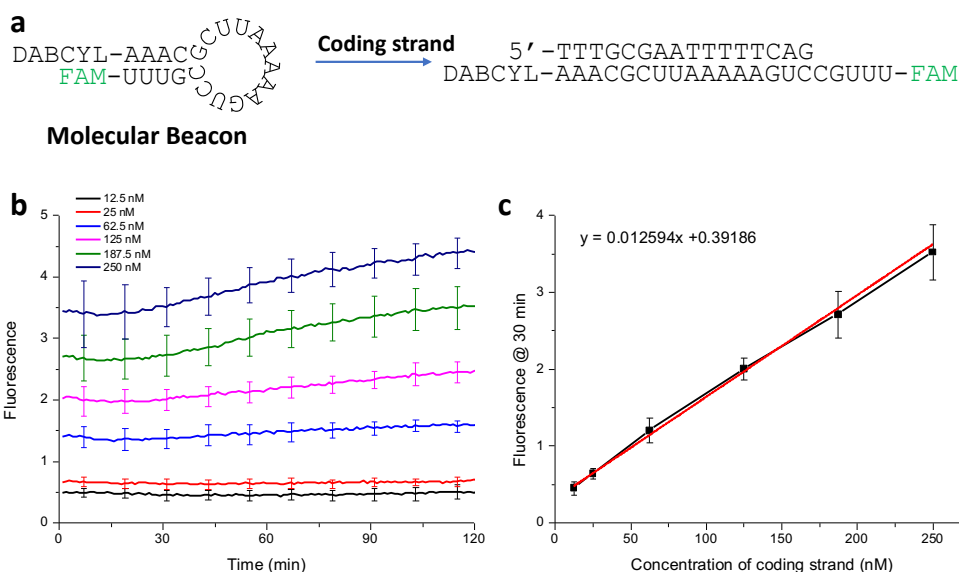


Figure 3-10. MB fluorescence experiment for transcription calibration. (a) Schematic representation of hybridization between the coding strand of the rotaxane axle with the same sequence to a part of the T7RNAP-generated RNA (fw4, suppl. Table S3 for the sequence) and MB. (b) MB fluorescence of different concentrations of coding strand ODN. (c) The calibration curve that correlated coding strand concentration with fluorescence at time-point 30 min and the corresponding fitting equation. Error bars: S.D.,  $n = 3$ .

In the presence of different equivalents of T7RNAP, the corresponding transcription rates of rotaxane samples were calculated based on the above calibration curve (Figure 3-11). The 25 nM template concentration (the concentration of rotaxane) and 30 min time point were applied in the section. Measurements in the presence of 2, 4, and 8 equivalents of T7RNAP exhibited transcription rates of  $12.92 \pm 1.81$ ,  $9.77 \pm 1.77$ , and  $7.99 \pm 1.28$  minutes per cycle, respectively. The efficiency of transcription can be enhanced by increasing the amount of T7RNAP. In comparison with a common transcription with T7RNAP, the transcription rate in the rotaxane actuator is relatively low. Most importantly, the amount of RNA produced at 30 mins is still increasing linearly, while the 2 to 4 transcription cycles have been performed according to varied amount of T7RNAP, which indicates that transcription in this system is automatically repeated without any external intervention.

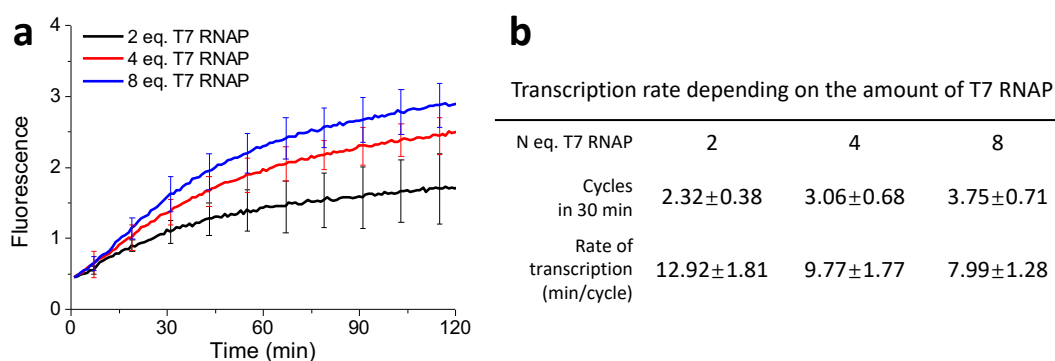


Figure 3-11. MB fluorescence experiment for transcriptional performance of rotaxane in the presence of different equivalents of T7RNAP. (a) Transcription performances of rotaxane in the presence of 2/4/8 eq. of T7RNAP at 25 nM template concentration. Error bars: S.D.,  $n = 3$  (b) Calculated transcription rates in average from (a). The calibration curve from Figure 3-10a is used to estimate the concentration of RNA produced by transcription.

Furthermore, the direct control of rotaxane transcription by the macrocycle was examined by the MB fluorescence experiment with the help of RO-TH (RO with toehold) and its complementary strand cRO-TH (see Supporting Table 1 for the sequences). Similar to the RO, RO-TH can release the macrocycle from the promoter gap of axle but has a 7-nt overhang, which allows cRO-TH to easily bind to the RO-TH and displace it from the macrocycle.<sup>18</sup> Thus, switching on and off the transcription was achieved by adding RO-TH and cRO-TH alternately to dehybridize and rehybridize macrocycle with the promoter gap, respectively (Figure 3-12a). As shown in Figure 3-12b, the fluorescence signal of dumbbell structure with or without addition RO-TH/cRO-TH has negligible change, as the negative control, indicating that RO-TH and cRO-TH have no effect on the dumbbell structure (red and black). Meanwhile, the signal of the rotaxane in the absence of RO-TH and cRO-TH is continuously increasing during the measurement (magenta). Moreover, the addition of RO-TH can significantly slow down or even pause the transcription, while adding cRO-TH afterwards restores the transcription (blue). These results demonstrate that the addition of RO-TH/cRO-TH can regulate the operation of the transcription in this system and strongly indicate the hybridization of macrocycle is a direct control of the rotaxane actuator.

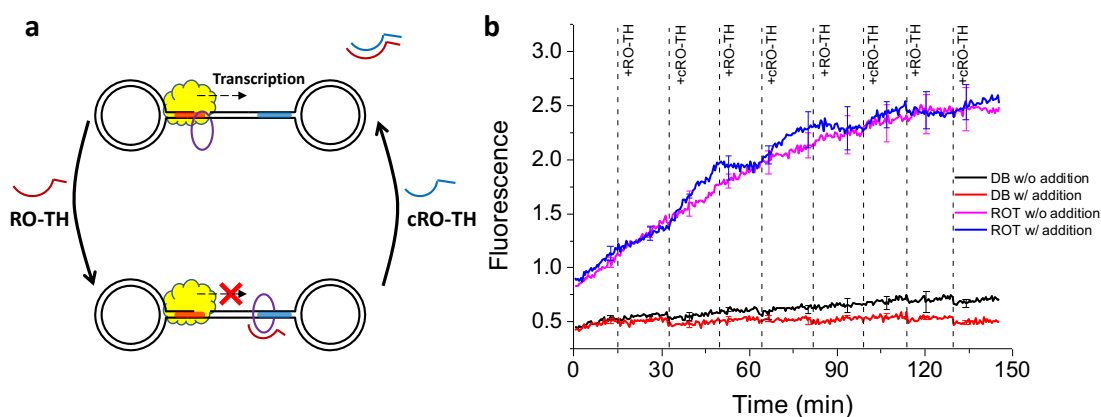


Figure 3-12. MB fluorescence experiment for switching on/off the transcription of rotaxane. (a) Schematic representation of transcription of ROT (blue) and DB (red) with addition of RO-TH and cRO-TH every 16 min alternatively. (b) MB fluorescence experiment of (a). Transcription of ROT (magenta) and DB (black) without adding RO-TH or cRO-TH as controls. Error bars: S.D.,  $n = 3$ .

### 3.1.5. Rehybridization of the macrocycle

The time necessary for macrocycle rehybridization to the promoter gap after transcription was studied. However, it is laborious to measure the time taken for hybridization of interlocked macrocycles in the rotaxane. Therefore, the time consumed for the rehybridization of the macrocycle is estimated based on the situation of the macrocycle hybridizing to a half-dumbbell version of rotaxane. The half-dumbbell was modified with a BHQ2 quencher at the margin of promoter gap in the rotaxane axle (Supporting Table 3, Axle MB-BHQ2), which can quench the fluorescence signal from a HEX fluorophore labeled on a reporter ODN (HEX-ODN1, Supporting Table 1) binding to the macrocycle. The HEX-ODN1 is complementary to a part of the macrocycle that cannot interfere with the hybridization between the macrocycle and the promoter gap of rotaxane. The combination of macrocycle and half-dumbbell constitutes a pseudo-rotaxane structure (Figure 3-13, left panel). The fluorescence signal of HEX can be quenched due to its close proximity to the BHQ2 quencher when the macrocycle/HEX-ODN 1 hybrid (macrocycle binding with HEX-ODN 1, Supporting Table 1) binds to the promoter gap. As a negative control, in the absence of the macrocycle, half dumbbell with only the HEX-ODN 1 shows the maximum HEX-fluorescence signal during the 10-min measurement (Figure 3-13, right panel, black curve). As a positive control, a pre-assembled pseudo-rotaxane formed by the macrocycle/HEX-ODN 1 hybrid presented a full quenched signal (Figure 3-13, blue curve). Then, the hybridization of the promoter gap with the macrocycle/HEX-ODN 1



was measured by adding macrocycle/HEX-ODN 1 hybrid to the half dumbbell at the zero time-point (Figure 3-13, red curve). The fluorescence intensity gradually dropped, during the 10-min hybridization process of above binary.

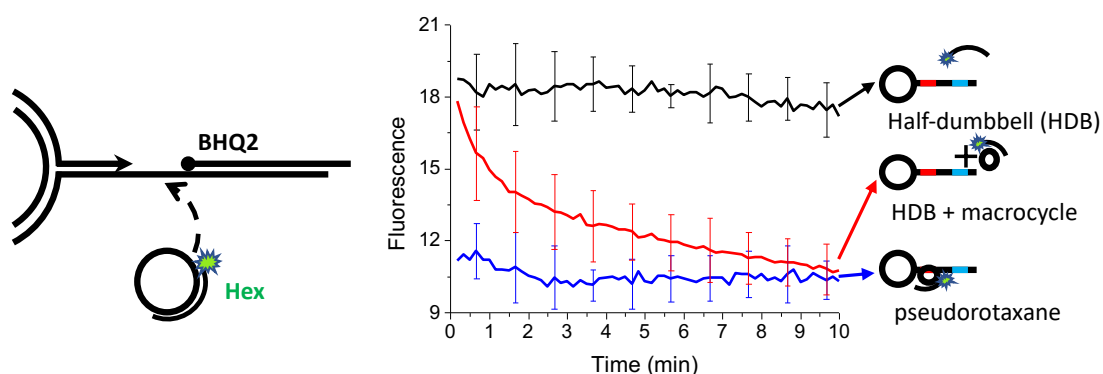


Figure 3-13. Macrocycle rehybridization investigation. Left panel: schematic representation of the process of macrocycle rehybridization. Right panel: the HEX fluorescence changes of half-dumbbell in absence (negative control, black) and presence (positive control, blue) of 50 nM of macrocycle. the HEX fluorescence change of addition of the macrocycle/HEX-ODN 1 hybrid (50 nM) to the half-dumbbell during 10 min (red). Error bars: S.D., n = 5.

Based on the fluorescence quenching curve, the rate constant of macrocycle hybridization was calculated by the nonlinear second-order fitting to the following equation<sup>119</sup>:

$$A_t = A_0 + (A_{inf} - A_0) \cdot \frac{C_0 \cdot k_{on} \cdot t}{1 + C_0 \cdot k_{on} \cdot t}$$

where  $A_t$  is the fluorescence intensity at time-point  $t$ ,  $A_0$  is the fluorescence intensity of the free macrocycle/HEX-ODN 1 hybrid at  $t = 0$ ,  $A_{inf}$  is the fluorescence intensity of the hybridized macrocycle/HEX-ODN 1 hybrid at equilibrium and  $C_0$  is the initial concentration (50 nM) of free macrocycle/HEX-ODN 1 hybrid.

The half-life ( $t_{1/2}$ ) of macrocycle hybridization was obtained at  $C_{1/2} = 1/2 C_0$  using the following equation:

$$\frac{1}{C_{1/2}} - \frac{1}{C_0} = k_{on} \cdot t_{1/2}$$

At  $C_{1/2} = 1/2 C_0$ , the half-life of macrocycle hybridization was calculated to be  $99.0 \pm 6.9$  s (Figure 3-14). In comparison with the time consumed for the transcription in the

rotaxane actuator, which takes several minutes per transcription cycle, the time required for macrocycle hybridization is considerably less. Due to the interlocked nature of the macrocycle in the rotaxane, the dehybridization of the macrocycle becomes more difficult than in the case of a non-interlocked macrocycle. Once released, the rehybridization of the interlocked macrocycle is faster than the non-interlocked macrocycle which takes more time to find its binding site in the bulky solution.<sup>48,120</sup> Therefore, the time of rehybridization of macrocycle to the promoter gap has little contribution to the entire transcription cycle. Considering that the elongation process of the transcription is a fast step, the rate-limiting step in each pulsatile cycle of rotaxane actuator should be the promoter recognition and the initiation of the transcription by the T7RNAP.

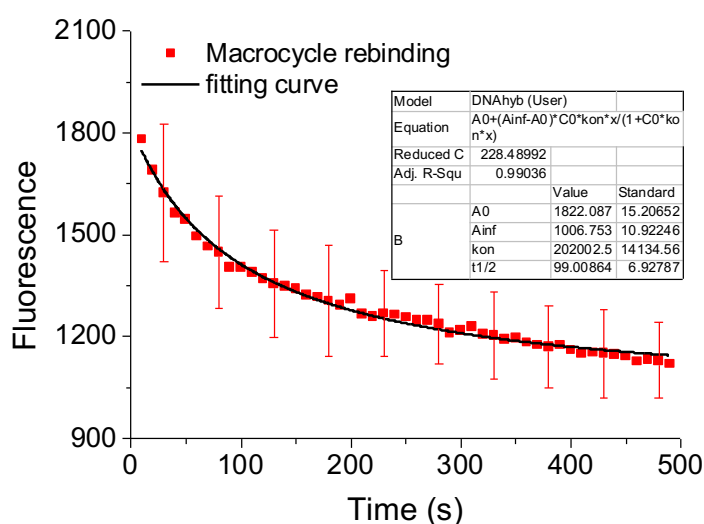


Figure 3-14. Non-linear fitting for the macrocycle rebinding curve. The inset table shows the fitted parameters of the equation. Error bars: S.D., n = 5.

### 3.1.6. Macrocycle releasing by T7RNAP

Fluorescence quenching experiments were also employed to investigate the release of macrocycle by T7RNAP with the HEX/BHQ2 fluorophore/quencher pair. As shown in the left panel of Figure 3-15, in the beginning, the macrocycle/HEX-ODN 1 hybrid was binding to the promoter gap, while the fluorescence signal of HEX was quenched by BHQ2 that located at the edge of promoter gap. Once macrocycle released, the fluorophore/quencher pair separates, and the fluorescence signal gradually grows. As a positive control, the addition of T7RNAP to the rotaxane with the macrocycle that is already released by RO, did not alter the high intensity of fluorescence (Figure 3-15, right panel, blue curve). In contrast, by adding T7RNAP to the rotaxane with hybridized

macrocycle, the quenched fluorescence signal slowly recovered to a plateau that is below the level of blue curve (Figure 3-15 right panel, red curve), which is the maximum intensity can be reached for the rotaxane with released macrocycle. The results are consistent with the idea that the macrocycle binding to the promoter gap of rotaxane can be released by T7RNAP. However, since the measurements were performed in a bulky solution, the equilibrium between released and rehybridized macrocycles coexists in this case, which is reflected in the lower maximum level of fluorescence.

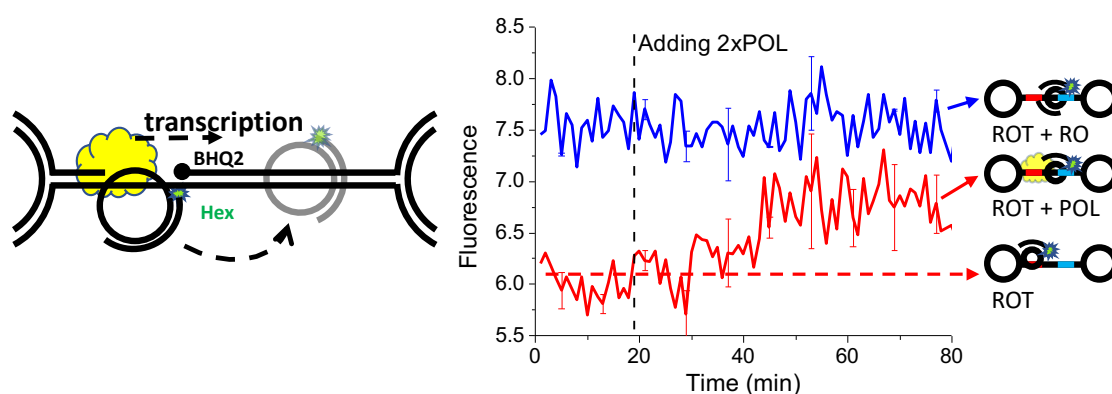


Figure 3-15. Kinetics of macrocycle release by T7RNAP. Left panel: schematic representation of macrocycle releasing by T7RNAP. Right panel: the HEX fluorescence change of the release of the macrocycle/HEX-ODN 1 hybrid by T7RNAP. The addition of T7RNAP to the hybridized rotaxane (25 nM) after 18 min in absence (red curve) and in presence (blue curve) of RO. Error bars: S.D.,  $n = 3$ .

### 3.1.7. Movement direction of macrocycle forced by T7RNAP

The direction preference of the macrocycle after being released by T7RNAP was studied by inserting an extra gap in the downstream part of the axle. Given that only C and T are present at the initial 6 bases of the template strand in the axle (Supporting Table 3 for the sequences of the axles), to start the transcription, just ATP and GTP are sufficient. Meanwhile, the macrocycle can still be released from the promoter gap. However, the T7RNAP could stall in the middle of the axle, because UTP and CTP are required in the subsequent transcription process. Once released, the macrocycle is expected to move in the range between the stalling T7RNAP and the downstream stopper (Figure 3-16, left panel, Supporting Table 3, Axle MB-2Gaps). As shown in the left panel of Figure 3-16, an additional gap that is also in between has the possibility

to capture the macrocycle, and if so, a BHQ2 labelled at the margin of this gap can quench the fluorescence signal of the HEX modified reporter strand (HEX-ODN2, Supporting Table 1) that has the same binding feature with HEX-ODN1. Thus, if the T7RNAP releases the macrocycle as expected and forces the macrocycle to move to the downstream region of the axle, the HEX-fluorescence will be quenched; else, the signal will persist. As shown in the right panel of Figure 3-16, the addition of the T7RNAP to the rotaxane with an additional gap makes the fluorescence signal HEX reduced during the entire 120-min measurement (red curve). In contrast, the macrocycle was pre-released and bound to the downstream gap in the presence of pGO, and the addition of T7RNAP will not change the quenched fluorescence signal. (magenta curve). However, both fluorescence curves failed to approach the entire quenching level of the negative control, where the fluorescence signal of HEX was also measured in the presence of pGO but without adding T7RNAP (blue curve). The possible reason is that T7RNAP may skip a few nucleobases and continue to transcribe the following DNA, thereby also detaching the macrocycle from the second gap.<sup>115</sup> Based on these results, it is demonstrated that the T7RNAP cannot only release the macrocycle from the promoter gap but also confine it in the range between the T7RNAP and the downstream stopper, namely, in the direction of transcription.

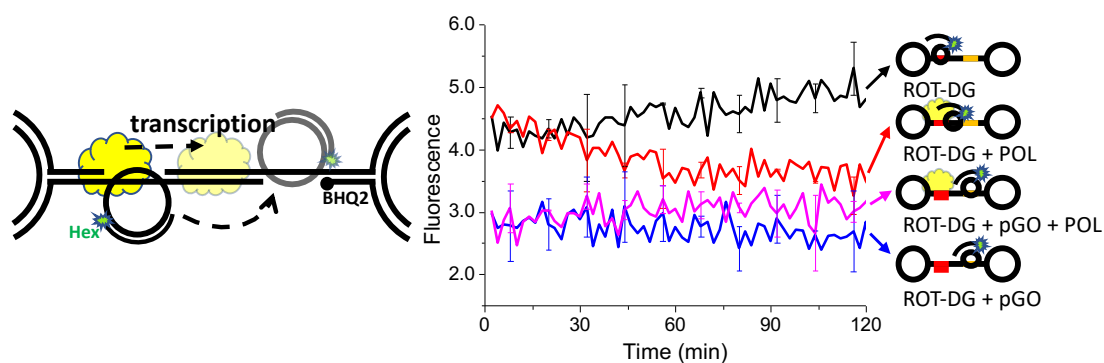


Figure 3-16. Moving direction of the macrocycle. Left panel: schematic representation of the direction of movement of the macrocycle released by T7RNAP. Right panel: the HEX fluorescence changes of the rotaxane with double gap (ROT-DG, 25 nM) in absence (black curve, positive control) and presence of the promoter gap ODN (pGO, blue curve, negative control). The HEX fluorescence of the addition of T7RNAP to ROT-DG in absence (red curve) and presence (magenta curve) of the pGO. All the cases were measured for 120 min. Error bars: S.D.,  $n = 3$ . The HEX-ODNs were present at 20 nM in all experiments.

### 3.1.8. Termination of transcription and dethreading investigation

Two successive Class II terminator sequences of T7RNAP were utilized to terminate the transcription and release the T7RNAP from the axle of the rotaxane. According to the approximately 55% termination efficiency of one terminator sequence, a portion of T7RNAP can still bypass the terminator and continue to transcribe the following DNA template.<sup>112</sup> Thus, the transcription could terminate at the first terminator or the second terminator, or even at the end of the axle by the help of three-way junction that connect the axle and the downstream stopper. As shown in Figure 3-17a, the transcript of the transcription was checked by PAGE gel with urea for denaturing. Three ssDNA strands were applied as markers to point out the three possible positions that are corresponding to the relative transcripts with different lengths. And for the sample of rotaxane after transcription, three major bands were appearing at the gel. The appearing bands have a gel mobility that is comparable to ssDNA strands that have similar length to transcript as expected, when the transcription stops at the first or the second terminator sequence or at the three-way junction. Slight differences in the gel mobility can be attributed to the fact that the reference ODN are ssDNA while the transcript is RNA. A smear occurred, while a fraction of the sample cannot enter the gel and stayed in the gel pocket.

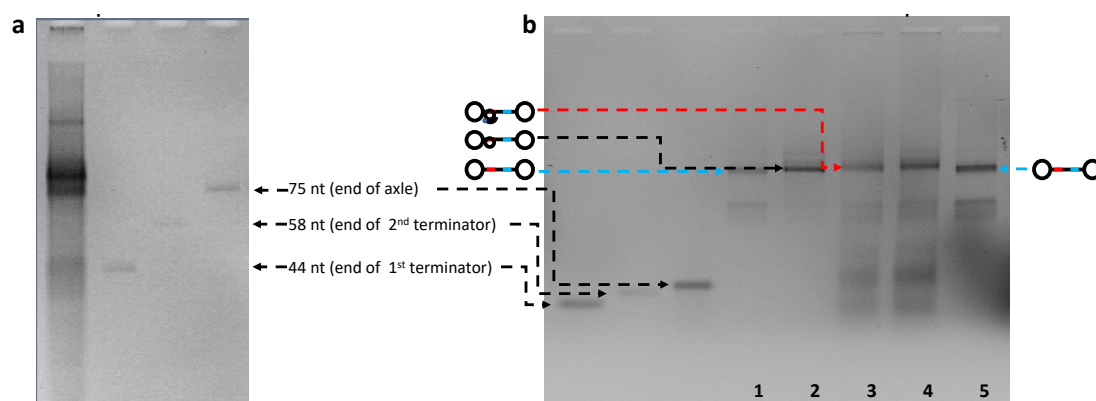


Figure 3-17. Rotaxane after transcription. (a) and (b) gel analysis ((a) PAGE with urea, 12 %, 50 min at 200V; (b) agarose gel, 2.5%, 70 min at 120 V) of RNA transcripts produced by transcription of rotaxane. 44 nt, 58 nt and 75 nt are corresponding ssDNA marker. Lane 1 Dumbbell; Lane 2 Rotaxane without biotin-ODN; Lane 3 Rotaxane with biotin-ODN; Lane 4 Rotaxane with biotin-ODN after transcription; Lane 5 Dumbbell.

---

To assess if the rotaxane can be disassembled after transcription, due to the dethreading of the small macrocycle, the transcription experiments were repeated, and gel analysis was performed afterwards. The transcription products were checked on an agarose gel to visualize the rotaxane together with the transcript. As shown in Figure 3-17b, in the agarose gel, the rotaxane has a slightly lower mobility in the gel compared to the dumbbell (lane 2 and lane 1 respectively). For the rotaxane after transcription, the appearance of additional high mobility bands was presented in the gel, besides the bands that also appeared in the PAGE gel (lane 3 and lane 4). It is also noticeable that no longer transcript with very low gel mobility is formed and also no additional heavy smearing is noticeable indicating the termination happens only in three very precise positions. The band corresponding to the rotaxane is maintained, and the formation of an additional band with gel mobility corresponding to the dumbbell is not visible after the transcription.

AFM measurements were performed to further investigate the samples after transcription. As above mentioned, the biotin-ODN was utilized to better visualize the macrocycle of the rotaxane, which hybridized to the macrocycle and then incubated with streptavidin. As shown in Figure 3-18, most of the rotaxane after transcription shows a small knot on the axle that in the above interpretation corresponds to the small macrocycle. Some of the structures also clearly show the presence of the macrocycle on the rotaxane, due to the bright dot corresponding to the streptavidin connected to it. However, the number of structures that have the streptavidin connected to it is low, probably due to low attachment efficiency of the streptavidin to the biotin-ODN and a low hybridization of the short biotin-ODN to the macrocycle. Another possible reason is that the streptavidin can be moved away from the structure by physical interaction with the cantilever during the AFM scan. To summarize, dethreading of the macrocycle may occur but in a very small fraction of rotaxane structures and it should not heavily affect the overall performance and mechanism of action of the system.

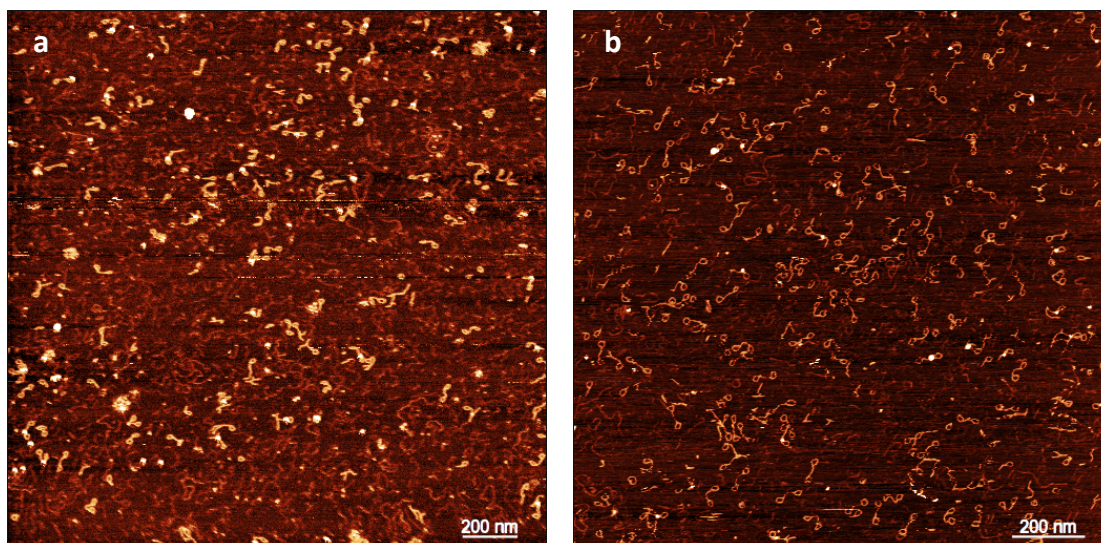


Figure 3-18. AFM measurements of the rotaxane after transcription with biotin-ODN and streptavidin.

Above results show that the terminator sequences are important to prevent the macrocycle from dethreading. In direct comparison with the original rotaxane system that contained the terminators, a further experiment indicates that no dethreading occurs even in the absence of the terminator sequences. As shown in Figure 3-19a, the transcription experiments directly compare the rotaxane with terminator sequences and without terminator sequences, observing a reduced transcription rate in the rotaxane without terminator sequences. To test whether the macrocycle was dethreading, the samples were checked on an agarose gel after transcription. The biotin-ODN was added to the samples, which can hybridize to the macrocycle without interfering with its hybridization to the axle. This biotin-ODN serves as an attachment point for streptavidin added after the transcription that increases the molecular size of the rotaxane sample so that it can be unambiguously distinguished from the dumbbell. After transcription the rotaxane bands are clearly visible independent of the presence of the terminator sequences (Figure 3-19b). Hybridization of the macrocycle from the outside to the axle has been excluded on a second gel (Figure 3-19c). One hypothesis is that the macrocycle forms a mechanical barrier for the polymerase once it hits the three-way junction on the axle/ring-stopper connection and this steric hindrance is sufficient to stall the polymerase and impede further transcription. Noteworthy, the overall transcription rate is reduced compared to the rotaxane with two terminator sequences, probably because the polymerase is held up at the three-way junction but is not able to efficiently detach from the axle due to the missing terminator sequence. This mechanism would sequester the macrocycle for a longer time before allowing the

reset of the rotaxane system.

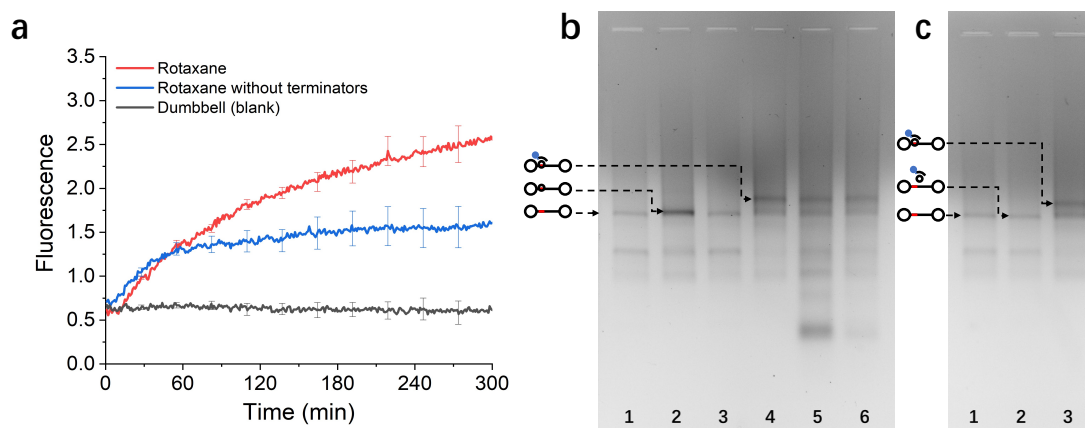


Figure 3-19. MB fluorescence experiment for the comparison between rotaxane with and without terminator sequences. (a) MB fluorescence of transcriptions dumbbell structure (black), rotaxane (red) and rotaxane without terminator sequences (blue) at 20 nM template concentration. Error bars: S.D.,  $n = 3$ . (b) Gel analysis (agarose, 2.5%, 90 min at 80 V) of RNA transcripts produced by transcription of rotaxane. Lane 1: Dumbbell; Lane 2: Rotaxane without biotin-ODN; Lane 3: Dumbbell with biotin-ODN and streptavidin; Lane 4: Rotaxane with biotin-ODN and streptavidin; Lane 5: Rotaxane with biotin-ODN after transcription and addition of streptavidin; Lane 6: Rotaxane without terminator sequences with biotin-ODN after transcription and addition of streptavidin. (c) Gel analysis (agarose, 2.5%, 90 min at 80 V) of dumbbell with outside (unthreaded) macrocycle. Lane 1: Dumbbell; Lane 2: Dumbbell and outside macrocycle with biotin-ODN and streptavidin; Lane 3: Rotaxane with biotin-ODN and streptavidin.

### 3.1.9. Investigation of the dynamic stability of the macrocycle in the rotaxane by molecular dynamics simulations

To access the stability of designed rotaxane in the term of the macrocycle dethreading, molecular dynamics simulations were performed by using the oxDNA2 model.<sup>44–46,121</sup> The rotaxane with the ss-macrocycle that is not hybridized to a reporter strand was simulated, and the relative position of the macrocycle to the rotaxane axle was recorded. As shown in Figure 3-20, the resulting position histogram of the macrocycle illustrates that the macrocycle never visits any position of both ring stoppers. The result supports the observation from experiments that the macrocycle is unlikely to dethread



from the dumbbell of the rotaxane without any external force, and thus the correct formation of the rotaxane can be confirmed.

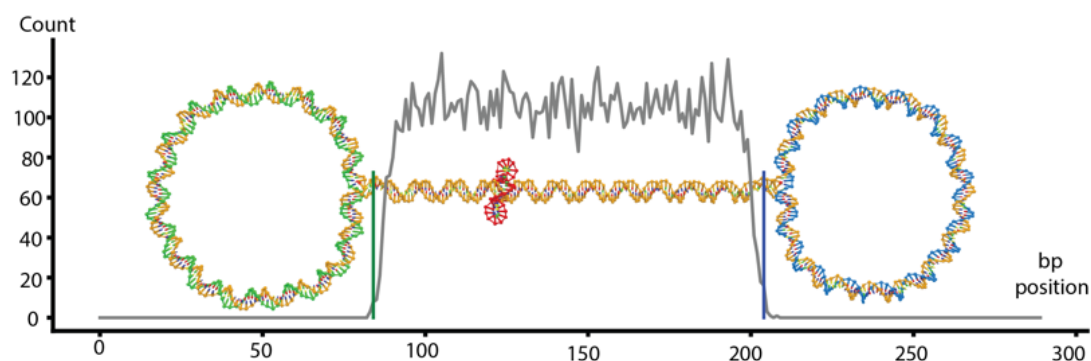


Figure 3-20. Macrocycle position histogram for rotaxane (ROT) without reporter ODN. The position of the macrocycle ring is said to be the closest base pair on the dumbbell structure. The histogram is plotted as a summary of 3 replica runs, corresponding in total to 66  $\mu$ s simulation time. A schematic of the system is represented in the inset picture. Green line denotes beginning of the left stopper ring, blue line denotes the start of the right stopper ring. The simulations were performed by Dr. Michael Matthies and Professor Petr Šulc at the Arizona State University.

Furthermore, to investigate whether the T7RNAP may force the macrocycle dethread through downstream stopper, another set of oxDNA simulations was performed by exerting a series of constant forces on the macrocycle to simulate the effect of T7RNAP on the macrocycle of the rotaxane (Supporting Table 5). To simplify, the simulations were performed with an incomplete rotaxane system, which only contains the threading macrocycle, the axle and the downstream stopper connecting to the axle, while another end of the axle was pinned down to a certain point in the simulation box. A representative initial state is shown in Figure 3-21.

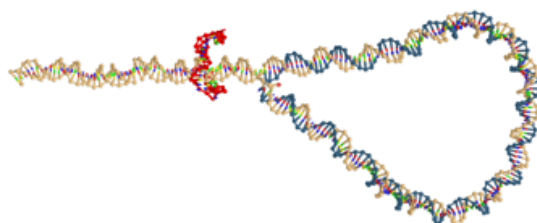


Figure 3-21. Representative initial state of the macrocycle force pushing experiments for ROT without reporter ODN. Strands corresponding to half of the rotaxane are

marked as yellow and blue. The macrocycle ring to which the force is applied is displayed in red. The simulations were performed by Dr. Michael Matthies and Professor Petr Šulc at the Arizona State University.

As shown in Figure 3-22, in the presence of 10, 20, 30 or 40 pN force exerting on the macrocycle, the simulated position plots of the macrocycle relative to the pinned point of axle present two stall points, which are located at the end of the axle and at the middle of the downstream stopper, while there is a "tail" curve for the macrocycle dethreading. Even in the case of 10 pN (twice less than the actual force that T7RNAP can apply<sup>122</sup>), dethreading of the macrocycle can be observed. And a representative state prior to the dethreading is shown in Figure 3-23, in which some of the stacking bonds of the ring stopper breaks owing to the constant stress from exerted force. The dethreading of the macrocycle can be observed in the presence or absence of a reporter strand (same sequence with HEX-ODN1, Supporting Table 1) that can bind to the macrocycle and contract it to a small dimension.

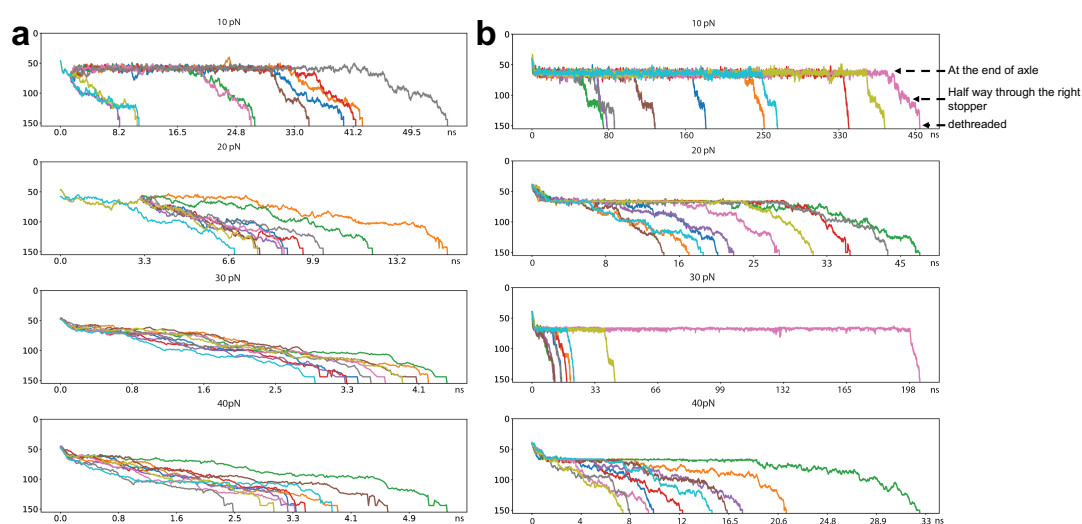


Figure 3-22. Simulations of rotaxane in the presence of 10, 20, 30 or 40 pN force exerting on the macrocycle. (a) and (b) Macrocycle position plots of half of the rotaxane axle pinned to one point with four constant forces pushing against the macrocycle ring for ROT without and with reporter ODN respectively. Position of the macrocycle is plotted on the y-scale, x-scale denotes the simulation time point. A position past 150 denotes dethreading of the macrocycle of the rotaxane structure. The simulations were performed by Dr. Michael Matthies and Professor Petr Šulc at the Arizona State University.

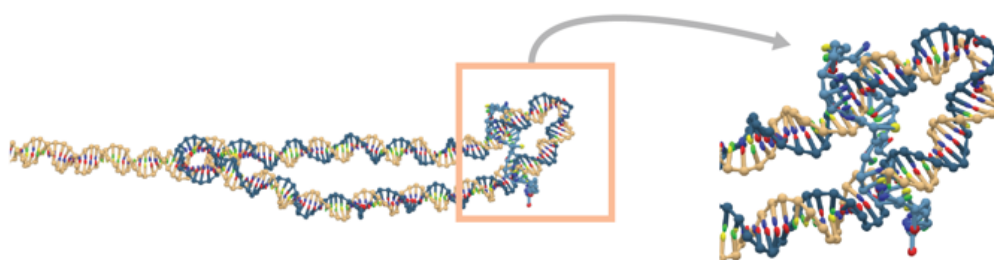


Figure 3-23. A representative state prior to the dethreading during simulation.

However, the above-mentioned gel experiments and AFM measurements of the investigation on the macrocycle dethreading supported that dethreading of the macrocycle in the rotaxane with ring stoppers is less likely to happen or may occur in a very small fraction (Chapter 3.1.8). Compared to the experiment results, the simulations indicated that the macrocycle dethreading has a high possibility to occur in the system of the rotaxane with ring stopper. One possible reason is that the simulations did not consider the presence of two terminator sequences located at the end of axle in tandem and would underestimate the robustness of subsequent three-way junction from the ring stopper, which have enough capability to terminate or stop the transcription and prevent the T7RNAP from continuing to push the macrocycle over the downstream stopper. The simulations were performed by Dr. Michael Matthies and Professor Petr Šulc at the Arizona State University.

---

## 3.2. Spherical stopper (SST) optimization for the rotaxane actuator

Inspired by the previous work on DNA rotaxane, the spherical stopper (SST) that consists of two dsDNA ring and connect by 4-way junctions can prevent the macrocycle from dethreading and therefore improve the dynamic stability of DNA rotaxane.<sup>58</sup> Hence, in this chapter, a spherical stopper that combines two 168 dsDNA rings was used to displace the ring stopper attached to the downstream axle of the original rotaxane. The transcription behavior of this SST optimized rotaxane was evaluated and compared to the original one. And modelling simulation verified the better performance of SST in preventing the macrocycle from dethreading.

### 3.2.1. Design and assembly of the SST-optimized rotaxane

The design of SST-optimized rotaxane is basically the same as the original rotaxane except for an SST instead of a ring stopper (Figure 3-24). The axle and macrocycle are kept unchanged in this design and can still initiate the transcription when the macrocycle is hybridizing with the axle.

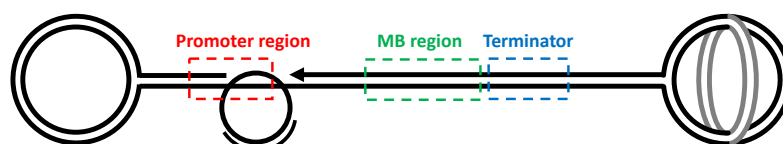


Figure 3-24. The design of the SST-optimized DNA rotaxane.

For the assembly of the spherical stopper, two component DNA rings of spherical stoppers were first assembled separately as ring stoppers without further purification. Two halves were mixed together subsequently and heated the mixture to 35 °C then annealed to room temperature programmatically. The crude products of the spherical stopper were also purified by HPLC (Supporting Figure 2 for the AFM images of purified SST). The assembly process of rotaxane with a spherical stopper is similar to that of rotaxane with ring stoppers. The assembly of rotaxane with spherical stoppers was verified by agarose gel and AFM (Figure 3-25, Supporting Figure 3 for the supplementary images of rotaxane with one SST).

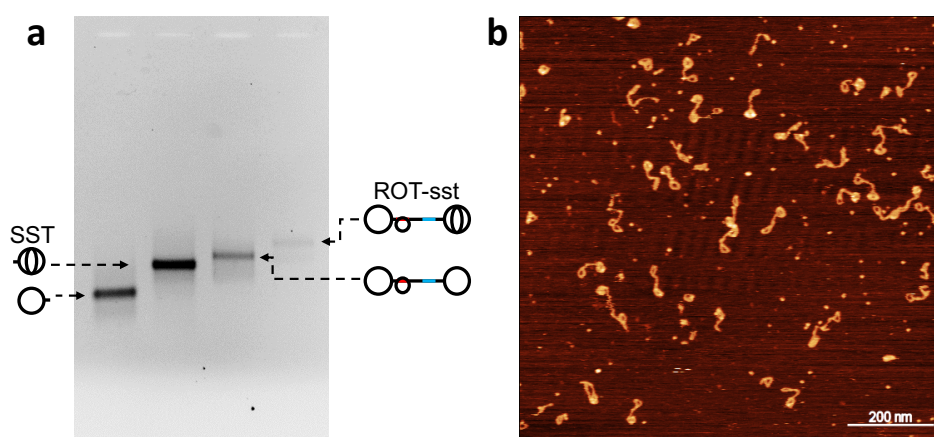


Figure 3-25. (a) Gel analysis (agarose, 1%, 20 min at 160 V) of spherical stopper (SST) and rotaxane with a spherical stopper (ROT-sst). (b) AFM measurement of ROT-sst.

### 3.2.2. Transcription behavior and comparison

The transcription of the rotaxane with one spherical stopper was used to compare with the original rotaxane with two ring stoppers. As shown in Figure 3-26, the signal of the rotaxane with one spherical stopper is almost the same as that of the rotaxane with two ring stoppers (green and red). However, in the presence of the pGO that can fill the promoter gap in both cases, the signal of the former is a bit lower than the latter (magenta and blue), probably due to the less purity of the sample of the rotaxane with one spherical stopper. Overall, the transcription of the SST-optimized rotaxane shows the similar pattern with the original rotaxane.

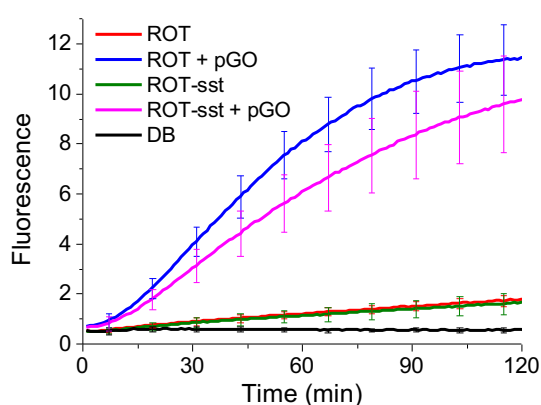


Figure 3-26. MB fluorescence experiment for the comparison of transcriptional behavior between original rotaxane and ROT-sst. MB fluorescence of transcriptions dumbbell structure (black), rotaxane (ROT, red), rotaxane adding promoter gap ODN (ROT + pGO, blue), rotaxane with spherical stopper (ROT-sst, green) and ROT-sst adding pGO (magenta) at 20 nM template concentration. The macrocycle is always

---

bound with a biotin-ODN in this experiment. Error bars: S.D., n = 3.

### 3.2.3. Investigation of the dynamic stability of the macrocycle in the SST-optimized rotaxane by molecular dynamics simulations

The SST-optimized rotaxane was also investigated by modelling simulation (Supporting Table 5). The setup of the model and simulation were exactly the same as the previous regime (chapter 3.1.9). Figure 3-27 presented a representative initial state of this system. And as shown in Figure 3-28, the macrocycle position plots indicate that the system is stable during the modelled time and does not dethread. As the simulated time for this system is twice as long as the simulated time for the previous design, it can be concluded that the macrocycle is unlikely to dethread in this design.

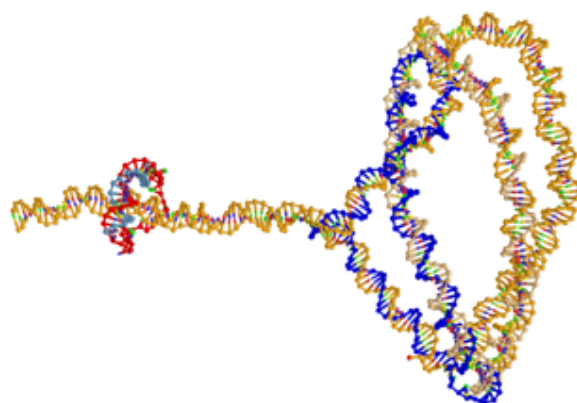


Figure 3-27. Representative initial state of the macrocycle force pushing experiments for ROT-sst with reporter ODN. Strands corresponding to half of the rotaxane are marked as yellow and blue. The macrocycle ring to which the force is applied is displayed in red. The hybridized reporter oligonucleotide is shown in light blue.

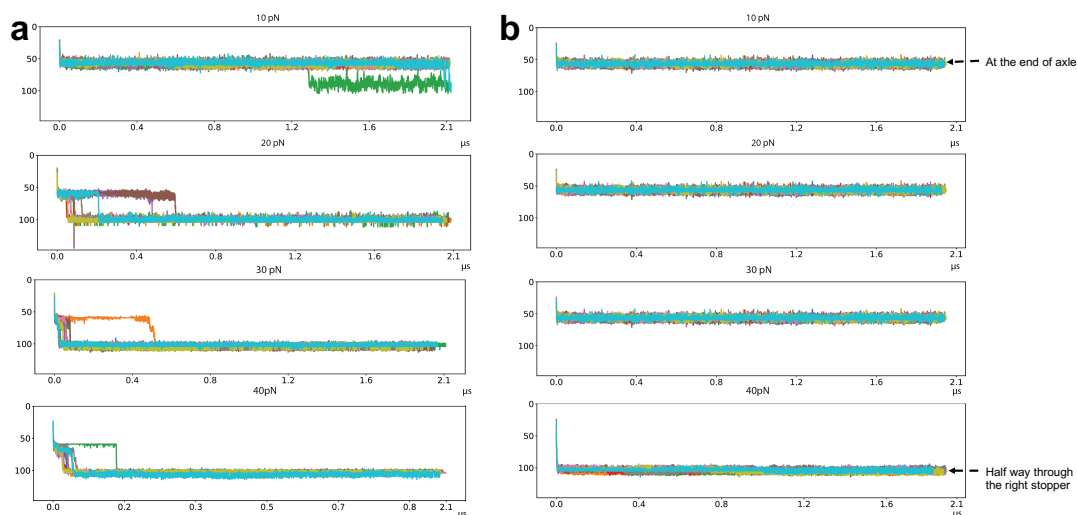


Figure 3-28. Simulations of ROT-sst in the presence of 10, 20, 30 or 40 pN force exerting on the macrocycle. (a) and (b) Macrocycle position plots of half of the rotaxane axle pinned to one point with four constant forces pushing against the macrocycle ring for ROT-sst without and with reporter ODN respectively. Position of the macrocycle is plotted on the y-scale, x-scale denotes the simulation time point. A position past 145 denotes dethreading of the macrocycle of the rotaxane structure. Position 60 corresponds to the axle end. Position 100 corresponds to the stopper ring. The simulations were performed by Dr. Michael Matthies and Professor Petr Šulc at the Arizona State University.

---

### **3.3. Investigation of macrocycle-mediated promoter properties**

The transcriptional behavior of the rotaxane actuator system is highly dependent on the construction of the macrocycle-mediated promoter. Hence, it is important to investigate the structural characteristic of this macrocycle-mediated promoter and its interaction with T7RNAP. Essentially, the rotaxane actuator is activated by filling the ss-gap region in the promoter region of the rotaxane axle. A promoter gap ODN (pGO) can cover this gap and restore the transcription of the system. The macrocycle contains the sequence of pGO, and at the same time, extends it and forms a closed loop. The effect of the tightly looped structure of macrocycle on the transcription of rotaxane actuator remains obscure. The direct comparison between activation strands (macrocycle, linear template of macrocycle, and pGO) for this system provides an insight into the properties of the macrocycle-mediated promoter.

#### **3.3.1. Design and assembly**

In this chapter, the design of the rotaxane system is essentially the same as the original rotaxane actuator, except that the ss-gap region on the axle is reduced to 10 nt (Figure 3-29). In this case, the activation strands (macrocycle, linear template of macrocycle, and pGO) can be compared directly as all elements have the same hybridization region (-5 to +5 relative to the transcription starting point, marked in red in Figure 3-29). Two ring stoppers are used in this design and the macrocycle remains unchanged. The macrocycle with its splint ODN (that has the same sequence with biotin-ODN and does not interfere with the hybridization between the macrocycle and the axle) is also included in the comparison, as a reporter strand is often required to monitor the status of the macrocycle and also to increase the rigidity of the macrocycle in the original design.



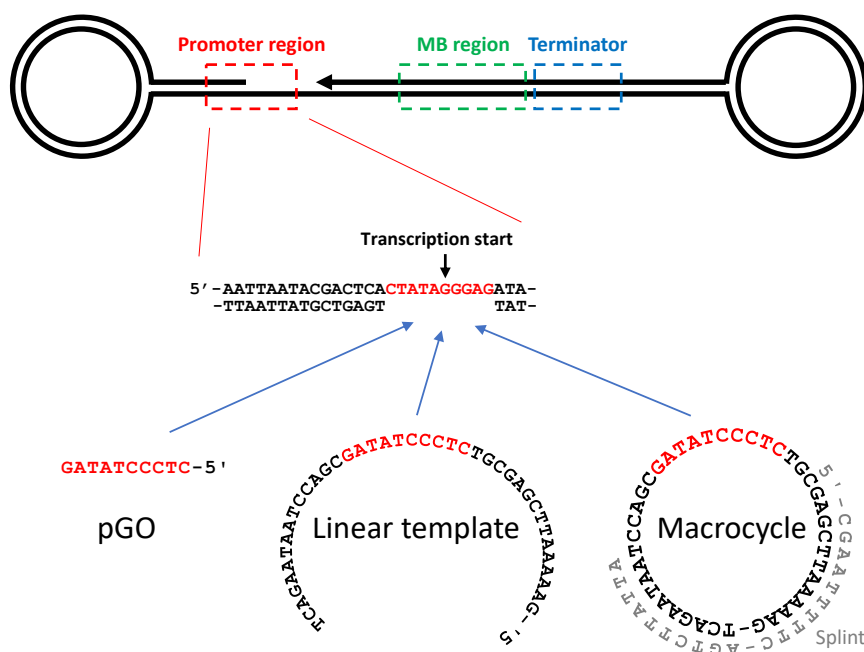


Figure 3-29. Schematic representation of the dumbbell/rotaxane system. The sequence of the promoter region of the axle containing 10 nt ss-gap region, and the sequences of activation strands for this design (pGO, linear template of macrocycle, and macrocycle with its splint ODN). The sequences for hybridization between the promoter gap and activation strands are marked in red.

The assembly of the macrocycle is the same as previously described (in chapter 3.1.2). Weak anion exchange (WAX) HPLC purification is applied to purify the macrocycle for a higher production yield, while NaOH (0.2 M) is used to denature the macrocycle-splint complex to obtain the ss-macrocycle (Figure 3-30a). The formation of ss-macrocycle and its hybridization with the axle were verified by PAGE gel electrophoresis (Figure 3-30b).

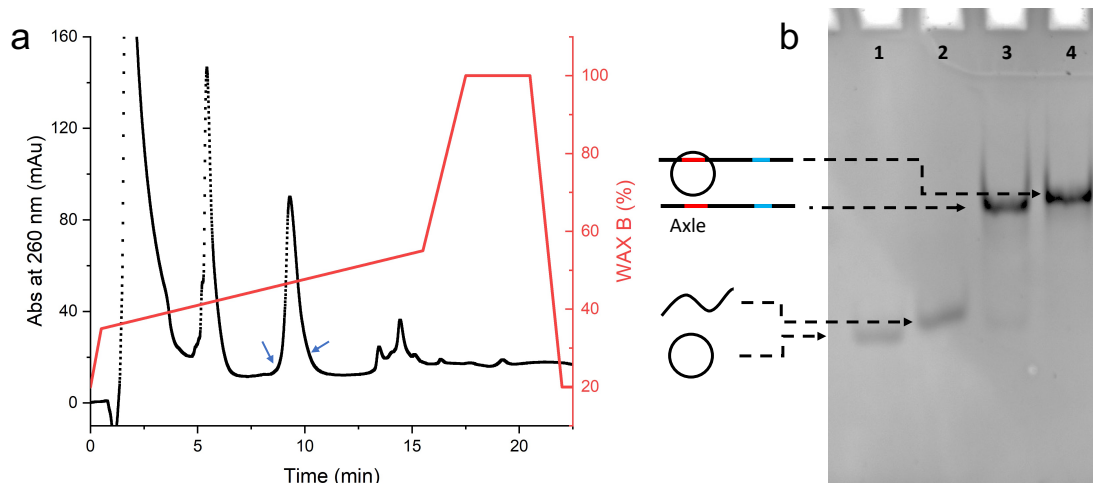


Figure 3-30. (a) HPLC purification for the macrocycle. The peak between two blue arrows was collected. (b) Gel analysis (PAGE with 10 mM MgCl<sub>2</sub>, 9%, 45 min at 150 V) of the formation of macrocycle and its hybridization with the rotaxane axle.

The rotaxane is assembled by capping method as described in chapter 3.1.2 and purified by weak anion exchange (WAX) HPLC (Figure 3-31a). The correct assembly of rotaxane was verified by agarose gel electrophoresis (Figure 3-31b). The threading of macrocycle can be confirmed by a bit slower mobility in gel analysis compared to the dumbbell structure without threading macrocycle (Figure 3-31b, lane 4 and lane 3). It is worth noting that the macrocycle still cannot hybridize to the dumbbell structure from outside (non-threading) in this condition (Figure 3-31b, lane 5).

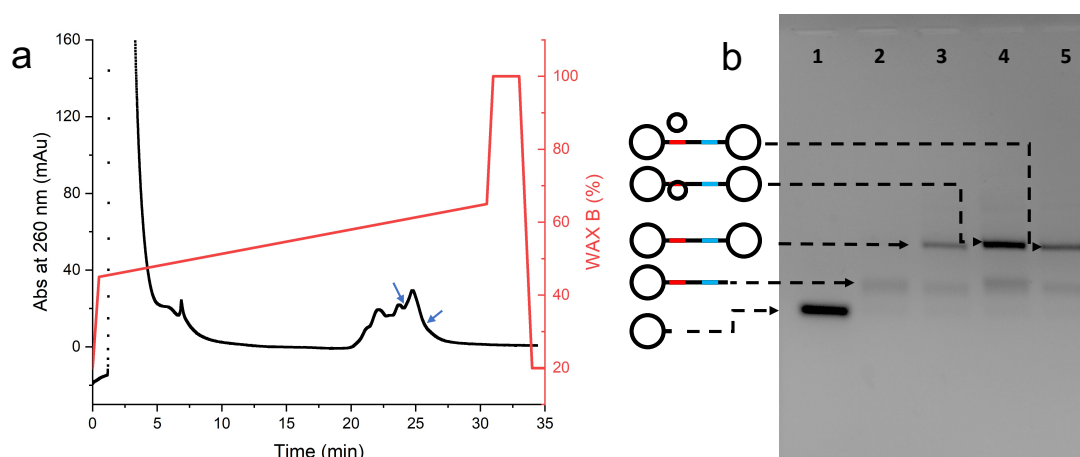


Figure 3-31. (a) HPLC purification for the rotaxane. The peak between two blue arrows was collected. (b) Gel analysis (agarose, 2.5%, 120 min at 80 V) of rotaxane assembly. Lane 1, left stopper; lane 2, assembly of left stopper and the axle; lane 3, dumbbell structure; lane 4, rotaxane; lane 5, dumbbell structure with outside macrocycle.

AFM was performed to further demonstrate the formation of the rotaxane. As shown in Figure 3-32, in the presence of biotin-ODN and streptavidin, several dumbbell-shaped structures, each with a bright dot, were observed on the mica surface, which indicated the formation of the designed DNA rotaxane.

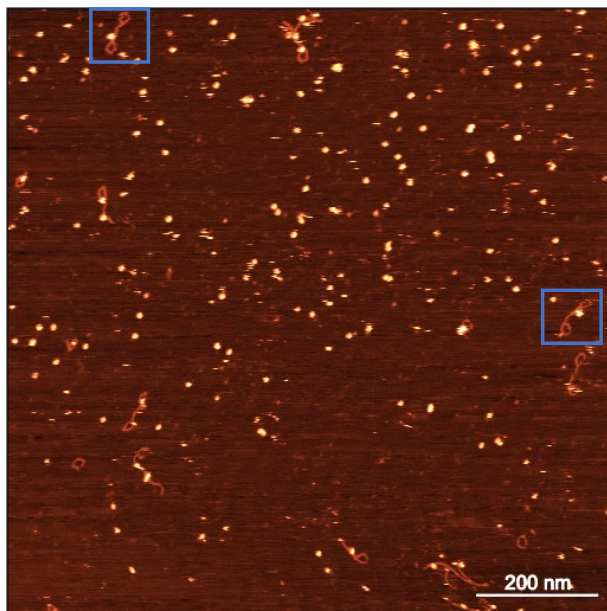


Figure 3-32. AFM measurement of the rotaxane with biotin ODN and streptavidin.

### 3.3.2. Transcriptional behaviors

The real-time MB fluorescence experiments were performed to compare the transcription performances of dumbbell or rotaxane systems with different activation strands at the same concentration: the non-threading ss-macrocycle with and without its splint ODN, the linear template of macrocycle, pGO with and without ligation, and rotaxane (threading macrocycle) with and without the splint ODN of macrocycle. As shown in Figure 3-33a, MB fluorescence signals were increasing during the 120-min transcription. Figure 3-33b shows the relative transcription rates calculated from Figure 3-33a for a better comparison.

As a negative control, the dumbbell structure lacking the macrocycle that contains the essential part of the promoter region presents a negligible signal of transcription (black). As a positive control, the dumbbell with ligated pGO, which has the complete promoter sequence, shows a dramatically increasing signal during transcription (brown). Its transcription rate was utilized to normalize all other signals in Figure 3-33b. The dumbbell in the presence of pGO (purple) or the linear template of macrocycle (green) shows similar results with the negative control. Both rotaxane with threading ss-

macrocycle (dark yellow) and dumbbell with non-threading ss-macrocycle (red) exhibited similar levels of increasing transcription signals. Their signal levels are much lower than the positive control but higher than the dumbbell with pGO or the linear template of macrocycle. In the presence of splint ODN that can bind to the macrocycle, the signal of rotaxane with threading macrocycle remains unchanged (cyan), whereas the signal of dumbbell with non-threading macrocycle is reduced a lot (blue).

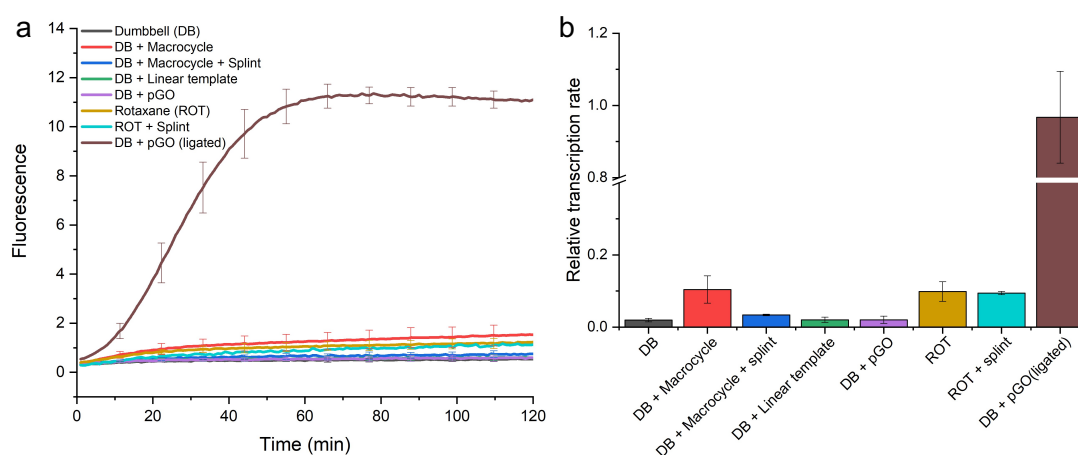


Figure 3-33. Molecular beacon (MB) fluorescence experiment for the transcriptional behaviors of the rotaxane/dumbbell systems in the presence of different activation strands at the same concentration. (a) Transcription of dumbbell (black), dumbbell with non-threading ss-macrocycle (red), dumbbell with non-threading macrocycle and splint ODN (blue), dumbbell with the linear template of macrocycle (green), dumbbell with pGO (purple), rotaxane (dark yellow), rotaxane with splint ODN (cyan), and dumbbell with pGO (ligated, brown) at 25 nM template concentration. Error bars: S.D.,  $n = 3$ . (b) Relative transcription rates from (a), same colors as in (a).

To further compare those cases with low fluorescence signals, the dumbbell systems were tested in the presence of 4 equivalent activation strands (Figure 3-34). Dumbbell (black) and dumbbell with ligated pGO (dark yellow) are also used as negative control and positive control, respectively. Dumbbell with pGO begins to present a certain fluorescence signal of transcription in this condition (purple). The signal level of the dumbbell with linear template of the macrocycle is even lower than the dumbbell with pGO (green). Dumbbell with non-threading ss-macrocycle shows higher signal level of transcription but still much lower than the positive control (red). In the presence of splint ODN, the signal of the dumbbell with non-threading macrocycle (blue) is also reduced but is higher than the dumbbell with pGO. In contrast, in the presence of splint ODN, the signal of dumbbell with ligated pGO remains unchanged (cyan), indicating that the splint ODN cannot repress the transcription directly and it should take effect by the

hybridization with ss-macrocycle.

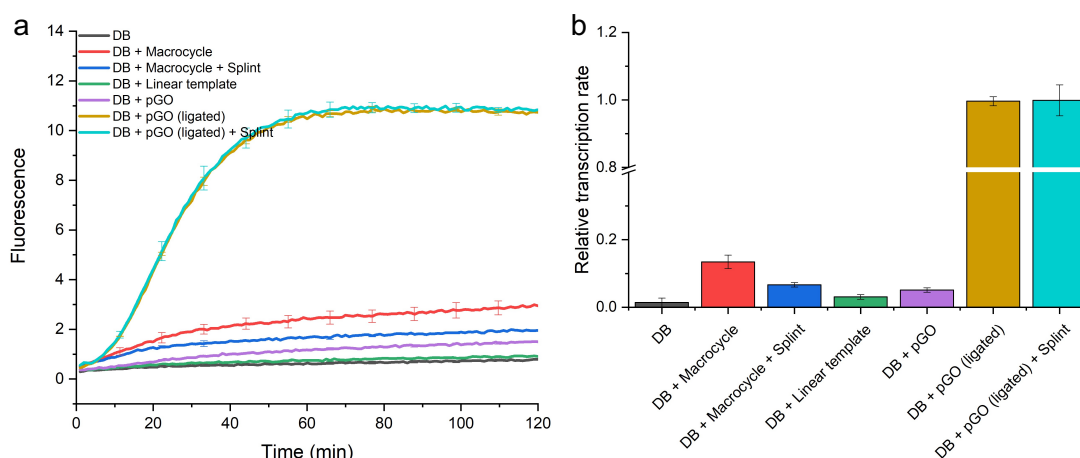


Figure 3-34. Molecular beacon (MB) fluorescence experiment for the transcriptional behaviors of the dumbbell systems in the presence of 4 equivalent of different activation strands. (a) Transcription of dumbbell (black), dumbbell with non-threading ss-macrocycle (red), dumbbell with non-threading macrocycle and splint ODN (blue), dumbbell with the linear template of macrocycle (green), dumbbell with pGO (purple), dumbbell with pGO (ligated, dark yellow), and dumbbell with and pGO (ligated) and splint ODN (cyan) at 40 nM template concentration. Error bars: S.D.,  $n = 4$ . (b) Relative transcription rates from (a), same colors as in (a).

The transcription performance in this design is mainly affected by the interactions among a ternary system: T7RNAP-incomplete promoter-activation strands (macrocycle/linear template of macrocycle/pGO). T7RNAP can bind to the binding sites on the incomplete promoter region of the axle but cannot start transcription without activation strands containing the essential part of promoter sequence. Activation strands can fill the promoter gap of the axle (from -5 to +5) and activate the transcription of T7RNAP.

pGO can completely cover the promoter gap of the axle but restore a very low level of transcription. One possible reason is that the gap region contains the unwinding part of the T7 promoter which will be dehybridized by T7RNAP during transcription initiation. Thus, once transcription starts, the hybridization between pGO and promoter gap is less stable and pGO (only 10 bp) may be released by T7RNAP, thus depriving T7RNAP of its pathway to the downstream template.

The linear template of macrocycle has the additional overhangs beside the same sequence as pGO, which would introduce extra steric hindrance to the transcription

---

initiation of T7RNAP and thus reduce its transcription performance.

The macrocycle is a tightly looped structure. The hybridization between the non-threading ss-macrocycle and the promoter gap of axle is similar to the interaction between DNA hairpin structures in which a kissing-loop complex is formed.<sup>123</sup> The kissing-loop complex presents lower stability compared to canonical dsDNA, which should even decrease the possibility of interaction between non-threading macrocycle and the promoter gap and further reduce its transcription performance. However, the fluorescence signal of its transcription is higher than that of the dumbbell with pGO (unligated) or the linear template of macrocycle, suggesting that there should be additional interactions beside the hybridization between the non-threading macrocycle and the promoter gap of the axle.

Previous research has reported that T7RNAP has the possibility to bind to small circular ssDNA (even smaller than T7RNAP itself) and perform the rolling circle RNA synthesis independent on canonical duplex DNA promoter.<sup>124,125</sup> And in some cases, the polymerase recognizes specific structures rather than the specific sequences. The small circular ssDNA mimics the transcriptional bubble structure that may attract polymerase binding.

Thus, combining the interaction between T7RNAP and incomplete promoter on the axle and the possible interaction between T7RNAP and circular ssDNA (ss-macrocycle), this trinary system could be relatively stable to start transcription.

The interactions in rotaxane with threading macrocycle are even complicated, which should include the hybridization between the macrocycle and promoter gap, the possible interaction between T7RNAP and the ss-macrocycle, and "catenand" effect in the interlocked rotaxane system. Unlike the kissing-loop complex between non-threading ss-macrocycle and the promoter gap, the threading macrocycle can bind to the gap region with higher stability. However, the intrinsic curvature of the macrocycle would bend the corresponding promoter structure, which could affect the recognition of T7RNAP and compromise its transcriptional performance.

A reporter strand (splint ODN at here) that binds to the free part of the ss-macrocycle but does not interfere with the hybridization of the macrocycle with the ss-gap region of the axle, is usually required to monitor the macrocycle. Based on the results, in the presence of splint ODN, the transcription performance of the dumbbell with the non-threading macrocycle is much reduced, whereas the transcriptional ability of the rotaxane remains unchanged. And the splint ODN cannot directly repress the transcription of T7RNAP. Thus, the hybridization between splint ODN and the ss-

macrocycle is the key point. The hybridization of the splint ODN with the macrocycle enhances the rigidity of the single-stranded structure of the macrocycle, while increasing the internal tension compared to the ss-macrocycle, which would affect the ability of the macrocycle-splint complex to bind to the promoter gap of axle. In addition, the partially double-stranded structure of the macrocycle-splint ODN complex would also affect the possible interaction between the T7RNAP and circular ssDNA.

Comparing these two systems, the rotaxane with the threading macrocycle can provide stable transcription performance, even in the presence or absence of reporter strands.

To sum up, the comparison of transcription behavior between above systems reveals several factors that influence the transcription performance of this macrocycle-mediate promoter: 1) the stability of hybridization between macrocycle and the promoter gap of axle; 2) hybridization mode (threading or non-threading); 3) the addition of reporter strands; 4) the possible interaction between T7RNAP and the macrocycle.

---

## 4. Discussion and Outlook

### 4.1. Design and mechanism

Two challenges inevitably arise when designing DNA rotaxanes. **One is the stability of the macrocycle threading.** The macrocycle should hold a suitable dimension relative to the bulky stoppers to ensure that it will not dethread when the rotaxane transfers from the hybridized state to the interlocked state. As described in the first DNA rotaxane paper, the lifetime of the macrocycle threading is highly dependent on the size ratio of the macrocycle/stopper.<sup>58</sup> For the rotaxane with 105bp-macrocycle / 168bp-stoppers, the lifetime of the macrocycle threading is around 3 hours. The present project is more demanding in terms of the size of the macrocycle to stay threaded, as the macrocycle not only needs to thread on the axle but also be subjected to the T7RNAP, which will constantly collide with the macrocycle during transcription.

Moreover, in this work, the macrocycle is designed to be 40 nt, which is small enough to be obstructed by two 168 bp dsDNA ring stoppers and even to be blocked by T7RNAP. A 20 nt reporter ODN can be used to contract the macrocycle to an even smaller size. An excessively long double-stranded part of the macrocycle will certainly enhance the tension in the macrocycle, but this will also increase the difficulty of achieving hybridization between the macrocycle and the promoter gap. Therefore, the reporter ODN can only be added after assembly and when necessary.

Several experiments were conducted to confirm the dynamic stability of this rotaxane actuator in the interlocked state. The gel analysis set out in Figure 3-5 shows that by adding RO to release the macrocycle and transfer the rotaxane from the hybridized state to the interlocked state, the macrocycle is still threaded on the axle of the rotaxane. Further, Figure 3-19c rules out the case in which the macrocycle hybridizes to the promoter gap from the outside. This is also consistent with the results of the modelling simulation without external forces (Figure 3-20).

T7RNAP will exert an external force (~25 pN) on the macrocycle.<sup>122</sup> A model investigation of the effect of the external forces (from 10 to 40 pN) on the macrocycle threading shows that the dethreading happens in all cases. However, the gel analysis and AFM measurements in Figure 3-17 to Figure 3-19, indicate that the dethreading of the macrocycle may occur following transcription but is in a small margin and should not seriously affect the performance of the system. Possible reasons for this discrepancy are the presence of two tandem terminator sequences in the downstream



portion of the axle and the fact that the simulation might underestimate the robustness of the subsequent three-way junction from the ring stopper.

The use of spherical stoppers unambiguously solves this issue. According to previous reports, the rotaxane with spherical stoppers can maintain the interlocked stability, even after seven days.<sup>58</sup> This coincides with the modelling simulations detailed in section 3.2, where the macrocycle is constantly threading with respect to the downstream spherical stopper while external forces (10 to 40 pN) are present. As such, it can be concluded that the macrocycle is unlikely to dethread in this design.

Another challenge of the rotaxane design is **how to integrate it with practical applications**. Rotaxanes are always designed to switch between static and mobile states, or between two "stations" (two static states), by introducing external stimuli.<sup>117</sup> For DNA rotaxanes, the stimuli can take the form of an external DNA strand with the help of strand displacement, H<sup>+</sup> and cations that can induce conformational change in DNA, light with the help of azobenzene-modified bases, and even temperature.<sup>58,61,74,126</sup> It is easy to achieve precise control by adding external stimuli; even so, it still suffers from additional manipulation and cannot be easily automated due to a lack of autonomous dynamic elements. One of the advantages of DNA is its biocompatibility and potential to interact with other biomolecules, such as proteins, which can be used to generate directional forces to create biohybrid artificial nanostructures capable of autonomous and repetitive motion.

By combining DNA rotaxane with T7RNAP, this work demonstrates the effectiveness of an automated linear actuator, where the linear motion of T7RNAP along the DNA track can be transferred to the translational displacement of the macrocycle in the rotaxane.

During transcription, T7RNAP will unwind part of the DNA template, making it possible to release the DNA macrocycle from its hybridized position, thus switching the rotaxane from the static state to the mobile state. Notably, the subtle design of the hybridization position of the macrocycle also matters in this instance. As mentioned above, the T7 promoter is made up of three parts: two binding sites for the T7RNAP and an unwinding region which prepares for the transcription initiation. Theoretically, all locations in the DNA template between the unwinding region of the promoter and the downstream terminator sequences are able to be unwound by T7RNAP during transcription. As reported, T7RNAP is able to bypass any gaps less than 10 nt on the DNA template, although it does so with very low efficiency. It is possible that T7RNAP may stall at the margin of a gap in the coding region of the DNA template and cannot release the

---

macrocycle hybridizing with that gap. To ensure the macrocycle can be released by T7RNAP, it is best to place the macrocycle in the unwinding region of the T7 promoter for hybridization. Furthermore, the fluorophore quenching experiments in section 3.1.6 demonstrate that the macrocycle can be released during transcription.

Another question arises here as to which direction the macrocycle will move in after it is released. In this work, the macrocycle is expected to move in the direction of transcription and reach the downstream part of the axle. Otherwise, the macrocycle would rehybridize with the promoter gap immediately following release. Hence, part of the macrocycle is designed to participate in the unwinding event of initiation, while the remaining part of the macrocycle is located outside the promoter region to ensure that once released, the macrocycle will move towards the downstream axle. A suitable dimension of the macrocycle is another prerequisite to ensure that the macrocycle can be effectively confined by the T7RNAP and the downstream stopper. In this way, the T7RNAP moves along the axle unidirectionally, while the margins that macrocycle can move become gradually smaller, resulting in an overall displacement of the macrocycle from its original anchoring region to the terminator sequences of T7RNAP in the downstream axle.

In this design, as the macrocycle contains a fragment of the promoter sequence in the template strand that is necessary to initiate transcription, the hybridization of the macrocycle to the promoter gap is a precondition for starting transcription. In other words, the hybridization of the macrocycle can directly control the transcription. Investigations into the transcription behavior of the rotaxane actuator demonstrated that only the hybridization of the macrocycle can initiate transcription; in the absence of the macrocycle, the transcription can almost completely shut down (Figure 3-8 and Figure 3-12).

All of the above processes happened within a designed operation cycle of the DNA rotaxane actuator. As long as the NTP-fuel necessary to power transcription is present, this cycle can run repetitively and autonomously with an automated pulsatile movement of the macrocycle. The system has the potential to be developed as an automatic linear machine, such as a transport system analogous to the microtubules along which the kinesin travels. Its limitations are the length, stiffness of the axle, and the position of terminator sequences, which determine its stability, effectiveness, and usefulness as a transmission system.

## 4.2. The factors that affect the transcription rate in the rotaxane actuator

It is worth discussing the factors that affect the transcription rate in this rotaxane actuator. In this actuator, an operation cycle can be divided into four stages: transcription initiation, elongation, termination, and macrocycle rehybridization.

The introduction of the macrocycle-mediated promoter in this system is the most important factor affecting initiation efficiency. The stability of hybridization between the macrocycle and the promoter gap is the basis for the transcriptional performance of this reconstructed promoter. A threading macrocycle can provide a stable performance in this transcription system. However, it is evident that the small ring shape of the macrocycle leads to an intrinsic bend in the promoter region, creating a three-dimensional distortion in the sequence. Furthermore, the fact that the macrocycle has to be displaced from the promoter region during the transcription introduces additional steric hindrance to the polymerase transcription initiation. In particular, a  $\beta$ -hairpin loop of T7RNAP intercalating into the interval between base pairs -4 and -5,<sup>106</sup> manipulating the melting of the promoter sequence at initiation, is definitely affected by the steric hindrance from the macrocycle loop. When taken together, all these characteristics will reduce the initiation efficiency. A possible interaction between T7RNAP and the circular ssDNA (the macrocycle at here) could increase the stability of the interaction among the ternary system: T7RNAP-incomplete promoter-macrocycle, which would promote a better performance of transcription in this system. However, this interaction requires further investigation.

In comparison, elongation of transcription is a rapid process that should not be a negative factor impacting the whole transcription rate.

Termination occurs when the T7RNAP encounters a signal from a specific sequence, i.e., the terminator. In this design, two tandem class II terminator sequences are set up in the downstream axle. Based on the results in previous reports, each class II terminator provides an approximately 55% termination efficiency.<sup>112</sup> Two successive terminators can ensure approximately 80% efficiency in stopping transcription. Moreover, the comparison of rotaxanes with and without terminator sequences in section 3.1.8 indicates that the presence of terminators significantly influences the transcription rate. This makes sense because the T7RNAP is very likely to stall at the end of the downstream axle and the macrocycle is cornered in a small place between the T7RNAP and the stopper for a longer period of time before the system is allowed

---

to reset. Therefore, the presence of terminators helps to complete the transcription cycle by detaching the T7RNAP from the axle and allowing the macrocycle to rehybridize to the promoter gap and restart the transcription process.

The time consumed by macrocycle rehybridization was also estimated by using the macrocycle to hybridize to a half-dumbbell structure of the rotaxane. The half-life of macrocycle hybridization was calculated to be  $99.0 \pm 6.9$  s. For the interlocked macrocycle in the rotaxane, the rehybridization time should be less than this figure, because the interlocked nature renders the reactants co-localized.<sup>48,120</sup> Once released, rehybridization of the interlocked macrocycle is faster than the non-interlocked macrocycle, which requires more time to locate its binding site in the bulky solution.

In summary, in light of the negligible impact of the elongation step, the influence of the macrocycle-mediated promoter on T7 RNAP recognition and transcription initiation, and the reconstitution of the promoter after one transcription cycle, as well as the presence of terminator sequences, significantly influence the transcription rate.

### 4.3. Interlocked macrocycle-mediated transcriptional control

Gene expression is a fundamental process taking place in all organisms. In this process, genetic information is decoded from DNA to produce various proteins with different physiological functions. To avoid unnecessary waste of material and energy as well as toxicity to the host cell, a delicate regulatory mechanism is essential for the expression of each gene expression.<sup>88</sup> In the process of moving from DNA to protein expression, transcriptional control ensures that the process does not produce excess intermediates. Therefore, in the context of an artificial gene expression system, transcriptional regulation is paramount.

In addition to protein regulators, nucleic acid-based regulators are also emerging. One prevalent example is STARs (small transcriptional activating RNAs), which can regulate expression at the transcriptional level by applying a small non-coding RNA to hybridize to RNA transcript encoded by DNA terminator sequence. This prevents the RNA transcripts from forming a hairpin structure, therefore suspending the termination and continuing transcription elongation.<sup>92</sup>

Few DNA-based regulatory components have been reported, most of which are based on manipulating the interactions between RNAP and the related promoter sequence to realize more favorable binding of RNAP to the DNA template, by complementing an incomplete promoter region.<sup>95-97</sup> Notably, one limitation is the sequence of the promoter, such as the promoter for T7RNAP, which is relatively conserved and does not allow much modification. Previous research has focused on the upstream region of the promoter sequence, making it single-stranded to function as an anchor for its complementary sequence-RNAP fusion to activate the transcription upon binding. However, this approach is both complicated and costly.<sup>98</sup>

Another limitation is that, to activate transcription, a strand containing part of the promoter sequence should be added manually, thus reducing the integrity of the system. Moreover, its single-stranded nature means it is less likely to be sufficient stable in vivo.<sup>127</sup>

The design of an interlocked macrocycle-mediated promoter offers the possibility of achieving a fully DNA-based regulatory element with high integrity. As described above, the control of transcription through this system is based on the incomplete promoter sequence with a single-stranded gap region. The sequence on the macrocycle can fill

---

the gap and complete the double-stranded promoter sequence, which can subsequently be recognized by T7RNAP and activate transcription. Moreover, the design ensures that once transcription begins, T7RNAP can release the macrocycle from the promoter gap and restrict it to the downstream direction. This will block the macrocycle from returning to its anchor site, thus preventing further transcription. With the help of downstream terminator sequences, transcription stops and T7RNAP detaches. Owing to its interlocking nature, the macrocycle wanders and hybridizes to its original binding site driven by the one-dimensional Brownian motion. Rehybridization of the macrocycle resets the promoter, serving as a prerequisite for T7RNAP recognition and the initiation of a new transcription cycle.

Unlike the transcriptional regulation achieved by the addition of external stimuli, the interlocked macrocycle-controlled transcription is self-regulated and fully automated without the need for any intervention, as long as the NTP-fuel is available. Also, unlike the regulation by feedback circuits, this design regulates at the level of transcriptional initiation and does not produce any intermediate to realize the regulation. However, it is also possible to combine this system with feedback circuits. If the generated RNA transcript contains the releasing sequence for the macrocycle, then the accumulation of RNA will gradually block the hybridization of the macrocycle with the promoter gap, thus establishing a product-controlled negative feedback inhibition mechanism and preventing new transcription cycles from initiating. In this case, the system has the potential to develop self-regulating artificial RNA (mRNA, ncRNA, or miRNA) expression systems with integrated transcriptional controls that can be used as biocompatible automatons.

Finally, the construction of such interlocked macrocycle-mediated promoter has the potential to be incorporated into other gene expression systems, by simply transplanting the promoter design into target systems. The design also benefits from the macrocycle, a small circular DNA, which is relatively stable, even in the cellular environment. This makes it possible to apply the design in cells.

## 5. Materials and methods

### 5.1. Reagents

Reagents	Distributor
Oligodeoxynucleotides (ODNs)	Metabion, Ella Biotech or Microsynth
Milli-Q H <sub>2</sub> O	Barnstead Micro Pure; Thermo Fisher Scientific
10x T4 DNA ligase buffer	Thermo Fisher Scientific
T4 DNA ligase	Thermo Fisher Scientific
Tris	Carl Roth
MgCl <sub>2</sub>	Carl Roth
NaCl	Carl Roth
NaOH	Carl Roth
HCl	VWR Chemicals
Acetic acid	VWR Chemicals
EDTA	Panreac AppliChem
Glycerin	Carl Roth
Bromophenol blue	Carl Roth
Xylene cyanol	Merck
Poly-L-ornithine	Sigma Aldrich
Polyehylenimine	Polysciences
Acrylamide/bisacrylamide	Carl Roth
Ammonium persulfate (APS)	Carl Roth
Tetramethylethylenediamine (TEMED)	Carl Roth
Ethidium bromide (EtBr)	Carl Roth
Agarose	Carl Roth
NTPs	Jena Bioscience
RNasin	Promega
Dimethyl sulfoxide (DMSO)	Honeywell
Tris-HCl	Carl Roth
Mg(OAc) <sub>2</sub>	Sigma-Aldrich
Boric acid	Carl Roth

NTC buffer	MACHEREY-NAGEL
NT3 buffer	MACHEREY-NAGEL
NE buffer	MACHEREY-NAGEL

## 5.2. Buffer systems

Buffer	Recipe
10x DA buffer	100 mM Tris-HCl, 500 mM NaCl, 100 mM MgCl <sub>2</sub> at pH 7.5
1x DA buffer	10 mM Tris-HCl, 50 mM NaCl, 10 mM MgCl <sub>2</sub> at pH 7.5
WAX A buffer	20 mM Tris-HCl at pH 9
WAX B buffer	20 mM Tris-HCl, 1 M NaCl at pH 9
10x TAE buffer	400 mM Tris, 200 mM acetic acid, 10 mM EDTA
1x TAE buffer	40 mM Tris, 20 mM acetic acid, 1 mM EDTA
1x TBE buffer	90 mM Tris-borate, 2 mM EDTA
6x loading buffer	H <sub>2</sub> O (70 %), glycerol (30 %), bromophenol blue, xylene cyanol
1x Diffusion buffer	500 mM ammonium acetate, pH 8.0, 0.1% SDS, 1 mM EDTA, 10 mM magnesium acetate
5x Transcription buffer	200 mM Tris-HCl, 15 mM DTT, 50 mM NaCl, and 10 mM spermidine, pH 7.9

## 5.3. Equipment

Equipment	Producer
Centrifuge	Eppendorf
Vortex mixer	Velp Scientifica
Photometer (Nanodrop)	Eppendorf
Thermocycler	Eppendorf
Incubator	Eppendorf
Centrifugal filter 30K	ThermoAmicon Ultra
Centrifugal filter 100K	ThermoAmicon Ultra
HPLC system	Agilent/Hewlett-Packard 1100 Series
HPLC columns	TSKgel DAEA-NPR
AFM system	JPK
Mica sheets	Plano



## Materials and methods

Metal stub	Plano
Magnetic sample holder	JPK
AFM cantilever (USC-F0.3-k0.3-10)	NanoWorld Innovative Technologies
PAGE gel setup	Bio-Rad
Agarose gel setup	Bio-Rad
Power supply	Consort
Gel documentation system	Perkin Elmer
384-well plate	Perkin Elmer
Plate reader (Enspire)	Perkin Elmer
Plate reader (Varioskan)	Thermo Scientific
Microwave oven	BOSH
pH meter	IonoLab
UV/vis spectrometer	Perkin Elmer
Pipettes	Eppendorf

---

## 5.4. Methods

### 5.4.1. UV Absorption Spectroscopy – concentration of ODNs and DNA assemblies

DNA presents a 260-nm characteristic absorption, which can be utilized to calculate the DNA concentration in solution. Lambert-Beer law:  $A = \epsilon \cdot b \cdot c$  is used to calculate the concentration of a DNA sample, where A is the absorbance or OD (optical density) of the sample, c is the target concentration which needs to be calculated,  $\epsilon$  is the extinction coefficient of the DNA sequences and b is the optical path length. For a DNA sample with specific sequence, the  $\epsilon$  can be calculated from the sum of the  $\epsilon$  of each nucleotide. The characteristic  $\epsilon$  values of nucleotides are as follow: A-15300 l/mol\*cm, T-9000 l/mol\*cm, C-7400 l/mol\*cm and G-11700 l/mol\*cm.

### 5.4.2. DNA annealing program

DNA samples were annealed in order to assemble sufficiently. After mixing the ODNs in tubes, and then place the tubes into a thermocycler and use specific programs for different samples.

Program 4: For DNA rings, samples were firstly heated to 95°C for 5 min, and then annealed from 60°C to 15°C in 75 min. And finally incubate at 4°C.

Program 15: For spherical stoppers, two ring components were firstly heated to 95°C for 5 min, and then cooled down from 60°C to 15°C in 150 min. And finally incubate at 4°C.

Program 16: For spherical stoppers, after mixing two halves, the samples were cooled from 35°C to 10°C in 60 min.

## 5.5. Gel electrophoresis

### 5.5.1. Agarose Gel Electrophoresis

The formation of rotaxane was analyzed using agarose gel electrophoresis (2.5% agarose gel, 0.5× TAE buffer, 70 min at 120 V). Spherical stopper and rotaxane with spherical stopper assemblies were analyzed using agarose gel electrophoresis (1%

agarose gel, 0.5× TAE buffer, 20 min at 160 V). All gels were stained with ethidium bromide and visualized by UV irradiation.

### 5.5.2. Polyacrylamide Gel Electrophoresis (PAGE)

RNA transcripts from transcription experiments were checked by urea gel (12%, 1× TBE buffer, 45 min at 200 V). And threading assemblies were analyzed by PAGE gel (9%, containing 10 mM MgCl<sub>2</sub> in 1× TBE buffer, 60 min at 150 V). All gels were stained with ethidium bromide and visualized by UV irradiation.

### 5.5.3. Macherey-Nagel Gel and PCR Clean-up kit

For a single-stranded macrocycle sample, after using a clean razor blade to cut the target band of the rotaxane from PAGE gel, chop the gel slice and place it into one filter cup from Macherey-Nagel Gel and PCR Clean-up kit. Add 200 mL of diffusion buffer to each 100 mg of crushed gel. Incubate at 37 °C overnight. Centrifuge at 14000 rcf for 1 min and transfer the filtrate to a new filter cup. Mix 400 mL NTC buffer with each 200 mL filtrate and centrifuge at 11000 rcf for 1 min. Use 500 mL NT3 buffer to wash (centrifuge at 11000 rcf for 1 min) twice. Finally elute the DNA samples from the filter by incubating with 30 mL NE buffer or water for 1 min, and then centrifuge at 11000 rcf for 1min. The filtrate is the concentrated solution of the target DNA sample.

### 5.5.4. Freeze 'n squeeze

For rotaxane samples used for AFM image, after using a clean razor blade to cut the target band of the rotaxane from agarose gel, chop the gel slice and place it into one filter cup from Macherey-Nagel Gel and PCR Clean-up kit. Then place the filter and sample at -80 °C freezer for 20 min. Spin the sample at 16000 rcf for 6 min at room temperature. Collect the purified DNA from the collection tube of the filter and use a 30K or 100K filter to concentrate.

## 5.6. High Performance Liquid Chromatography (HPLC)

Ring stoppers and spherical stoppers were purified by weak anion exchange HPLC (column TSKgel DEAE-NPR 4.6 mm × 75 mm (TOSOH)). The isocratic gradient of WAX B buffer is starting from 0 to 0.5 min at 20% and then from 45% to 65% in 20 min (0.8 ml·min<sup>-1</sup> flow). Rotaxanes were similarly purified using an isocratic gradient of

---

WAX B buffer from 0 to 0.5 min at 20%, and the gradient was increased from 45% to 65% in 30 min (0.4 ml·min<sup>-1</sup> flow,). The macrocycle was purified an isocratic gradient from 0 to 0.5 min at 20% of WAX B buffer, and the gradient was increased from 35% to 55% in 20 min (0.4 ml·min<sup>-1</sup> flow).

## 5.7. Fluorescence experiments

### 5.7.1. MB fluorescence experiments.

Molecular beacon probes. Molecular beacons (MB) are hairpin-structured oligonucleotide probes that can hybridize with specific DNA or RNA strands, which is extensively applied to detect target sequences in real-time strategy. With a fluorophore and a relative quencher modified to the two ends of the probe strand, MB probes present their transformation situations whenever necessary if a fluorescence detector was in use. Owing to the special stem-loop structure, the design of MB probes can be divided into two sections. For the stem segment, self-hybridized sequences are applied to constitute the probe forming a hairpin in the absence of objectives. For the loop part of the probe, a specific sequence has strong affinity to the analyte which usually has completely complementary hybridization with the target. Consequently, the probe deforms to a double helix with a target strand and reinforces the fluorophore-quencher pair far away from each other and restores the fluorescence.

A fluorescence assay with a MB was performed to monitor the transcription in real-time. The corresponding DNA nanostructure or DNA template was incubated at 25 nM with 2.17 µl of MgCl<sub>2</sub> (300 mM), 50 nM (2 equiv.) / 100 nM (4 equiv.) / 200 nM (8 equiv.) T7RNAP, 10% DMSO, 26 µl of a mastermix (2.5× transcription buffer, 5 mM NTPs, RNAsin (1:20 vol/vol), and 1.5 µM of the MB) in a total volume of 65 µl. This volume was split into two samples of 30 µl each, loaded in a 384-well plate (Greiner Fluotrac 200, 384-well plate) and the FAM fluorescence (ex. 491 nm; em. 521 nm) was measured in an Enspire 2300 plate reader (Perkin Elmer) every 1 min at 37 °C for 2 h.

### 5.7.2. Fluorescence-quenching measurements.

Fluorescence measurements were performed on an EnSpire™ Multimode Reader (PerkinElmer). For macrocycle releasing and macrocycle release direction experiments, the rotaxane samples (containing BHQ2 modified ODNs as quenchers. Supporting Table 3, Axle MB-BHQ2 for Figure 3-15, Axle MB-2Gaps for Figure 3-16) were incubated at 25 nM with 10 mM MgCl<sub>2</sub>, 2 mM NTPs, 10% DMSO, 20 nM HEX

modified ODNs (HEX-ODN 1 for Figure 3-15 and HEX-ODN 2 for Figure 3-16, Supporting Table 1 for the sequences) and 50 nM (2 equiv.) T7RNAP in a total volume of 65  $\mu$ l. The final volume was split into two samples of 30  $\mu$ l each, loaded in a 384-well plate (Greiner Fluotrac 200, 384-well plate) and the HEX fluorescence (ex. 535 nm; em. 556 nm) was measured in an Enspire 2300 plate reader (Perkin Elmer) every 2 min at 37 °C for 80 and 120 min, respectively.

For macrocycle rebinding experiments, half dumbbell was assembled by left stopper and axle MB-BHQ2 (contain BHQ2 modified ODN as quencher, Supporting Table 3) incubated at 50 nM with 10 mM MgCl<sub>2</sub> in a total volume of 350  $\mu$ L. The final volume was split into ten samples of 30  $\mu$ l each, and loaded in a 384-well plate (Greiner Fluotrac 200, 384-well plate). 5  $\mu$ l macrocycle mixture (1 mM macrocycle with HEX modified ODN (HEX-ODN 1, Supporting Table 1) in 1 $\times$  DA buffer) or pure water was added to the wells of half dumbbell before measuring fluorescence. HEX fluorescence (ex. 535 nm; em. 556 nm) was immediately measured in an Enspire 2300 plate reader (Perkin Elmer) every 10 s at 37 °C for 10 min.

### 5.8. Atomic Force Microscopy (AFM)

DNA rotaxane samples for AFM imaging experiments were diluted to 5 nM and 2 equiv. of biotin-ODN was added to hybridize with the macrocycle bound to the axle. 10 equiv. of streptavidin was also added to better identify the presence of macrocycle hybridizing with the axle.

AFM imaging was performed with a NanoWizard (JPK Instrument AG) in Alternating Contact (AC) mode in air using ACTA 50 SPM probe (Si N-type 0.01-0.025 ohm/cm; L: 125  $\mu$ m, W: 30  $\mu$ m, T: 0.4  $\mu$ m). The surface of fresh cleaved mica was functionalized by deposition of 2  $\mu$ L poly-L-ornithine 0.01% solution for 1 min, washed with 800  $\mu$ L of water, and dried in a gentle air stream. Two  $\mu$ L of 1 nM sample was deposited on the functionalized surface for 2 min, rinsed with 200  $\mu$ L H<sub>2</sub>O, and dried in a gentle air stream. Image acquisition: with 512 x 512 pixel resolution for 700 x 700 nm or 1000 nm x 1000 nm.

### 5.9. Assembly of DNA nanostructures

#### 5.9.1. Assembly of 168 bp ring stoppers.

For assembly of the ring stoppers, the ODNs (Supporting Table 2) were mixed to 4  $\mu$ M

---

concentration with NaCl (40 mM) in 1× ligase buffer (50 mM Tris·HCl, 10 mM MgCl<sub>2</sub>, 10 mM DTT, 1 mM ATP, pH 7.5) were heated to 95 °C for 5 min and annealed from 60 °C to 15 °C in 75min. T4 DNA Ligase (1 μL/100 μL, 10 U)) was added and ligated overnight at 15 °C. The products were purified by HPLC and concentrated using Amicon Ultra-30K centrifugal filters. The buffer is exchanged to 1x DA buffer (10 mM Tris, 10 mM MgCl<sub>2</sub>, 100 mM NaCl, pH 7.5) by spinning twice the sample and adding 400 μl of the buffer each time. Samples are recovered by inverting and spinning the filter tubes.

### 5.9.2. Synthesis of 40 nt single-stranded macrocycle.

The process followed the instruction from previous publication.<sup>118</sup> Briefly, single-stranded linear DNA template (20 μM, 2μL, Table S1), splint (100 μM, 5μL) and T4 DNA Ligase (1 μL/10 μL, 10 U) were mixed in 0.05× ligase buffer (20 μL in total) and incubated at 20 °C. Additional linear DNA template (20 μM, 25 μL) was separate into 7 portions and each portion was added to the mixture with 20 min interval time. The mixture was incubated at 20 °C overnight. The single-stranded macrocycle was purified by extraction from urea gel (12%) using Macherey-Nagel kit (ssDNA clean-up protocol). The single-stranded macrocycle can also be purified by HPLC with the addition of 0.2 M NaOH before injection and concentrated using Amicon Ultra-10K centrifugal filters

### 5.9.3. Assembly of axle.

For assembly of the axle, the ODNs (Supporting Table 3) were mixed to 5 μM concentration in a 1× ligase buffer and 1× DA buffer were heated to 65 °C for 5 min and then cooled down to room temperature. And T4 DNA Ligase (1 μL/100 μL, 10 U) was added and ligated overnight at 15 °C.

### 5.9.4. Assembly of rotaxane.

Assembly of the DNA rotaxane described in this work was using previously reported threading and capping methods.<sup>53</sup> Firstly, mix 40 nt single-stranded macrocycle and preassembled axle (1.1:1 equiv.) and incubate at 4 °C overnight to obtain threading. Subsequently, the mixture and 1.1 equiv. of both stoppers were mixed in a 1×ligase buffer. After incubation at 15 °C for 2h, T4 DNA Ligase (1 μL/100 μL, 10 U) was added and ligated 15 °C for 2 h. Ligation was tested on 2.5% agarose gel. And the DNA rotaxane was purified by HPLC and concentrated using Amicon Ultra-100K centrifugal

filters. The buffer is exchanged to 1x DA buffer by spinning twice the sample and adding 420  $\mu$ l of the buffer each time. Samples are recovered by inverting and spinning the filter tubes.

### 5.9.5. Assembly of spherical stopper (SST)

The ODNs (Supporting Table 4) for two parts of spherical stoppers (SST-Half1 and SST-Half2) were assembled separately as described for the 168 bp ring stoppers but not HPLC purified. After ligation, the two parts were heated to 35 °C and then mixed in equimolar amounts. The sample was cooled in the thermocycler from 35 °C to 10 °C in 60 min. After addition of ligase, the spherical stopper was ligated at 15 °C overnight. The products were purified and concentrated as ring stoppers.

### 5.9.6. Assembly of rotaxane with one spherical stopper (ROT-sst)

Assembly of ROT-sst is following the assembly method of rotaxane instead of right ring stopper with spherical stopper. The products were purified by gel extraction ('freeze-and-squeeze') and concentrated using Amicon Ultra-100K centrifugal filters. The buffer is exchanged to 1x DA buffer by spinning twice the sample and adding 420  $\mu$ l of the buffer each time. Samples are recovered by inverting and spinning the filter tubes.

## 5.10. Molecular dynamics simulations of DNA nanostructures.

### 5.10.1. Modeling construction

The simulation models of DNA rotaxane structures are built by oxView. Briefly, use sequences of interest to create double stranded or ssDNA "columns" in B-form, and then, change the spatial positions of the different DNA "columns" and use the "Ligate" function to connect them. After constructing the brief ensemble of the complete structure, "Rigid-body dynamics" function can be used to preliminarily relax the structure. Export the "simulation files" of the structure to prepare for the further simulations.

---

### 5.10.2. oxDNA molecular dynamics simulation

The simulations were performed by Dr. Michael Matthies and Professor Petr Šulc at the Arizona State University.

The coarse-grained molecular dynamics simulations were performed using the oxDNA2 software package, using the sequence-dependent parametrization of the hydrogen-bonding stacking interactions. The temperature of all modelled systems was set at 25°C and the salt concentration was set to 1M of NaCl. Simulations were performed using an Andersen-like thermostat.

Minimization. The constructed structures need to be performed minimization simulation firstly. The minimization was performed using the CPU implementation of the code. Simulation time step was 0.0165 ps. 100,000 steps of minimization were enough to minimize the bond length within the structures.

Relax. After minimization of the structures, a 100,000 steps brief Monte Carlo simulation and a 10,000,000 steps dynamics simulation was needed for relaxing the structure (Simulation time step was 0.00033 ps.).

Molecular dynamics simulation. Simulations of the rotaxane without the reporter strand attached to the macrocycle were performed using the GPU implementation of the code. Three replicas of the system were run for at least 16.5  $\mu$ s (1,000,000,000 steps). Resulting in 66  $\mu$ s of total observation time.

### 5.10.3. Simulation with external constant forces

The simulations were performed by Dr. Michael Matthies and Professor Petr Šulc at the Arizona State University.

Simulations of half of the rotaxane axle pinned to one point with a constant force pushing against the macrocycle ring were performed using the CPU implementation of the code.

The pinning was realized by introducing a spring potential  $\frac{k}{2}(r - r_0)^2$ , acting on the last base pairs of the DNA duplex part of the rotaxane (whose position is  $r$ ), with the stiffness  $k = 1140$  pN/nm. ( $r_0 = (0,0,0)$ ) The pushing force, substituting the effect the polymerase was modelled using a constant force acting separately on the center of mass of each nucleotide in the macrocycle ring in the  $y$ -axis direction, perpendicular



## Materials and methods

---

to the plane in which the end base pairs of the duplex were pinned. The force reported in Table S5 corresponds to the sum of all the forces acting on each individual nucleotide in the macrocycle ring, so the individual constant force acting on each nucleotide is the value reported in column "force [pN]" divided by the number of nucleotides in the macrocycle.

Four different systems were studied, the simulation setup is summarized in Supporting Table 5. The replicas were run for at least minimum simulated time (min. simulated time)  $\mu\text{s}$  and at maximum for maximum simulated time (max. simulated time)  $\mu\text{s}$ .

The plots of the position of the macrocycle on the rotaxane and the position histogram use a relative coordinate system. The center of mass (cms) of base pairs starting from half of the first rotaxane stopper ring till the axle, the axle and half of the second rotaxane stopper ring were calculated and enumerated from 0 to N. The cms for the macrocycle ring was computed. The macrocycle position is said to be the number of the cms on the dumbbell, closest to the macrocycle cms. All calculations were performed using the scipy python library.

---

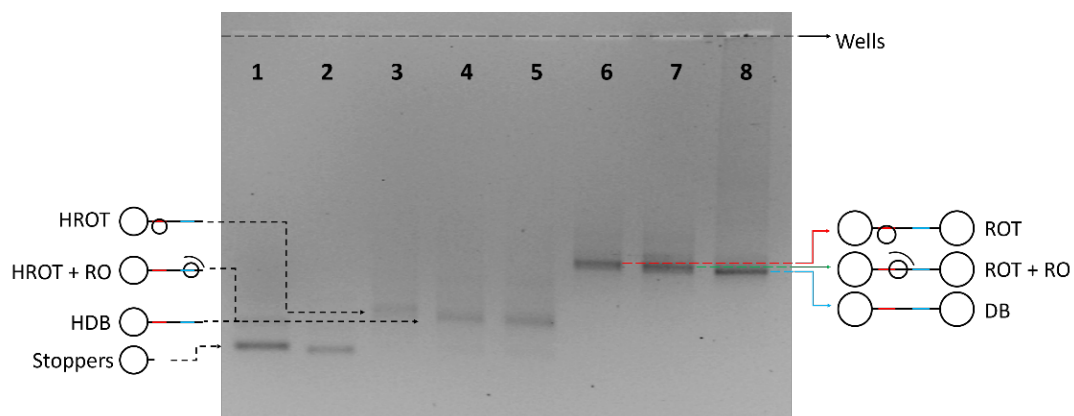
## 6. Appendix

### 6.1. List of Abbreviations

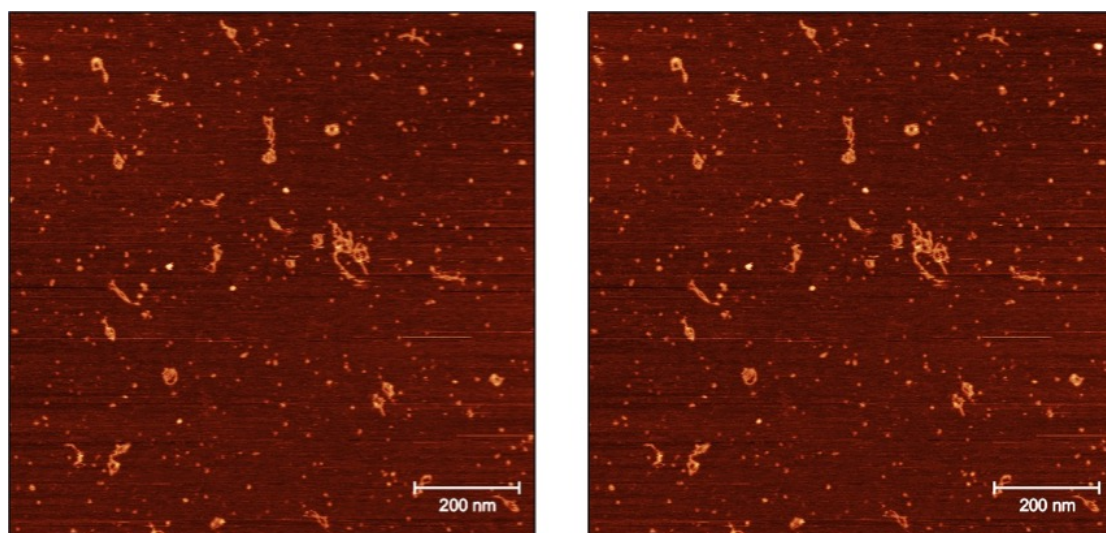
3D	three-dimensional
A	adenine
AFM	atomic force microscope
Arg	Arginine
Asn	Asparagine
BHQ2	black hole quencher 2
C	cytosine
CG	coarse-grained
CREs	cis-regulatory elements
cRO	complementary releasing oligonucleotide
DB	dumbbell
DCR	daisy chain rotaxane
DMSO	dimethyl sulfoxide
DNA	deoxyribonucleic acid
ds	double-stranded
G	guanine
GFP	green fluorescence protein
Gln	Glutamine
HEX-ODN	Hex-modified ODN
HPLC	High Performance Liquid Chromatography
IC	initiation complex
iGEM	International Genetically Engineered Machine
MB	molecular beacon
MIM	mechanically interlocked molecule
mRNA	message RNA
ncRNA	non-coding RNA
NTP	nucleoside triphosphate
ODN	oligonucleotide
PAGE	polyacrylamide gel electrophoresis
pcRNA	pseudo-complementary peptide nucleic acid
pGO	promoter gap ODN
PX	paranemic crossover
RBS	ribosome binding site
RNA	ribonucleic acid
RNAP	ribonucleic acid polymerase
RO	releasing oligonucleotide
ROT-sst	rotaxane with spherical stopper
ss	single-stranded

SST	spherical stopper
STARs	small transcriptional activating RNAs
T	thymine
TEM	transmission electron microscopy
TH	toehold
Trp	Tryptophan
U	uracil
Val	Valine
WAX	weak anion exchange

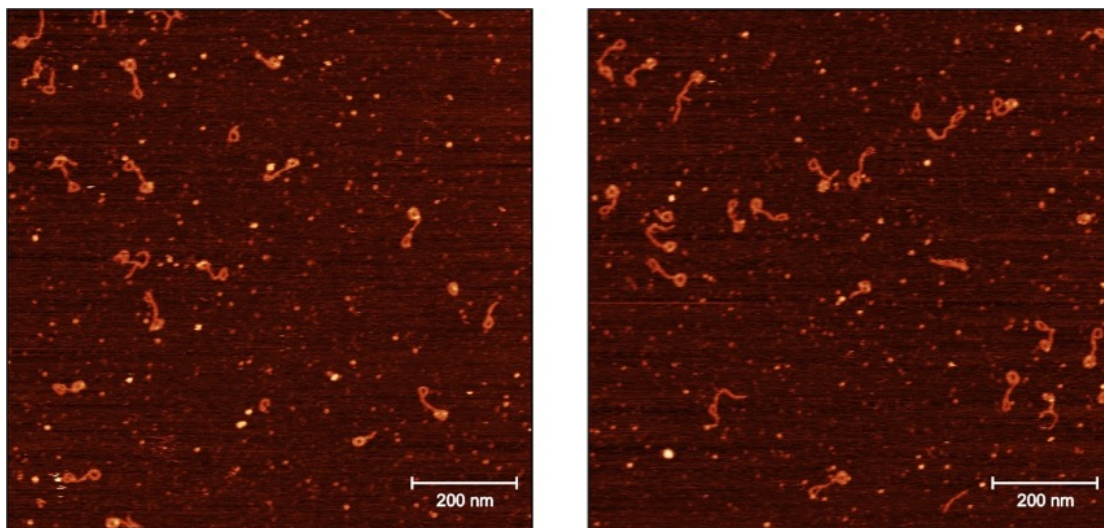
## 6.2. Supplementary Data



Supporting Figure 1. A supplementary gel analysis of rotaxane assembly.



Supporting Figure 2. Supplementary AFM measurements of spherical stoppers




Supporting Figure 3. Supplementary AFM measurements of the rotaxane with one spherical stopper

## 6.3. Tables

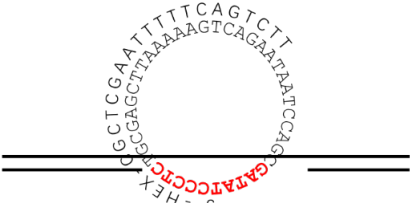
Supporting Table 1. Macrocycle and binding ODNs.

Name	Sequence
Ring10-4 (linear template)	5'-P-GAAAAATTCGAGCGTCTCCCTATAGCGACCTAATAAGACT
nbE (splint)	CGAATTTTTTCAGTCTTATTA
RO (release ODN)	GGTCGCTATAGGGAGACG
RO-TH (RO with toehold)	GCACGTGAGGTCGCTATAGGGAGACG
cRO- TH (complementary RO-TH)	CGTCTCCCTATAGCGACCTCACGTGC
nbE-bio (biotin modified ODN, biotin-ODN)	CGAATTTTTTCAGTCTTATTA-biotin
cRing4-Hex (HEX-ODN 1)	HEX-CGCTCGAATTTTTTCAGTCTT
cRing3-Hex (HEX-ODN 2)	TTTTTCAGTCTTATTAGGTC-HEX

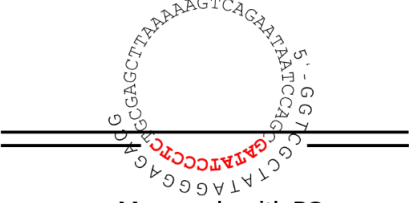


Macrocycle with splint or biotin modified ODN




Macrocycle with Hex ODN-1



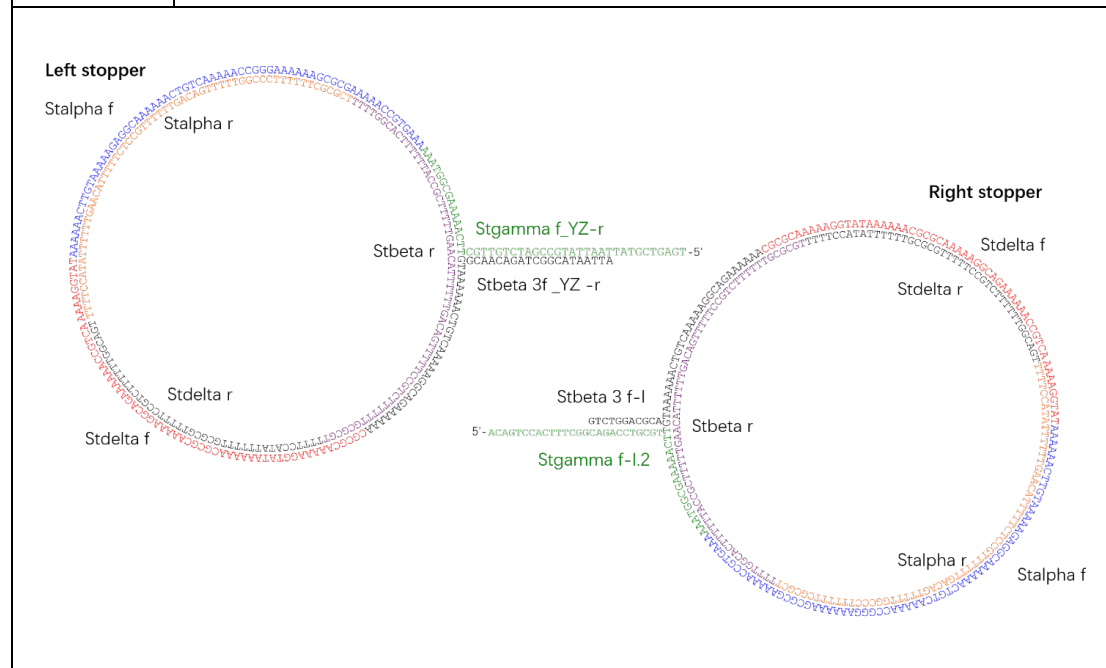
Macrocycle with RO



Macrocycle with Hex ODN-2

Supporting Table 2. Stoppers.

Name	Sequence
Stalpha r	5'-P- TTTTCCATATTTTTGAACATTTTTCTCCGTTTTTTGACAGTTTTTGGCCCTTTTTTCGCGCT
Stalpha f	5'-P- AAAGTGCCAAAAAGCGCGAAAAAAGGGCCAAAAACTGTCAAAAAACGGAGAAAAATGTTCA AAAA
Stbeta r	5'-P- TTTTGGCACTTTTTACCGCTTTTTGAACATTTTTGACAGTTTTCCGTCTTTTTGCGCGT
Stdelta r	5'-P-TTTTCCATATTTTTGCGCGTTTTTCCGTCTTTTTGGCAGT
Stdelta f	5'-P-ATATGGAAAACTGCCAAAAAGACGGAAAAACGCGCAAAAAATATGGAAAAACGCGC
Stgamma f_YZ-r	5'-P-TGAGTCGTATTAATTATGCCGATCTGTTGCTTCAAAAAGCGGTAAA
Stbeta 3 f_YZ-r	5'-P-AAAAAGACGGAAAAACTGTCAAAAAATGGCAACAGATGGCATAATTA
Stgamma f-I.2	5'-P-ACAGTCCACTTTCGGCAGACCTGCGTTTCAAAAAGCGGTAAA
Stbeta 3 f-I	5'-P-AAAAAGACGGAAAAACTGTCAAAAAATGACGCAGGTCTG



Supporting Table 3. Axles.

Name	Sequence
<b>Axle MB (for Figure 3-8 to 3-12)</b>	
Axle-T7_rev1	5'-P-CCGAAAGTGGACTGTAAAACAGATAATCAAAACAGATACTGAAA
Axle-T7_rev4-23	5'-P-AATTCGCAAACATACCTAACAAT
Axle-T7_rev4	5'-P-AATTCGCAAACATACCTAACAATAT
Axle-T7_fw4 (coding DNA)	5'-P- ATACGACTCACTATAGGGAGATATTGTTAGGTATGTTTGCGAATTTTTCAGTATCTGTTTTG ATT-ATCTGTTTT
Gap-Axle4-23 (promoter gap ODN, pGO in chapter 3.1)	5'-P-ATCTCCCTATAG
Gap-Axle4 (promoter gap ODN, pGO in chapter 3.3)	5'-P-CTCCCTATAG
<b>Axle nMB (for Figure 3-8 and 3-12)</b>	
Fw4-nonMB	5'-P- ATACGACTCACTATAGGGAGATATTGTTAGGTATGGTAAATCGGGAGTAAGCTATCTGTTTT GA-TTATCTGTTTT
Rev1-nonMB	5'-P-CCGAAAGTGGACTGTAAAACAGATAATCAAAACAGATAGCTTAC
Rev4-23-nonMB	TCCCGATTTACCATACCTAACAAT
<b>Axle MB-BHQ2 (for Figure 3-13 and Figure 3-15)</b>	
Axle-T7_rev1	5'-P-CCGAAAGTGGACTGTAAAACAGATAATCAAAACAGATACTGAAA
Rev4-23BHQ2	AATTCGCAAACATACCTAACAAT-BHQ2
Axle-T7_fw4	5'-P- ATACGACTCACTATAGGGAGATATTGTTAGGTATGTTTGCGAATTTTTCAGTATCTGTTTTG A-TTATCTGTTTT
<b>Axle MB-2Gaps (for Figure 3-16)</b>	
Fw4st_short	5'-P- ATACGACTCACTATAGGGAGATATTGTTAGGTATGTTTGCGAATTTTTCAGAAGCACTGTCCG AT
Rev1_extend	5'-P- CCGAAAGTGGACTGTCATACCTAACAATATCTCGGGAGACGCTATCGACAGTGCTTCTGAA A
Axle-T7_rev4-23	5'-P-AATTCGCAAACATACCTAACAAT
Fw3-BHQ2	BHQ2-GAGATATTGTTAGGTATG
<b>Axle MB-without terminator sequences (for Figure 3-19)</b>	

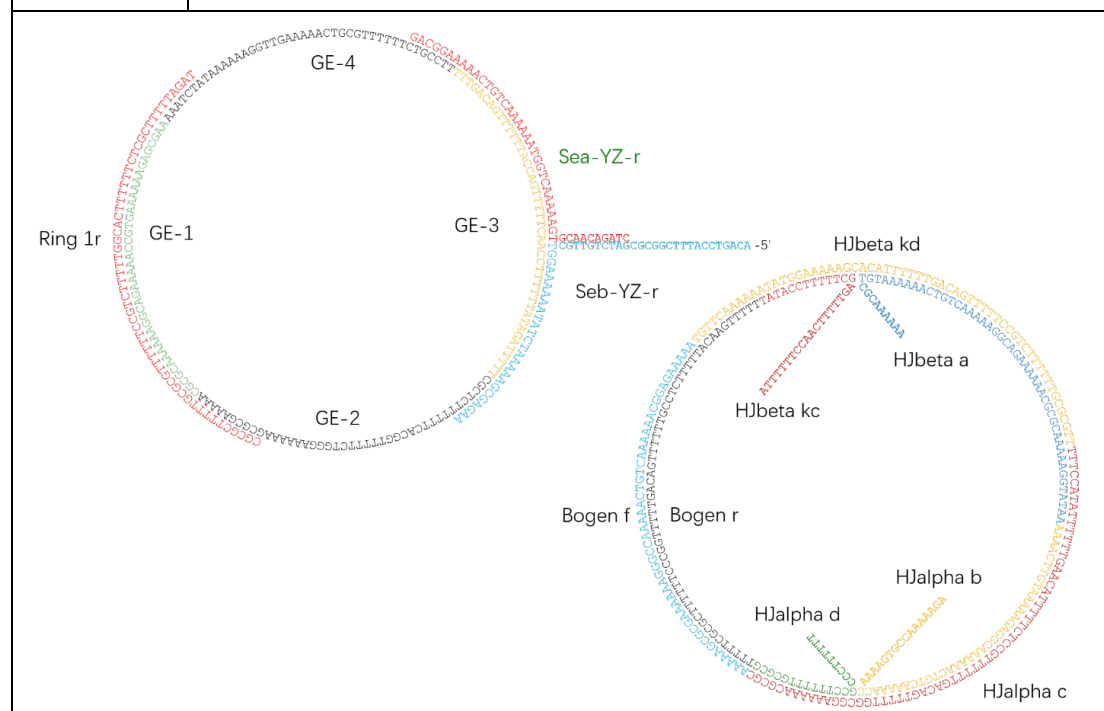


## Appendix

Axle-T7_fw4nt	5'-P- ATACGACTCACTATAGGGAGATATTGTTAGGTATGTTTGCGAATTTTTTCAGGTAAATCGGGA GT-AAGCACTGTC
Axle- T7_rev1nt	5'-P-CCGAAAGTGGACTGTGACAGTGCTTACTCCCGATTACCTGAAA
<p style="text-align: center; color: red; margin: 0;"><b>Gap-Axle4-23 (promoter Gap ODN, pGO)</b></p> <p style="text-align: center; color: red; margin: 0;"><b>GATATCCCTCTA</b></p> <div style="display: flex; justify-content: space-between; margin: 5px 0;"> <span style="font-size: small;">Axle-T7_rev4-23</span> <span style="font-size: small;">Axle-T7_rev 1</span> </div> <p style="font-size: x-small; margin: 0;">TAACAATCCATACAAACGCTTA AAGTCATAGACAAAATAAGACAAAATGTCAGGTGAAAGCC</p> <p style="margin: 0;"> <b>Axle MB</b> 5'-<u>ATACGACTCACTATAGGGAGA</u>TATTGTTAGGTATGTTGCGAATTTTCAGTATCTGTTTGATTATCTGTTTT  <span style="margin-left: 100px;">Axle-T7_fw4</span> </p> <div style="display: flex; justify-content: space-between; margin: 5px 0;"> <span style="font-size: small;">Rev4-23-nonMB</span> <span style="font-size: small;">Rev1-nonMB</span> </div> <p style="font-size: x-small; margin: 0;">TAACAATCCATACAAACGCTTA ATTTCGATAGACAAAATAAGACAAAATGTCAGGTGAAAGCC</p> <p style="margin: 0;"> <b>Axle nMB</b> 5'-ATACGACTCACTATAGGGAGATATTGTTAGGTATGTTGCGAATTTTCAGTATCTGTTTGATTATCTGTTTT  <span style="margin-left: 100px;">Fw4-nonMB</span> </p> <div style="display: flex; justify-content: space-between; margin: 5px 0;"> <span style="font-size: small;">Rev4-23BHQ2</span> <span style="font-size: small;">Axle-T7_rev1</span> </div> <p style="font-size: x-small; margin: 0;"><b>BHQ2</b>-TAACAATCCATACAAACGCTTA AAGTCATAGACAAAATAAGACAAAATGTCAGGTGAAAGCC</p> <p style="margin: 0;"> <b>Axle MB-BHQ2</b> 5'-<u>ATACGACTCACTATAGGGAGA</u>TATTGTTAGGTATGTTGCGAATTTTCAGTATCTGTTTGATTATCTGTTTT  <span style="margin-left: 100px;">Axle-T7_fw4</span> </p> <div style="display: flex; justify-content: space-between; margin: 5px 0;"> <span style="font-size: small;">Axle-T7_rev4-23</span> <span style="font-size: small;">Rev1_extend</span> </div> <p style="font-size: x-small; margin: 0;">TAACAATCCATACAAACGCTTA AAGTCATAGACAAAATAAGACAAAATGTCAGGTGAAAGCC</p> <p style="margin: 0;"> <b>Axle MB-2Gaps</b> 5'-ATACGACTCACTATAGGGAGATATTGTTAGGTATGTTGCGAATTTTCAGTATCTGTTTGATTATCTGTTTT  <span style="margin-left: 100px;">Fw4st_short</span> <span style="margin-left: 100px;">5'-<b>BHQ2</b>-GAGATATTGTTAGGTATG</span> <span style="margin-left: 100px;">Fw3-BHQ2</span> </p> <div style="display: flex; justify-content: space-between; margin: 5px 0;"> <span style="font-size: small;">Axle-T7_rev4-23</span> <span style="font-size: small;">Axle-T7_rev 1nt</span> </div> <p style="font-size: x-small; margin: 0;">TAACAATCCATACAAACGCTTA AAGTCATTAGCCCTCATTTCGTGACAGTGTGTCAGGTGAAAGCC</p> <p style="margin: 0;"> <b>Axle MB-without terminators</b> 5'-<u>ATACGACTCACTATAGGGAGA</u>TATTGTTAGGTATGTTGCGAATTTTCAGTAAATCGGAGTAAGCACTGTC  <span style="margin-left: 100px;">Axle-T7_fw4nt</span> </p>	

Supporting Table 4. Spherical stopper (SST).

Name	Sequence
<b>SST-Half1</b>	
SEa-YZ-r	5'-P-GACGGAAAACTGTCAAAAAATGTTCAAAAAGTGAACAGATC
SEb-YZ-r	5'-P-ACAGTCCATTTTCGGGATCTGTTGCTGGAAAAATATCTAAAAAGCGAGAA
Ring1r	5'-P-CGCGCTTTTTGCGCGTTTTTCCGTCTTTTTGGCACTTTTTCTCGCTTTTAGAT
GE-1	5'-P-AAGCGAGAAAAAGTGCCAAAAAGACGGAAAAACGCGC
GE-2	5'-P-AAAAAGCGCGAAAAAAGGGTCTTTTTGGCACTTTTTCTCGC
GE-3	5'-P-TTTTAGATATTTTTCCAACTTTTGAACATTTTTGACAGTTT
GE-4	5'-P-TTCCGTCTTTTTGCGTCAAAAAGTTGAAAAAATATCTAAA
<b>SST-Half2</b>	
Bogen r	5'-P-TTTTTGAACATTTTTCTCCGTTTTTGGACAGTTTTTGGCCCTTTTTT
HJbeta kc	5'-P-ATTTTTTCCAACTTTTTGAGCTTTTTCCATAT
HJbeta a	5'-P-AATATGGAAAAACGCGCAAAAAAGACGGAAAAACTGTCAAAAAATGTCGCAAAAA
HJalpha b	5'-P-AAAAGTGCCAAAAAGACCAAAAACTGTCAAAAAACGGAGAAAAATGTTCAAAA
HJalpha d	5'-P-CGCGCTTTTTGCGCGTTTTTCCGCCCTTTTTT
HJalpha c	5'-P- TTTTCCATATTTTTGAACATTTTTCTCCGTTTTTGGACAGTTTTTGGCGGAAAAACGCGC
Bogen f	5'-P-AAAAAGCGCGAAAAAAGGGCCAAAACTGTCAAAAAACGGAGAAAAA
HJbeta kd	5'-P-TGTTCAAAAAATATGGAAAAGCACATTTTTTGGACAGTTTTTCCGTCTTTTTGCGCGTT



## Appendix

Supporting Table 5. A summary of oxDNA simulations with force. The first column indicates if reported strand was (+) or was not (-) present on the macrocycle. Second column indicates if the stopper was a ring sequence (-) or the more “spherical” (+) one.

	Reporter Strand	Spherical stopper	# of Replicas	force pN	Min simulated time $\mu$ s	max simulated time $\mu$ s
1	-	-	10	10	0.69	0.75
2	-	-	10	20	0.72	0.73
3	-	-	10	30	0.71	0.74
4	-	-	10	40	0.73	0.74
5	+	-	10	10	0.73	0.74
6	+	-	10	20	0.74	0.76
7	+	-	10	30	0.71	0.73
8	+	-	10	40	0.72	0.73
9	-	+	10	10	2.07	2.09
10	-	+	10	20	2.02	2.05
11	-	+	10	30	1.98	2.07
12	-	+	10	40	0.88	0.91
13	+	+	10	10	1.92	2.01
14	+	+	10	20	1.95	2.01
15	+	+	10	30	1.94	1.97
16	+	+	10	40	1.88	1.95

---

## 7. References

1. *DNA nanotechnology: methods and protocols*. (Humana Press, 2011).
2. Seeman, N. C. & Kallenbach, N. R. Design of immobile nucleic acid junctions. *Biophys. J.* **44**, 201–209 (1983).
3. Yan, H., Zhang, X., Shen, Z. & Seeman, N. C. A robust DNA mechanical device controlled by hybridization topology. *Nature* **415**, 62 (2002).
4. Seeman, N. C. *Structural DNA Nanotechnology*. (Cambridge University Press, 2016). doi:10.1017/CBO9781139015516.
5. Chargaff, E., Lipshitz, R. & Green, C. Composition of the Desoxyribose Nucleic Acids of Four Genera of Sea-Urchin. *J. Biol. Chem.* **195**, 155–160 (1952).
6. Watson, J. D. & Crick, F. H. C. Molecular Structure of Nucleic Acids: A Structure for Deoxyribose Nucleic Acid. *Nature* **171**, 737–738 (1953).
7. Pettersen, E. F. *et al.* UCSF ChimeraX: Structure visualization for researchers, educators, and developers. *Protein Sci.* **30**, 70–82 (2021).
8. MacDonald, D., Herbert, K., Zhang, X., Polgruto, T. & Lu, P. Solution structure of an A-tract DNA bend. *J. Mol. Biol.* **306**, 1081–1098 (2001).
9. Curuksu, J., Zakrzewska, K. & Zacharias, M. Magnitude and direction of DNA bending induced by screw-axis orientation: influence of sequence, mismatches and abasic sites. *Nucleic Acids Res.* **36**, 2268–2283 (2008).
10. Zhao, J., Bacolla, A., Wang, G. & Vasquez, K. M. Non-B DNA structure-induced genetic instability and evolution. *Cell. Mol. Life Sci.* **67**, 43–62 (2010).
11. Green, S. J., Lubrich, D. & Turberfield, A. J. DNA Hairpins: Fuel for Autonomous DNA Devices. *Biophys. J.* **91**, 2966–2975 (2006).
12. King, J. J. *et al.* DNA G-Quadruplex and i-Motif Structure Formation Is Interdependent in Human Cells. *J. Am. Chem. Soc.* **142**, 20600–20604 (2020).
13. Holliday, R. A mechanism for gene conversion in fungi. *Genet. Res.* **5**, 282–304 (1964).
14. Seeman, N. C. Nucleic acid junctions and lattices. *J. Theor. Biol.* **99**, 237–247 (1982).
15. Mandel, M. & Marmur, J. [109] Use of ultraviolet absorbance-temperature profile for determining the guanine plus cytosine content of DNA. in *Methods in Enzymology* vol. 12 195–206 (Elsevier, 1968).
16. Kornberg, R. D. The molecular basis of eukaryotic transcription. *Proc. Natl. Acad. Sci.* **104**, 12955–12961 (2007).
17. Zhang, D. Y. & Winfree, E. Control of DNA Strand Displacement Kinetics Using Toehold Exchange. *J. Am. Chem. Soc.* **131**, 17303–17314 (2009).
18. Tang, W. *et al.* DNA Strand Displacement Reaction: A Powerful Tool for

- Discriminating Single Nucleotide Variants. *Top. Curr. Chem.* **378**, 10 (2020).
19. Engelen, W., Janssen, B. M. G. & Merkx, M. DNA-based control of protein activity. *Chem. Commun.* **52**, 3598–3610 (2016).
20. Frank-Kamenetskii, M. D. & Lazurkin, Yu. S. Conformational Changes in DNA Molecules. *Annu. Rev. Biophys. Bioeng.* **3**, 127–150 (1974).
21. Jaekel, Stegemann, & Saccà. Manipulating Enzymes Properties with DNA Nanostructures. *Molecules* **24**, 3694 (2019).
22. Chen, J. & Seeman, N. C. Synthesis from DNA of a molecule with the connectivity of a cube. *Nature* **350**, 631–633 (1991).
23. Evans, C. G. & Winfree, E. Physical principles for DNA tile self-assembly. *Chem. Soc. Rev.* **46**, 3808–3829 (2017).
24. Lehman, I. R. DNA Ligase: Structure, Mechanism, and Function: The joining of DNA chains by DNA ligase is an essential component of DNA repair. replication, and recombination. *Science* **186**, 790–797 (1974).
25. Seeman, N. C. DNA in a material world. *Nature* **421**, 427–431 (2003).
26. Rothmund, P. W. K. Folding DNA to create nanoscale shapes and patterns. *Nature* **440**, 297–302 (2006).
27. Saccà, B. & Niemeyer, C. M. DNA Origami: The Art of Folding DNA. *Angew. Chem. Int. Ed.* **51**, 58–66 (2011).
28. Daljit Singh, J. K., Luu, M. T., Abbas, A. & Wickham, S. F. J. Switchable DNA-origami nanostructures that respond to their environment and their applications. *Biophys. Rev.* **10**, 1283–1293 (2018).
29. Seeman, N. C. From genes to machines: DNA nanomechanical devices. *Trends Biochem. Sci.* **30**, 119–125 (2005).
30. Kelly, T. R. Molecular Motors: Synthetic DNA-Based Walkers Inspired by Kinesin. *Angew. Chem. Int. Ed.* **44**, 4124–4127 (2005).
31. Tian, Y., He, Y., Chen, Y., Yin, P. & Mao, C. A DNAzyme That Walks Processively and Autonomously along a One-Dimensional Track. *Angew. Chem. Int. Ed.* **44**, 4355–4358 (2005).
32. Beissenhirtz, M. K. & Willner, I. DNA-based machines. *Org. Biomol. Chem.* **4**, 3392–3401 (2006).
33. Zhao, S. *et al.* Boolean logic gate based on DNA strand displacement for biosensing: current and emerging strategies. *Nanoscale Horiz.* **6**, 298–310 (2021).
34. Qian, L. & Winfree, E. Scaling Up Digital Circuit Computation with DNA Strand Displacement Cascades. *Science* **332**, 1196–1201 (2011).
35. Podila, R. & Brown, J. M. Toxicity of Engineered Nanomaterials: A Physicochemical Perspective: TOXICITY OF ENGINEERED NANOMATERIALS. *J. Biochem. Mol. Toxicol.* **27**, 50–55 (2013).

- 
36. Qu, X. *et al.* An Exonuclease III-Powered, On-Particle Stochastic DNA Walker. *Angew. Chem. Int. Ed.* **56**, 1855–1858 (2017).
37. Yehl, K. *et al.* High-speed DNA-based rolling motors powered by RNase H. *Nat. Nanotechnol.* **11**, 184–190 (2015).
38. Douglas, S. M. *et al.* Rapid prototyping of 3D DNA-origami shapes with caDNAno. *Nucleic Acids Res.* **37**, 5001–5006 (2009).
39. Williams, S. *et al.* Tiamat: A Three-Dimensional Editing Tool for Complex DNA Structures. in *DNA Computing* (eds. Goel, A., Simmel, F. C. & Sosík, P.) vol. 5347 90–101 (Springer Berlin Heidelberg, 2009).
40. Pan, K. *et al.* Lattice-free prediction of three-dimensional structure of programmed DNA assemblies. *Nat. Commun.* **5**, 5578 (2014).
41. Veneziano, R. *et al.* Designer nanoscale DNA assemblies programmed from the top down. *Science* **352**, 1534–1534 (2016).
42. Jun, H. *et al.* Autonomously designed free-form 2D DNA origami. *Sci. Adv.* **5**, eaav0655 (2019).
43. Pérez, A., Luque, F. J. & Orozco, M. Frontiers in Molecular Dynamics Simulations of DNA. *Acc. Chem. Res.* **45**, 196–205 (2012).
44. Šulc, P. *et al.* Sequence-dependent thermodynamics of a coarse-grained DNA model. *J. Chem. Phys.* **137**, 135101 (2012).
45. Ouldridge, T. E., Louis, A. A. & Doye, J. P. K. Structural, mechanical, and thermodynamic properties of a coarse-grained DNA model. *J. Chem. Phys.* **134**, 085101 (2011).
46. Snodin, B. E. K. *et al.* Introducing improved structural properties and salt dependence into a coarse-grained model of DNA. *J. Chem. Phys.* **142**, 234901 (2015).
47. Sengar, A., Ouldridge, T. E., Henrich, O., Rovigatti, L. & Šulc, P. A Primer on the oxDNA Model of DNA: When to Use it, How to Simulate it and How to Interpret the Results. *Front. Mol. Biosci.* **8**, (2021).
48. Bruns, C. J. & Stoddart, J. F. *The Nature of the Mechanical Bond.* (2016).
49. Stoddart, J. F. Mechanically Interlocked Molecules (MIMs)—Molecular Shuttles, Switches, and Machines (Nobel Lecture). *Angew. Chem. Int. Ed.* **56**, 11094–11125 (2017).
50. Sauvage, J.-P. From Chemical Topology to Molecular Machines (Nobel Lecture). *Angew. Chem. Int. Ed.* n/a-n/a (2017) doi:10.1002/anie.201702992.
51. Sauvage, J.-P. & Gaspard, P. *From Non-Covalent Assemblies to Molecular Machines.* (2010).
52. Jester, S.-S. & Famulok, M. Mechanically interlocked DNA nanostructures for functional devices. *Acc. Chem. Res.* **47**, 1700–9 (2014).

53. Valero, J. *et al.* Design, assembly, characterization, and operation of double-stranded interlocked DNA nanostructures. *Nat. Protoc.* **14**, 2818–2855 (2019).
54. Schill, G. *Catenanes, rotaxanes, and knots.* (1971).
55. Schomburg, I. Nomenklatur der Rotaxane und Pseudorotaxane. *Angew. Chem.* **121**, 4719–4738 (2009).
56. Dietrich-Buchecker, C. O., Sauvage, J. P. & Kintzinger, J. P. Une nouvelle famille de molecules : les metallo-catenanes. *Tetrahedron Lett.* **24**, 5095–5098 (1983).
57. Parham, A. H., Windisch, B. & Vögtle, F. Chemical Reactions in the Axle of Rotaxanes – Steric Hindrance by the Wheel. *Eur. J. Org. Chem.* **1999**, 1233–1238 (1999).
58. Ackermann, D. *et al.* A double-stranded DNA rotaxane. *Nat. Nanotechnol.* **5**, 436–442 (2010).
59. Ulanovsky, L., Bodner, M., Trifonov, E. N. & Choder, M. Curved DNA: design, synthesis, and circularization. *Proc. Natl. Acad. Sci.* **83**, 862–866 (1986).
60. Ackermann, D., Jester, S.-S. & Famulok, M. Design Strategy for DNA Rotaxanes with a Mechanically Reinforced PX100 Axle. *Angew. Chem. Int. Ed.* **51**, 6771–6775 (2012).
61. Lohmann, F., Ackermann, D. & Famulok, M. Reversible light switch for macrocycle mobility in a DNA rotaxane. *J. Am. Chem. Soc.* **134**, 11884–7 (2012).
62. Ackermann, D. & Famulok, M. Pseudo-complementary PNA actuators as reversible switches in dynamic DNA nanotechnology. *Nucleic Acids Res.* **41**, 4729–4739 (2013).
63. Weigandt, J., Chung, C., Jester, S. & Famulok, M. Daisy Chain Rotaxanes Made from Interlocked DNA Nanostructures. *Angew. Chem. Int. Ed.* **55**, 5512–5516 (2016).
64. Liu, X., Lu, C.-H. & Willner, I. Switchable Reconfiguration of Nucleic Acid Nanostructures by Stimuli-Responsive DNA Machines. *Acc. Chem. Res.* **47**, 1673–1680 (2014).
65. Lu, C.-H., Ceconello, A. & Willner, I. Recent Advances in the Synthesis and Functions of Reconfigurable Interlocked DNA Nanostructures. *J. Am. Chem. Soc.* **138**, 5172–5185 (2016).
66. Lu, C.-H. *et al.* Switchable Reconfiguration of a Seven-Ring Interlocked DNA Catenane Nanostructure. *Nano Lett.* **15**, 7133–7137 (2015).
67. Sannohe, Y. & Sugiyama, H. Single strand DNA catenane synthesis using the formation of G-quadruplex structure. *Bioorg. Med. Chem.* **20**, 2030–2034 (2012).
68. Lohmann, F., Valero, J. & Famulok, M. A novel family of structurally stable double stranded DNA catenanes. *Chem. Commun.* **50**, 6091–6093 (2014).
69. Valero, J., Lohmann, F., Keppner, D. & Famulok, M. Single-Stranded Tile

- 
- Stoppers for Interlocked DNA Architectures. *ChemBioChem* **17**, 1146–1149 (2016).
70. List, J., Falgenhauer, E., Kopperger, E., Pardatscher, G. & Simmel, F. C. Long-range movement of large mechanically interlocked DNA nanostructures. *Nat. Commun.* **7**, 12414 (2016).
71. Chao, Y.-C. *et al.* NanoMuscle: controllable contraction and extension of mechanically interlocked DNA origami. *Nanoscale* (2019) doi:10.1039/C9NR06314E.
72. Lohmann, F., Weigandt, J., Valero, J. & Famulok, M. Logic Gating by Macrocyclic Displacement Using a Double-Stranded DNA [3]Rotaxane Shuttle. *Angew. Chem. Int. Ed.* **53**, 10372–10376 (2014).
73. Centola, M., Valero, J. & Famulok, M. Allosteric Control of Oxidative Catalysis by a DNA Rotaxane Nanostructure. *J. Am. Chem. Soc.* (2017) doi:10.1021/jacs.7b08839.
74. Ma, Y., Centola, M., Keppner, D. & Famulok, M. Interlocked DNA Nanojoints for Reversible Thermal Sensing. *Angew. Chem. Int. Ed.* **59**, 12455–12459 (2020).
75. Valero, J., Pal, N., Dhakal, S., Walter, N. G. & Famulok, M. A bio-hybrid DNA rotor–stator nanoengine that moves along predefined tracks. *Nat. Nanotechnol.* **1** (2018) doi:10.1038/s41565-018-0109-z.
76. Cameron, D. E., Bashor, C. J. & Collins, J. J. A brief history of synthetic biology. *Nat. Rev. Microbiol.* **12**, 381–390 (2014).
77. Meng, F. & Ellis, T. The second decade of synthetic biology: 2010–2020. *Nat. Commun.* **11**, 5174 (2020).
78. Nakano, T. *Molecular communication*. (Cambridge University Press, 2013).
79. Flores Bueso, Y. & Tangney, M. Synthetic Biology in the Driving Seat of the Bioeconomy. *Trends Biotechnol.* **35**, 373–378 (2017).
80. Schwille, P. Bottom-Up Synthetic Biology: Engineering in a Tinkerer’s World. *Science* **333**, 1252–1254 (2011).
81. English, M. A., Gayet, R. V. & Collins, J. J. Designing Biological Circuits: Synthetic Biology Within the Operon Model and Beyond. *Annu. Rev. Biochem.* **90**, 221–244 (2021).
82. Jacob, F. & Monod, J. On the Regulation of Gene Activity. *Cold Spring Harb. Symp. Quant. Biol.* **26**, 193–211 (1961).
83. Nobel prizes and restriction enzymes. *Gene* **4**, 181–182 (1978).
84. Gardner, T. S., Cantor, C. R. & Collins, J. J. Construction of a genetic toggle switch in *Escherichia coli*. *Nature* **403**, 339–342 (2000).
85. Elowitz, M. B. & Leibler, S. A synthetic oscillatory network of transcriptional regulators. *Nature* **403**, 335–338 (2000).
86. Stricker, J. *et al.* A fast, robust and tunable synthetic gene oscillator. *Nature* **456**, 516–519 (2008).



87. Smanski, M. J. *et al.* Synthetic biology to access and expand nature's chemical diversity. *Nat. Rev. Microbiol.* **14**, 135–149 (2016).
88. Alberts, B. *Molecular biology of the cell.* (Garland Science, Taylor and Francis Group, 2015).
89. Jungmann, R., Renner, S. & Simmel, F. C. From DNA nanotechnology to synthetic biology. *HFSP J.* **2**, 99–109 (2008).
90. Isaacs, F. J. *et al.* Engineered riboregulators enable post-transcriptional control of gene expression. *Nat. Biotechnol.* **22**, 841–847 (2004).
91. Green, A. A., Silver, P. A., Collins, J. J. & Yin, P. Toehold switches: de-novo-designed regulators of gene expression. *Cell* **159**, 925–939 (2014).
92. Chappell, J., Takahashi, M. K. & Lucks, J. B. Creating small transcription activating RNAs. *Nat. Chem. Biol.* **11**, 214–220 (2015).
93. Wittkopp, P. J. & Kalay, G. Cis-regulatory elements: molecular mechanisms and evolutionary processes underlying divergence. *Nat. Rev. Genet.* **13**, 59–69 (2012).
94. Lifton, R. P., Goldberg, M. L., Karp, R. W. & Hogness, D. S. The Organization of the Histone Genes in *Drosophila melanogaster*: Functional and Evolutionary Implications. *Cold Spring Harb. Symp. Quant. Biol.* **42**, 1047–1051 (1978).
95. Kim, J., Hopfield, J. J. & Winfree, E. Neural network computation by in vitro transcriptional circuits. *Adv. Neural Inf. Process. Syst.* **17**, 681–688 (2004).
96. Kim, J., White, K. S. & Winfree, E. Construction of an *in vitro* bistable circuit from synthetic transcriptional switches. *Mol. Syst. Biol.* **2**, 68 (2006).
97. Kim, J. & Winfree, E. Synthetic in vitro transcriptional oscillators. *Mol. Syst. Biol.* **7**, 465 (2011).
98. Chou, L. Y. T. & Shih, W. M. In Vitro Transcriptional Regulation via Nucleic-Acid-Based Transcription Factors. *ACS Synth. Biol.* **8**, 2558–2565 (2019).
99. Green, A. A. Synthetic bionanotechnology: synthetic biology finds a toehold in nanotechnology. *Emerg. Top. Life Sci.* **3**, 507–516 (2019).
100. Jeong, D. *et al.* Cell-Free Synthetic Biology Platform for Engineering Synthetic Biological Circuits and Systems. *Methods Protoc.* **2**, 39 (2019).
101. Sousa, R. T7 RNA Polymerase. in *Encyclopedia of Biological Chemistry* 355–359 (Elsevier, 2013). doi:10.1016/B978-0-12-378630-2.00267-X.
102. Ikeda, R. A. & Richardson, C. C. Interactions of the RNA polymerase of bacteriophage T7 with its promoter during binding and initiation of transcription. *Proc. Natl. Acad. Sci.* **83**, 3614–3618 (1986).
103. Martin, C. T. & Coleman, J. E. Kinetic analysis of T7 RNA polymerase-promoter interactions with small synthetic promoters. *Biochemistry* **26**, 2690–2696 (1987).
104. Strothkamp, R. E., Oakley, J. L. & Coleman, J. E. Promoter melting by T7

- 
- ribonucleic acid polymerase as detected by single-stranded endonuclease digestion. *Biochemistry* **19**, 1074–1080 (1980).
105. Osterman, H. L. & Coleman, J. E. T7 Ribonucleic acid polymerase-promoter interactions. *Biochemistry* **20**, 4884–4892 (1981).
106. Jeruzalmi, D., Cheetham, G. M. T. & Steitz, T. A. Structural basis for initiation of transcription from an RNA polymerase–promoter complex. *Nature* **399**, 80 (1999).
107. Cheetham, G. M. & Steitz, T. A. Insights into transcription: structure and function of single-subunit DNA-dependent RNA polymerases. *Curr. Opin. Struct. Biol.* **10**, 117–123 (2000).
108. Diaz, G. A., Rong, M., McAllister, W. T. & Durbin, R. K. The Stability of Abortively Cycling T7 RNA Polymerase Complexes Depends upon Template Conformation. *Biochemistry* **35**, 10837–10843 (1996).
109. Bai, L., Shundrovsky, A. & Wang, M. D. Chapter 9. Kinetic Modeling of Transcription Elongation. in *RSC Biomolecular Sciences* (eds. Buc, H. & Strick, T.) 263–280 (Royal Society of Chemistry, 2009). doi:10.1039/9781847559982-00263.
110. Maslak, M. & Martin, C. T. Kinetic analysis of T7 RNA polymerase transcription initiation from promoters containing single-stranded regions. *Biochemistry* **32**, 4281–4285 (1993).
111. Ma, K., Temiakov, D., Anikin, M. & McAllister, W. T. Probing conformational changes in T7 RNA polymerase during initiation and termination by using engineered disulfide linkages. *Proc. Natl. Acad. Sci.* **102**, 17612–17617 (2005).
112. Lyakhov, D. L. *et al.* Pausing and termination by bacteriophage T7 RNA polymerase<sup>11</sup> Edited by M. Gottesman. *J. Mol. Biol.* **280**, 201–213 (1998).
113. Újvári, A. & Martin, C. T. Identification of a minimal binding element within the T7 RNA polymerase promoter<sup>11</sup> Edited by R. Ebright. *J. Mol. Biol.* **273**, 775–781 (1997).
114. Zhou, W. & Doetsch, P. W. Transcription bypass or blockage at single-strand breaks on the DNA template strand: Effect of different 3' and 5' flanking groups on the T7 RNA polymerase elongation complex. *Biochemistry* **33**, 14926–14934 (1994).
115. Zhou, W., Reines, D. & Doetsch, P. W. T7 RNA polymerase bypass of large gaps on the template strand reveals a critical role of the nontemplate strand in elongation. *Cell* **82**, 577–585 (1995).
116. Chen, Z. & Zhang, Y. Dimethyl sulfoxide targets phage RNA polymerases to promote transcription. *Biochem. Biophys. Res. Commun.* **333**, 664–670 (2005).
117. Tian, H. & Wang, Q.-C. Recent progress on switchable rotaxanes. *Chem. Soc. Rev.* **35**, 361–374 (2006).

118. An, R. *et al.* Highly efficient preparation of single-stranded DNA rings by T4 ligase at abnormally low Mg(II) concentration. *Nucleic Acids Res.* **45**, e139–e139 (2017).
119. Gao, Y. Secondary structure effects on DNA hybridization kinetics: a solution versus surface comparison. *Nucleic Acids Res.* **34**, 3370–3377 (2006).
120. Albrecht-Gary, A. M., Saad, Z., Dietrich-Buchecker, C. O. & Sauvage, J. P. Interlocked macrocyclic ligands: a kinetic catenand effect in copper(I) complexes. *J. Am. Chem. Soc.* **107**, 3205–3209 (1985).
121. Rovigatti, L., Šulc, P., Reguly, I. Z. & Romano, F. A comparison between parallelization approaches in molecular dynamics simulations on GPUs. *J. Comput. Chem.* **36**, 1–8 (2015).
122. Thomen, P. *et al.* T7 RNA polymerase studied by force measurements varying cofactor concentration. *Biophys. J.* **95**, 2423–2433 (2008).
123. Barth, A., Kobbe, D. & Focke, M. DNA–DNA kissing complexes as a new tool for the assembly of DNA nanostructures. *Nucleic Acids Res.* **44**, 1502–1513 (2016).
124. Daubendiek, S. L., Ryan, K. & Kool, E. T. Rolling-Circle RNA Synthesis: Circular Oligonucleotides as Efficient Substrates for T7 RNA Polymerase. *J. Am. Chem. Soc.* **117**, 7818–7819 (1995).
125. Daubendiek, S. L. & Kool, E. T. Generation of catalytic RNAs by rolling transcription of synthetic DNA nanocircles. *Nat. Biotechnol.* **15**, 273–277 (1997).
126. Li, T., Lohmann, F. & Famulok, M. Interlocked DNA nanostructures controlled by a reversible logic circuit. *Nat. Commun.* **5**, ncomms5940 (2014).
127. Chan, K. *et al.* Base Damage within Single-Strand DNA Underlies In Vivo Hypermutability Induced by a Ubiquitous Environmental Agent. *PLoS Genet.* **8**, e1003149 (2012).

---

## 8. Acknowledgements

I would like to thank those who have helped me during my PhD studies. Their kindness has brightened my days, made my life in Bonn more fulfilling and meaningful, and given me the courage and determination to overcome difficulties.

I would like to begin by expressing my sincere gratitude to my supervisor, Professor Michael Famulok. Your kind help and guidance have been a source of motivation for me.

I would like to thank the Chinese Scholarship Council for providing me with this great opportunity to study at the University of Bonn, which is an amazing place.

I am fortunate enough to work with lovely people in the DNA nanotech group at the LIMES institute of University of Bonn. Dr. Julián Valero, Mathias Centola, Dr. Yinzhou Ma, Marko Škugor, Michael Haydell, Daniel Keppner, many thanks for your frequent help and support in daily life and in the lab.

I would like to thank Dr. Michael Matthies and Professor Petr Šulc at the Arizona State University for helping me with the coarse-grained simulation of my system, which is definitely a highlight of this project.

I would like to thank all the staff of the Famulok and Mayer groups for the very friendly and cozy working atmosphere.

I must express my very profound gratitude to my parents and to my wife for providing me with unfailing support and continuous encouragement throughout my years of study and through the process of researching. This accomplishment would not have been possible without them. Thank you.